Relationship between the natural frequencies and fatigue life of NBG-18 graphite

Renier Markgraaff

B-Eng (Mechanical)

Dissertation submitted in partial fulfilment of the requirements for the degree

Master of Engineering

School of Nuclear Engineering

At

North-West University

Potchefstroom Campus

Supervisor: Dr. J.G. Roberts

Co-Supervisor: Prof. J. Markgraaff

Potchefstroom

2010

EXECUTIVE SUMMARY

NBG-18 graphite is developed by SGL Carbon for the Pebble Bed Modular Reactor Company (PBMR), and is used as the preferred material for the internal graphite core structures of a high-temperature gas-cooled nuclear reactor (HTR). The NBG-18 graphite is manufactured using pitch coke, and is vibrationally molded.

To assess the structural behaviour of graphite many destructive techniques have been performed in the past. Though the destructive techniques are easy and in some cases relative inexpensive to perform, these methods lead to waste material and require cumbersome time consuming sample preparations.

To overcome this problem numerous non-destructive testing techniques are available such as sonic resonance, resonant inspection, ultrasonic testing, low and multi-frequency Eddy current analysis, acoustic emission and impulse excitation techniques.

The Hammer Impulse Excitation technique was used as a method in predicting the fatigue life of NBG-18 graphite by focussing on the application of modal frequency analysis of determined natural frequencies. Moreover, the typical fatigue characteristics of NBG-18 graphite were determined across a comprehensive set of load ranges.

In order to be able to correlate modal frequency parameters with fatigue life, suitable uniaxial fatigue test specimen geometry needed to be obtained. The uniaxial fatigue test specimens were manufactured from two NBG-18 graphite sample blocks. The relationship between natural frequencies of uniaxial test specimens, fatigue life, sample positioning and sample orientation was investigated for different principle stress ratios.

Load ratios $R = -\infty$ and $R = +2$ tested proved to show the highest *r*-values for the Pearson correlation coefficients investigated. However, there was no significant trend found between the natural frequency and the fatigue life.

Keywords: NBG-18 nuclear graphite, hammer impulse excitation, fatigue, natural frequency, relationship

ACKNOWLEDGEMENTS

This dissertation is dedicated to the memory of my mother, Hester Elizabeth Markgraaff.

First of all I would like to thank Prof. Johan Markgraaff and Dr. Johan Roberts of the North-West University for their professional support, interesting discussions and valuable comments.

I would also like to thank:

PBMR (Pty) Ltd for placing the Graphite Fatigue contract on the North-West University, which enabled this effort.

Prof. Danie Hattingh, Dr. Annelize Els-Botes, William Rall and Gideon Gouws from the Automotive Components Test Centre at Nelson Mandela Metropolitan University, who performed the uniaxial tests for me.

My father Philip, brother Armand, Tersia, stepmother Ida and my friends, for all their support encouragement and love.

God, for making everything possible.

TABLE OF CONTENTS PAGE

TABLE OF FIGURES PAGE

LIST OF TABLES PAGE

NOMENCLATURE

AE	Acoustic Emission
ASTM	American Society for Testing and Materials
CAD	Computer-Aided Design
DSP	Digital Signal Processing
EMI	Electromagnetic Induced Interference
FEA	Finite Element Analysis
FFT	Fast Fourier Transform
FRF	Frequency Response Function
HIE	Hammer Impulse Excitation
HTR	High Temperature Gas Cooled Nuclear Reactor
NDT	Non-destructive technique
PBMR	Pebble Bed Modular Reactor
RI	Resonant Inspection
UT	Ultrasonic Testing

LIST OF SYMBOLS

a	Acceleration response function
D	Grip diameter of specimen [mm]
d	Uniform section diameter of the sample [mm]
d	Diameter of the gauge section [mm]
E	Modulus of elasticity [MPa]
F	Input force
F	Axial force [N]
G	Strain gauge factor
H	Transfer function

h	Grip height in collet [mm]
l	Length of rod [mm]
n	Factor of safety
p	Clamping pressure between collet and graphite [MPa]
R	Load ratio
R_c	Shunt resistor value
S_{ut}	Ultimate tensile strength of graphite [MPa]
Ŭ	Angular misalignment angle relative to force line [rad]
ε	Parallel misalignment [mm]
Ů	Simulated strain
μ	Coefficient of friction between graphite and collet material
ρ	Population correlation
σ_{min}	Minimum stress [MPa]
σ_{max}	Maximum stress [MPa]
ν	Poissonôs ratio
ξ	Damping ratio
ω	Angular velocity [rad/s]

CHAPTER 1

1. INTRODUCTION

Graphite is used as moderator and structural material in nuclear reactors. The reactor core of the Pebble Bed Modular Reactor (PBMR) which is presently developed in South Africa by Pebble Bed Modular Reactor (Pty) Ltd. contains graphite core liners that form the boundaries of the annular volume which bounds the fuel pebbles, house the reactivity control mechanisms, and forms the cool gas inlet path and hot gas outlet port of the reactor. Graphite used in nuclear reactors as a material, can withstand temperatures of up to 2800 °C, which is significantly higher than the maximum temperature of 1600 °C that can be attained in a PBMR in extreme conditions. In addition to these structural functions, it also has a nuclear absorption function, which includes absorbing neutrons from the nuclear reaction thereby protecting the steel liner of the reactor pressure vessel from radiation heat and radiation damage.

The PBMR uses carbon spherical fuel elements called pebbles, which are approximately the size of a tennis ball. The pebbles are machined out of graphite. Thousands of uranium fuel particles, enclosed in composite coatings of pyrolytic carbon, silicon carbide and porous carbon are imbedded in a graphite matrix, which are contained within every pebble. The composite coatings (TRISO coatings) shown in Figure 1, which surrounds the uranium fuel particles within each pebble, forms a miniature pressure vessel, that prevents the release of fission products generated during nuclear decay.

During power-up and shutdown commissioning excursion, fatigue stresses are caused in the PBMR reactor core where stresses can lead to the failure of structural components. A reactor core will roughly go through approximately 50 of these cycles through its lifetime. There are also stresses caused by power excursions in transitions of the reactor to facilitate variations in electrical power, which is the result of load following. In order to minimize the probability of such failures the nuclear graphite must be devoid of inherent structural discontinuities. Due to the importance of these

issues a new grade of graphite NBG-18 has been developed by SGL Carbon in conjunction with PBMR, which is claimed to meet international nuclear safety requirements of the material for the graphite core structure. NBG-18 graphite is manufactured using pitch coke, and is vibrationally molded.

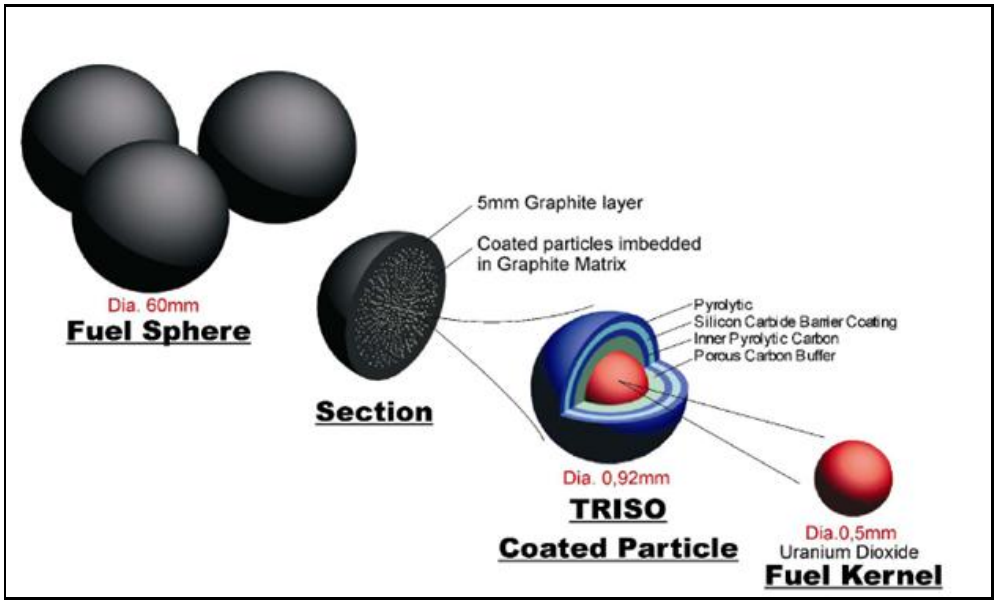

Figure 1: Fuel form (Modified after PBMR 2003)

To assess the structural behaviour of graphite many a test has been performed in the past. Tests methods include tests to determine flexural strength of manufactured carbon and graphite components by using four point loading at room temperature according to ASTM[1] C651 (2005), and methods to determine compressive strength of carbon and graphite carried out according to ASTM C695 (2005) all of which are destructive techniques.

Though the destructive techniques are easy and sometimes relatively inexpensive to perform, these methods lead to waste material and require cumbersome time consuming sample preparations.

To overcome this problem numerous non-destructive testing techniques are available such as sonic resonance, resonant inspection, low and multi-frequency Eddy current analysis, acoustic emission and hammer excitation techniques. In fact a standard method ASTM C747 (2005) based on sonic resonance, to determine the modulus of elasticity and fundamental frequencies of graphite and carbon exist.

According to Hands (1997) resonant inspection can detect cracks, voids, and hardness variations, dimensional variations, bonding problems, misshaped parts and changes in material properties.

Acoustic emission according to Anon (2006:1) is a good technique to monitor and study the mechanical properties of materials by assessing the degree of plastic deformation a material has undergone at different stages of crack propagation. It has also been used to determine degrees of corrosion, friction and mechanical impact mechanisms and leaks in materials and components.

According to Bosomworth (2005) the impulse excitation technique is a very precise and repeatable way to measure the dynamic elastic properties of materials and to detect defects. The hammer impulse excitation technique is said to be one of the easiest methods for this type of application.

1.1 Research Scope

This study outlines non-destructive techniques based on excited vibration to determine fatigue properties of graphite and aims to determine the feasibility of application of the impulse excitation technique to predict the fatigue life of NBG-18 graphite. The dissertation focuses on the application of modal frequency analysis of determined natural frequencies to obtain this objective.

[1]American Society for Testing and Materials (ASTM)

CHAPTER 2

2. REVIEW OF NON-DESTRUCTIVE TECHNIQUES

2.1 Introduction

This chapter conducts a literature survey on the applicability of non-destructive techniques (NDTôs) by reviewing NDTôs such as acoustic emission, ultrasonic testing and impulse excitation techniques in order to gain a better understanding of the relevant practices, and what their advantages and disadvantages entail and to determine their applicability towards the scope of the research.

For many years materials have been examined and inspected, using methods that do not involve the destruction of the material or components. Hughes (1879) discovered and formulated a technique, utilizing eddy-currents to distinguish between genuine and counterfeit coins. Shortly after that Roentgen discovered X-rays and utilized this phenomenon to detect flaws in the barrel of his gun.

Traditionally NDTôs were applied to parts that had already been fabricated to ensure that the finished products did not contain discontinuities, and would perform as originally designed. According to McClung (2007) other techniques developed which involved the examination of materials during processing to ensure that expensive processing of material into shapes would not be wasted due to faulty materials.

NDTôs can be divided into two groups namely volume orientated methods and surface orientated methods. Resonant inspection, acoustic emission, ultrasonic testing and the hammer impulse excitation technique are all volume orientated NDT methods as shown in Figure 2.

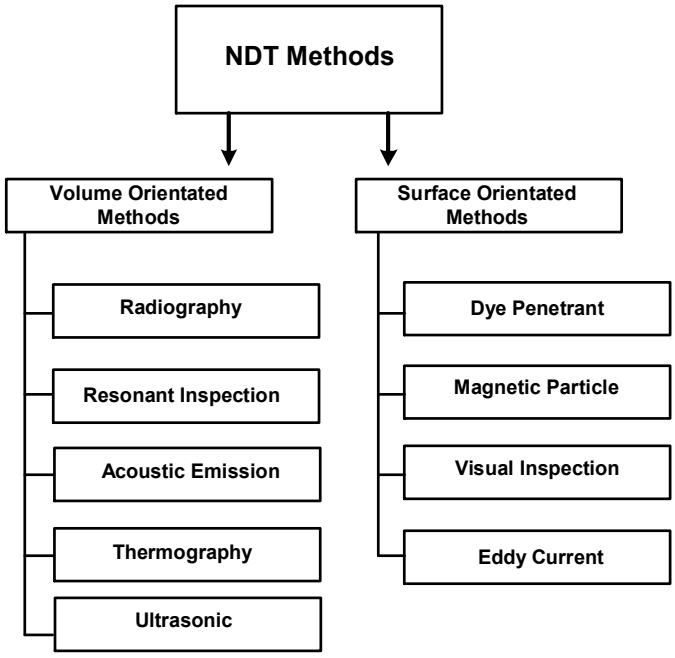

Figure 2: Classification of NDT methods

In order to understand the basic ideas behind volume orientated NDTôs applicable to this research the first part of the chapter explains the basic principles of natural frequency origination. The second part of the chapter is dedicated to resonant inspection, acoustic emission and the hammer impulse excitation technique. The third part of the chapter discusses the use of modal frequency analysis techniques, as a non-destructive tool to characterize and quantify fatigue behaviour of materials.

2.2 Basic Principles

2.2.1 Natural Frequencies

According to (Irvine, 2000) all structures whether it is a building, a bridge or an aircraft wing has at least one or more natural frequencies. A natural frequency can be described as the frequency at which a structure would start to oscillate, when it is disturbed from its position of rest and starts to vibrate freely without the influence of external forces. A vibratory system having *n* degrees of freedom will generally have *n* distinctive natural frequencies of vibration.

2.2.2 Resonance

Resonance according to McMaster (1959) can be explained as a periodic disturbing force applied to a body, causing the amplitude of vibration of the body to approximate that of the disturbing force. When the frequency of the disturbing force approaches a natural frequency of vibration of the body, it causes the amplitude of vibration of the body to increase. The two frequencies become equal and the body reaches indefinitely large amplitude, which is known as resonance.

2.2.3 Modal Analysis

Modal analysis in the context of this research is a process where a structure is described in terms of its dynamic properties, in other words its natural characteristics namely its natural frequency, damping and mode shapes (Avitabile, 1998). Avitabile explains frequency analysis in terms of modes of vibration of a simple freely supported flat plate (Fig. 3), to which a constant force is applied at one of the corners of the plate. The applied force in this case is not a force in a static sense, causing static deformation in the plate, but a force that varies in a sinusoidal manner. The rate of oscillation of frequency of the constant force in this case will be changed, but the peak force will remain the same. The response of the plate due to this excitation is physically measured at one corner of the plate by means of an accelerometer shown in Figure 3.

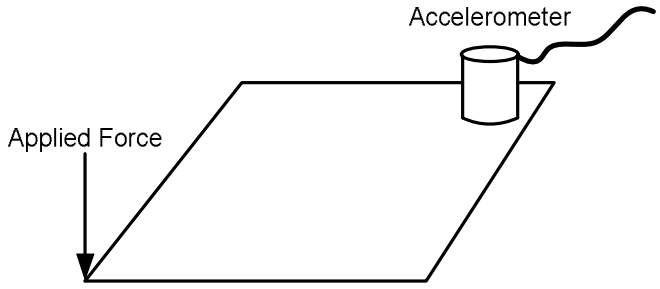

Figure 3: Simple Plate Excitation/Response Model

When measuring the response on the plate, a change occurs in the amplitude as the rate of oscillation of the input force is changed (Fig. 4). An increase and decrease in

amplitude can be noticed as time passes, depending on the rate of oscillation of the constant input force.

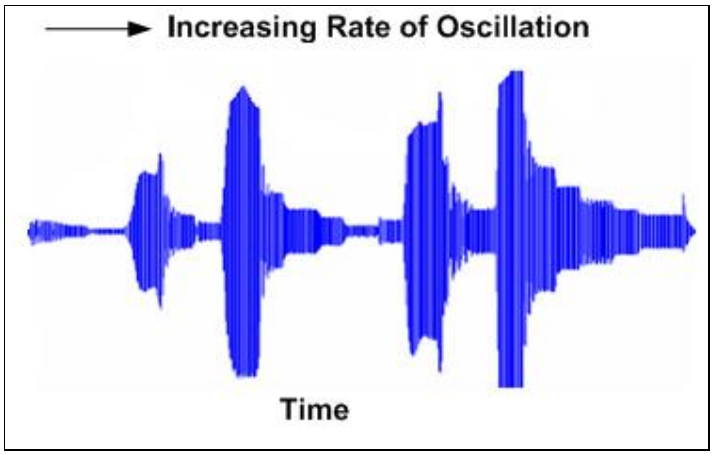

Figure 4: Simple Plate Response (Time Trace)

Thus, the response amplifies when a force is applied with a rate of oscillation that gets closer to the natural or resonant frequency of the system, and it reaches a maximum when the rate of oscillation is at the resonant frequency of the system. Taking this time data and transforming it to the frequency domain using the Fast Fourier Transform (FFT), makes it possible to compute a frequency response function (Fig. 5).

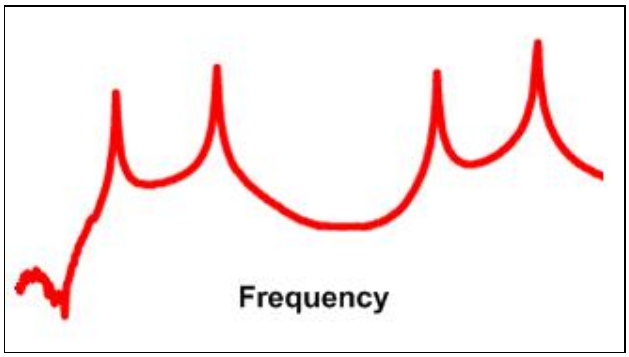

Figure 5: Simple Plate Frequency Response Function (Frequency Trace)

Peaks occur at resonant frequencies in this function, where it can be observed that the time response has a maximum value, which corresponds to the rate of oscillation of the input excitation.

An overlaid plot of the time trace (Fig. 4) and the frequency trace (Fig. 5), indicates that the maximum value of the time trace plot corresponds to the maximum value of the frequency plot. This makes it possible to either use the time trace or the frequency trace to determine the frequencies at which maximum amplitude increases occur.

According to Avitabile (1998)different deformation patterns exist at these natural frequencies in the structure (Fig. 6), which depends on the frequency used for the excitation force.

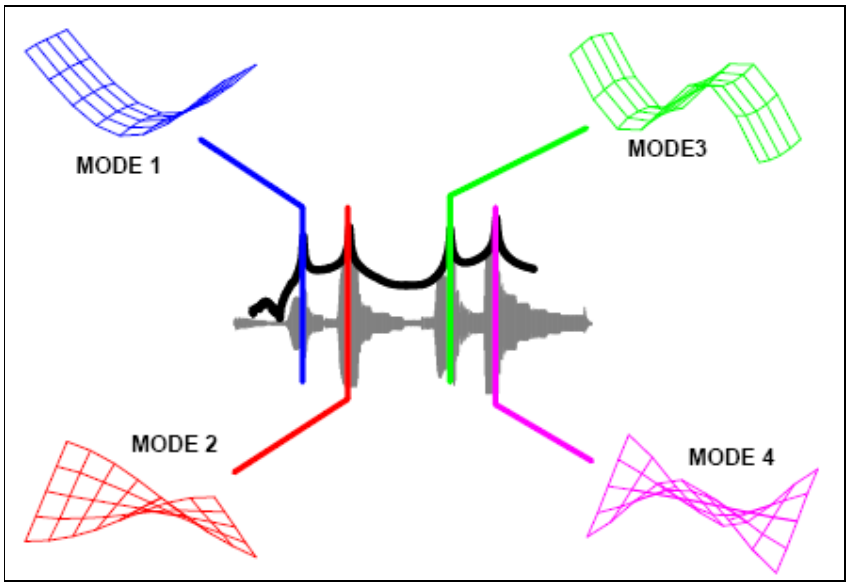

Figure 6: Simple plate sine dwell response

Figure 6 shows the deformation patterns that occur as a result of the excitation coinciding with one of the natural frequencies of the system. At the first natural frequency there is a first bending deformation pattern in the plate, referred to as Mode 1, and at the second natural frequency there is a first twisting deformation pattern in the plate, which is referred to as Mode 2. These deformation shapes are known as the mode shapes or shape factors of the structure. According to McMaster (1959) these shape factors include the geometrical design of the body and the dimensional factors of length, width and thickness. The physical-constants factors include the modulus of elasticity, density and the Poissonôs ratio of the test material. The natural frequency of mechanical vibration of a body is controlled by a number of factors which may be generalized in the following expression according to McMaster (1959):

Natural Frequency = (Shape Factor) x (Physical-constants Factor) (2.1)

2.2.4 Frequency Response Function

A frequency response function (FRF) is a transfer function, which can be used to perform vibration (frequency) analysis according to Irvine (2000).A frequency response function can be explained as the response of a material to an applied force as a function of frequency. The applied force and the response of the structure to the applied force are measured instantaneously according to Avitabile (1998). This response is either given in terms of displacement, velocity or acceleration. A signal process analyzer uses a Fast Fourier Transform (FFT) algorithm to transform the measured time data transformed from the time domain, to the frequency domain.

2.3 Non-Destructive Techniques and its Application on Graphite

2.3.1 Impulse Excitation Techniques

2.3.1.1 Introduction

Impulse Excitation techniques make it possible to determine the dynamic elastic properties of the materials tested. Specimens of the materials possess specific mechanical resonant frequencies, determined by their elastic modulus, mass, and the geometry of the test specimens according to ASTM E 1876-01 (2002).

Assuming that the specimen to be tested is vibrating freely, with no noticeable restraints, impulse excitation methods measure the resonant frequency of a specific geometry by exciting the specimen mechanically. Resulting mechanical vibrations is then picked up by a transducer (in other cases by an accelerometer) which transforms them into electrical signals. By varying the type of support and the impulse locations, different modes of transient vibrations are obtained. Signals are then analysed and

measured by isolating the resonant frequency of the signal analyzer, providing a reading which is either the frequency or the period of vibration of the specimen.

According to ASTM E 1876-01 (2002), the Youngôs modulus, the dynamic shear modulus and Poissonôs ratio can then be calculated by measuring the fundamental frequencies, the dimensions and the mass (or density) of the specimen.

The standard ASTM E 1876-01 (2002) test method is used for numerous applications like the development and characterization of materials, the generation of design data and for material integrity control purposes.

2.3.1.2 Applicability to Graphite

Modal testing by means of impulse excitation methods has been shown to have the potential to be a fast and accurate approach not only for characterization of material intrinsic properties, but for inspection and quality control as well.

Gibson (1999) showed that modal testing in either a single mode or multiple modes of vibration can be used to determine elastic moduli and damping factors. The test method ASTM C 747 (1993) covers the measurement of the fundamental transverse, longitudinal, and torsional frequencies of isotropic and anisotropic carbon and graphite materials. These measured resonant frequencies can be used to calculate dynamic elastic moduli for any grain orientations. The resonant frequency can be explained as a natural vibration frequency which is determined by the elastic moduli, density, and dimensions of the test specimen. Dynamic methods of determining the elastic moduli are based on the measurement of the fundamental resonant frequencies of a slender rod of circular or rectangular cross section. The resonant frequencies are related to the specimen dimensions and material properties.

Pardini *et al*. (2005) conducted modal analysis techniques to obtain the damping factor (ɜ) as well as the modulus of elasticity of two kinds of synthetic graphiteôs. The author and his colleagues machined graphite samples to nominal dimensions 11 x 11 X 250 mm, and tested in the vertical position (Z-direction) with a free-free boundary

condition by using two elastic strings at each extremity of the test specimens. This configuration was adopted after an extensive series of preliminary experiments was carried out. The experimental modal analysis was carried out by exciting the structure with an instrumented hammer. The hammer had a sensibility of 0.18 mV/N and its plastic tip was chosen in order to generate a well-defined spectrum in the frequency band from 0-5kHz. The results obtained were compared to numerical solutions of the problem using the finite element code ANSYS. In the simulations it was possible to obtain the natural frequencies and the modes of vibration. The spectral parameters were analysed and compared with the results obtained experimentally. The first four modes of vibration were taken into account in the study and an equation that could estimate the modulus of elasticity was proposed.

2.3.2 Acoustic Emission

2.3.2.1 Introduction

Acoustic Emission (AE), according to ASTM E 610-82 (2005) refers to the generation of transient elastic waves within a material, during the rapid release of energy from local sources within the material. According to Tuncel (2008:2) the temporary transient waves are created by the localized sources that occur in a state of stress. In metals the sources of these emissions are dislocation movement which accompanies plastic deformation and the initiation and extension of cracks in structures under stress.

Basic principles of acoustic emission according to Borum *et al*. (2006:7) imply that when a load is applied to a structure, it will begin to deform elastically, which is associated with changes in the structureôs stress distribution and the storage of elastic energy. With a further increase in the load, permanent microscopic deformation occurs, together with a release of the stored energy in the form of propagating elastic waves termed ñAcoustic Emissionsò. Sensors are coupled to the relevant structures by means of fluid coupling and are secured with adhesive bonds, tape or magnetic hold downs. Piezoelectric sensors outputs are amplified through a low noise preamplifier

and are then filtered to remove any extraneous noise and finally processing by suitable electronic equipment.

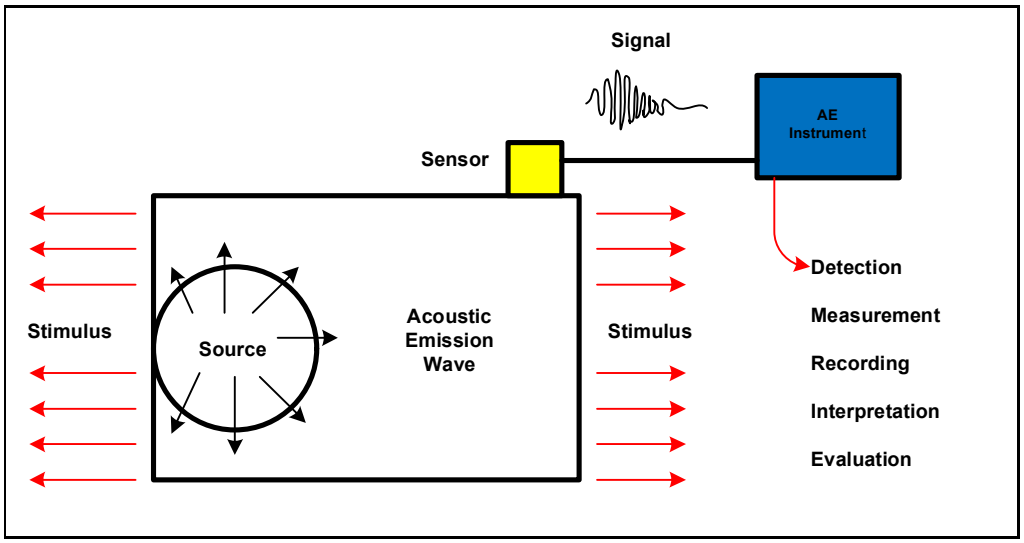

Figure 7: A Typical Acoustic Emission system

Melting, phase transformation, thermal stresses, cool down cracking and stress build-up can also be a source of AE. Above a certain level, these emissions can be detected and converted to voltage signals by piezoelectric transducers which are mounted on the surface of the structure.

Applications of AE in the laboratory can include the study of deformation, fracture and corrosion. It makes it possible to give an immediate indication of the response and behaviour of a material under stress, by being intimately connected with the materials strength, damage and failure.

Advantages of AE compared to conventional inspection methods include early and rapid detection of defects, flaws, cracks etc. The method records in real time and thus offers the possibility of on-line inspection which is a major advantage for monitoring and studying the initiation and growth of cracks, thus making AE an excellent means of observing indirectly microscopic processes that occur during deformation which is associated with micro cracking.

AE can also result in considerable reduction in plant maintenance costs, while at the same time increasing the available information about plant integrity. Another major advantage of AE is that it does not require access to the whole examination area, thus making the costs significantly less than with conventional NDT methods.

Although AE is a good technique to monitor and to study the mechanical properties of materials, the implementation of the technique is expensive when considering the testing of small components. AE is also very a time consuming process due to the fact that the relevant components has to be under some kind of stress situation in order for AE to occur, and thus have to be monitored continuously.

2.3.2.2 Applicability to Graphite

Countless AE tests have been performed on nuclear graphite samples under compression, tension and flexure loading to examine the deformation behaviour of graphite.

A substantial amount of AE occur during stressing of graphite (Neighbour *et al*., 1991) i.e. Burchell *et al*. (1985) measured flexural loading of several graphiteôs and found a near exponential growth in cumulative events from zero load to failure. Neighbour *et al*. (1991) presented an analysis of acoustic emission from samples of nuclear graphite IMI-24 that was subjected to three consecutive loads-unload cycles to, 5, 10 and 15 MPa in tension, compression and flexure. IMI-24 was used as the moderator in the British Advanced Gas-Cooled (AGR) nuclear reactors. IMI-24 is a polygranular, isotropic, molded graphite. AE was detected at the surface of stressed materials by a piezoelectric transducer. A wideband transducer with a frequency response of 0.1 to 1.1 MHz was coupled to the sample with petroleum jelly. The obtained signal was passed through a 60 dB pre-amplifier to an AE analyzer with a 25-channel amplitude sorter and ring down counter. The AE data was analysed by considering the cumulative number of AE events. An AE event can be defined in terms of the instrument threshold and a fixed deadtime of 100 µs. If the time that has elapsed since the last threshold crossing is greater than the deadtime, the next threshold crossing defines the beginning of a new event. The author and his

colleagues found that on the first cycle that cumulative acoustic emissions events in all loading modes increased progressively from zero stress. However it was observed that in subsequent cycles, acoustic emission recurred at stresses approaching but less than the previous stresses (i.e. a Felicity effect was observed in place of a Kaiser effect). A new parameter, the Recovery ratio B was proposed for characterizing the pattern of acoustic emission on cyclic loading of graphiteøs, and the exploration of the utility of AE method for determining residual stresses in nuclear graphiteøs.

Ioka *et al*. (1989) examined continuous-type AE from nuclear ï grade graphite under compressive loading in order to better understand the deformation behaviour of the graphite. The material used was fine grain size isotropic graphite, IG-11, manufactured by Toyo Tanso Co. Ltd., and was a candidate for the core structural material in a high temperature gas-cooled reactor (HTGR). An increase in strain in the initial stage of loading caused an increase in the AE for the graphite followed by a decreasing behaviour for further loading to the failure point. They proposed a model to explain qualitatively the phenomenon which was based on dislocation piled up at grain boundaries. Oxidized specimens were prepared to clarify the back stress effect at grain boundaries. AE for the oxidized specimens increased monotonically up to the point of failure, and a model was proposed which was supported by experimental results. A burst-type AE was observed due to some micro fractures in the graphite under external loading. A Qualitative relationship of total plastic strain rates by slip deformation and by micro cracking as a function of total strain was given from the AE behaviour, although the quantitative relationships of the graphite could not be determined under compressive loading.

2.3.3 Ultrasonic Testing

2.3.3.1 Introduction

Ultrasonic testing has been shown to be applicable to porous ceramics, including graphite materials and is used to evaluate the inner porous conditions. Ultrasonic waves are propagated into the body through interactions with a number of pores. These wave propagation characteristics in graphite are affected by the inner porous

conditions such as the porosity and pore size, which are changed by oxidation. The propagation characteristics are then analysed by statistical methods with cumulating of the time delay and the collision probability.

2.3.3.2 Applicability to Graphite

Ultrasonic testing (UT) as a non-destructive technique is applicable to porous ceramic materials including graphite according to *Ishihara et al*. (1995). Takatsubo *et al*. (1994) states that porous conditions in a porous body can be estimated by conducting an analysis on the UT signals, since the wave propagation signals in them depend highly upon their inner porous conditions. Shibata *et al.* (2001) showed that a wave propagation model which takes into account wave-pore interaction process is applicable to graphite in order to estimate inner porous condition changes caused by oxidation.

Shibata *et al.* (1999) developed an ultrasonic wave propagation model for the pulse-echo technique in which both diffusion and scattering losses could be treated as important factors of ultrasonic wave attenuation. This model was demonstrated by experimental data on ultrasonic signal characteristics of nuclear graphite. The authors proposed as an application of the model a new approach combining UT signals with fracture mechanics, to evaluate the mechanical strength of porous ceramics from the UT signal. Shibata *et al.* (2001) analyzed the wave propagation characteristics in the porous body by means of a propagation model which took account of wave-pore interaction process. The model assumes that spherical pores with radius r are located homogeneously throughout the body. When a wave then comes into collision with a pore as shown in Figure 8 it will go forward creeping through the pore edge with some probability as shown in the figure. There then exists a time delay between the creeping wave and the direct wave without collision.

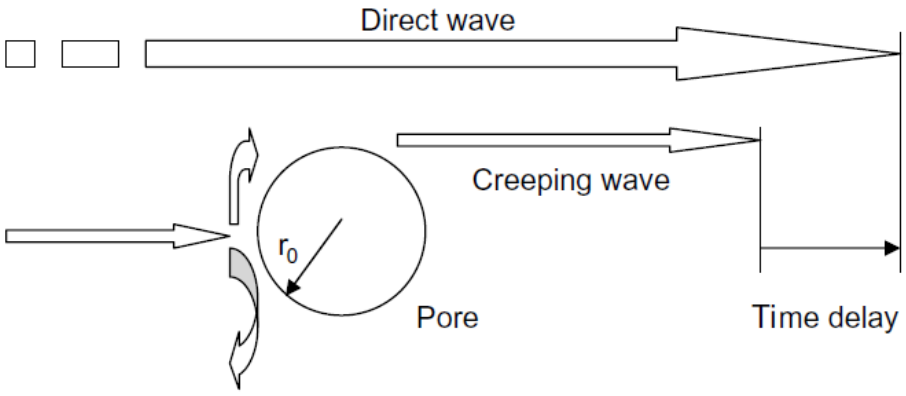

Figure 8: Wave-pore interaction model for propagation analysis (Modified after Shibata *et al.*, 2008)

Ultrasonic waves propagate through the body by interacting with a great number of pores. Propagation characteristics obtained are analyzed by statistical methods with cumulating of the time delay and collision probabilities. The propagated waveforms can then be expressed by Gaussian function with a height of *H* as follows according to Takatsubo *et al*. (1994):

$$H = 1/(t_w\sqrt{2\pi}), \tag{1}$$

$$t_w = \left[3\emptyset rL\left\{1-\pi(4\pi/3\emptyset)^{-2/3}\right\}\right]^{1/2} \times \left(\frac{\pi\beta}{\alpha}-2\right)/(4V_i), \tag{2}$$

$$\alpha = V_c/V_p, \tag{3}$$

$$\beta = 4L_p/(2\pi r), \tag{4}$$

Where L is the propagation length, V_i a sound velocity in an ideal polycrystals without pore, $\emptyset$ porosity, V_c and V_p respectively velocities of the creeping and direct waves and $4L_p$ a perimeter of the pore. Due to the result of this propagation analysis, the Youngôs modulus E of the porous body is evaluated as a normalized value by that of the ideal polycrystals E_i according to Takatsubo *et al*. (1994).

$$\frac{E}{E_i} = (1-\emptyset)/\left\{1+3\emptyset\left(\frac{\alpha\beta}{\alpha}-2\right)/8\right\}^2, \tag{5}$$

It was shown by Shibata *et al.* (2001) that the above propagation model is applicable to fine grained isotropic graphite, IG-110 in un-oxidized conditions. The authors calculated the porosity of IG-110 from its apparent volume density and the theoretical

density. However, for analysis of oxidized graphite the value is varied according to the oxidized conditions to take pore shape change in consideration. Thus, the authors developed a new analytical method by the ultrasonic wave propagation characteristics to evaluate the oxidation damage on the graphite components in the HTGR reactors in neutron irradiated conditions. In the end they concluded that the developed method shows promise to evaluate the oxidation damage on graphite components in HTGR reactors by means of a non-destructive way.

Ooka *et al.* (1993) applied UT to confirm structural integrity of core internal blocks as an acceptance test in the HTTR, a gas-cooled and graphite-moderated test reactor with thermal output of 30 MW and a coolant outlet temperature of 950°C at the maximum operating condition (Saito et al., 1994).

Shibata *et al.* (2008) investigated the applicability of the micro-indentation technique and ultrasonic wave methods to evaluate the degradation of graphite components of fine-grained isotropic graphiteôs of IG-110 and IG-430, candidate grades in the VHTR reactor. They found that micro-indentation behaviour was changed by applying the compressive strain on the graphite, and suggested that the residual stress could be measured directly, and that the change of ultrasonic wave velocity with 1 MHz by the uniform oxidation could be evaluated by the wave-propagation analysis with wave-pore interaction model. They tried to apply this combined approach to the acceptance test and the in-service inspection conditions of graphite components in the High temperature Test Reactor (HTTR). The authors concluded that the combined approach would be able to estimate the strength of graphite components under both un-oxidized and oxidized conditions and would so be applicable to both acceptance test and in-service inspection of graphite components.

2.4 Prediction of Fatigue Life using Modal Frequency Analysis

Countless research papers and articles speak of work that has been done on the prediction of fatigue life of different components ranging from welded joints to aircraft structural components, using different methods such as fracture mechanic theories and finite element analysis, which are mainly based on destructive testing. These methods are however considered approximate for they do not include all of the factors affecting fatigue life, which leads to a growing demand for a non-destructive test that can predict the fatigue life and overcome the problem of variability of results associated with destructive techniques.

Bishop *et al* (1963) states that experimental modal frequency analysis when used as a non-destructive tool helps to determine the reliability and integrity of machine components, by using the theory of resonance testing. Damir *et al* (2005) state that a huge amount of work has been performed on damage detection and identification by using modal parameters such as natural frequency, modal damping and mode shapes, for the simple reason that modal parameters are, by definition according to McNaughton (2002) functions of physical properties such as mass, stiffness or modulus of elasticity and hence of mechanical properties.

Doebling *et al.* (1996) examined changes in measured structural vibration and/or modal parameters by presenting a review of technical literature concerning the detection, location and characterization of structural damage. Owalbi *et al.* (2003) was able to detect structural damages such as the presence of cracks together with their location and size in beams, based on changes in natural frequencies and frequency response functions (FRFôs). They observed that the amplitude of bending modes of vibration increased as crack growth increased, which caused a decrease in natural frequency.

Tobgy (2002) investigated the ability of modal testing to estimate the fatigue life of standard fatigue specimens made of brass. He was able to do this by introducing random notches in brass specimens to achieve variability in the fatigue life of the specimens, and found that there is a correlation between fatigue life and corresponding modal parameters of each specimen.

Bedewi *et al.* (1997) investigated and correlated changes in modal parameters such as natural frequencies and damping ratios to fatigue failure life for selected graphite/epoxy composite specimens. They established this by monitoring the decrease in natural frequency and the increase in damping ratio as a function of number of cycles to failure to be able to predict the fatigue failure life.

Kessler *et al.*(2002) investigated the feasibility of modal analysis as a non-destructive tool in detecting damage in graphite/epoxy panels containing damage modes. By performing modal analysis together with a finite element model, they found strong correspondence between the extent of damage (or local stiffness) loss and reduction in natural frequency.

Damir *et al* (2005) investigated the feasibility of using experimental modal analysis, as a non-destructive means, to try to characterize and quantify the fatigue behaviour of grey and ductile cast iron. He investigated the response of modal parameters like natural frequencies, damping ratio, frequency response function (FRF) magnitude to variations in the microstructure of grey and ductile austempered cast iron, as a main factor affecting the fatigue life of the materials. His main objective was to find a correlation between the modal parameters and fatigue behaviour of the materials. In order to do this he conducted modal tests on standard specimens manufactured from grey and ductile austempered cast iron to extract the corresponding modal parameters. He conducted these tests on specimens of ductile cast iron and grey cast iron to check if modal parameters have the ability to respond to variations of microstructure constituents, that has an effect on the fatigue behaviour of the components. The microstructure variation between ductile cast iron and grey cast iron are due to the difference in graphite shape, which is nodular in ductile cast iron and flake type in grey cast iron. Mechanical properties of cast iron and more specifically its fatigue resistance are greatly affected by the graphite shape according to Anon (2001).

Damir *et al* (2005)performed rotating bending fatigue tests on the specimens to try and correlate modal parameters to fatigue behaviour. This enabled them to evaluate the ability of modal testing to predict the fatigue life of mechanical components.

The metallurgical characteristics like the microstructure of a material play a very important role in determining how a material will react to mechanical properties like fatigue behaviour of the material. Thus, the ability of measured modal parameters to respond to any change introduced in the microstructure of the material would give an indication of the ability of modal parameters to express the fatigue behaviour of mechanical components. Damir *et al* (2005) studied the response of modal parameters to changes occurred in microstructure of austempered ductile cast iron as a factor affecting the fatigue life of the material. He states that experimental modal analysis has proved to show great promise for fatigue evaluation and characterization for mechanical components. From his experimental work he found that material effective damping ratio (ε) showed the most noticeable response to changes in fatigue life and material hardness between the austempered ductile cast iron and grey cast iron and within each family tested. Also, for austempered ductile cast iron, the fatigue behaviour of the material is improved by the increase of the damping ratio. He concluded that these results obtained indicate the capability of modal testing, as a non-destructive tool, to characterize and quantify the fatigue life of grey and ductile cast iron, and that a high damping ratio corresponds to low hardness and higher fatigue life.

2.5 Review of the Fatigue Behaviour of Graphite

2.5.1 Introduction

Graphite in its natural form is an allotropic form of the element carbon which shows a well-developed layered structure, stacked parallel to each other in the sequence ABABé , in which the atoms are hexagonally arranged and forms the so called basal planes[5,9], as shown schematically in Figure 9.

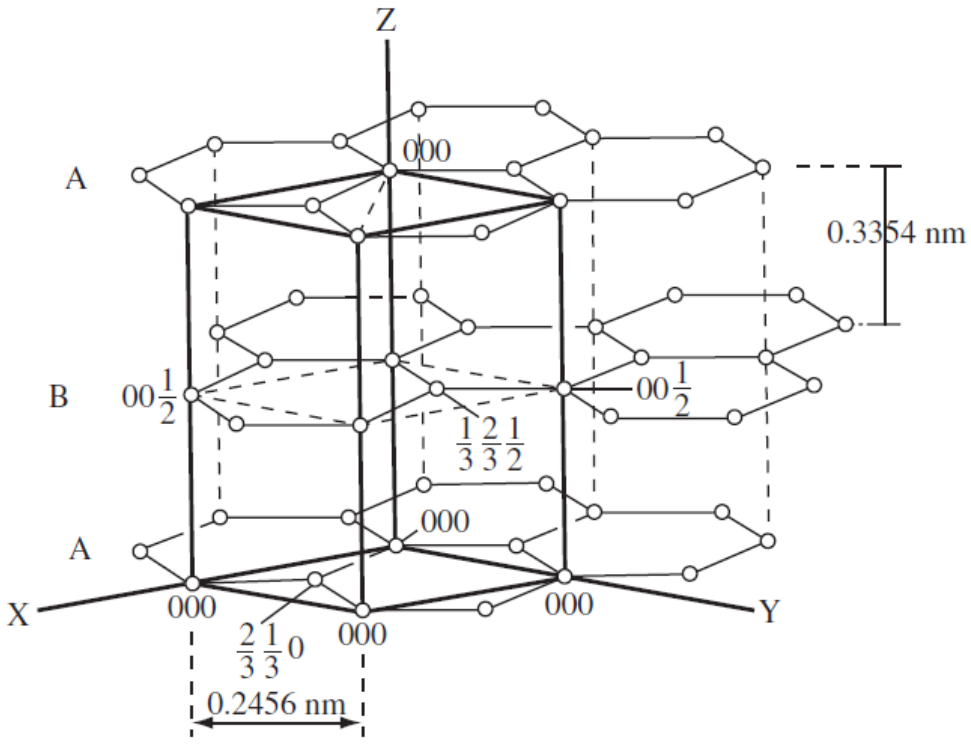

Figure 9: Representation of an ideal lattice of graphite

Natural graphite is anisotropic due to chemical bonds within graphite layers that are covalent and chemical bonds between layers that are weak forces of Van Der Waals. It shows higher strength and stiffness in basal planes and poor mechanical behaviour perpendicularly to the basal planes. Synthetic graphiteôs on the other hand which are particulate composites, shows a smaller degree of discrepancy among the mechanical properties, and thus macroscopically exhibit a mechanical behaviour closer to the isotropic. Synthetic graphiteôs are obtained from a mixture of coke and pitch binder, with small amounts of natural graphite, and is subjected to a series of thermal and mechanical treatments that ends with a graphitization process at a temperature of approximately 3000 ęC according to Friedrich *et al* (2002). Although the mechanical properties of graphite at approximately 20 ęC can only be considered moderate, graphiteôs can maintain these properties up to temperatures of about 2000 ęC in the absence of an oxidising atmosphere according to Polidoro (1987). Graphiteôs are classified according to the raw materials, as coarse, medium or fine grain, and are either processed by extruded or moulded techniques.

2.5.2 Morphology and Fracture Characteristics of Graphite

As mentioned above graphite formed body is graphitized by exposing it to temperatures in excess of 3000 ęC. Crack and void formation is a direct result of graphitization and varies within the volume of the billet. Cracks originate during the cool down period in the manufacturing process because of the existence of different thermal expansion coefficients of the a- and c-axis of graphiteôs hexagonal lattice structure. A void volume of between 10 and 25% exists in graphite. Different grades of graphite show widely different textures and pore-size distributions and also the presence of subcritical cracklike formations. These cracklike porosities can range from being fairly planar to having an ñonionò skin appearance according to Pardini *et al* (2005).

Pears *et al* (1970) identified two classes of defects, namely background and disparate. Background defects are small relative to the size of the filler particles and are also uniformly distributed. Background defects can include small blowholes, micro cracks, locations of weak cleavage within filler particles, shrinkage cracks and cavities, and small gas pockets (connected or unconnected porosity) within the binder residue. These defects are ever present. Disparate defects on the other hand are much larger than background defects and are most commonly blowholes, which may be elongated defects created during extrusion and may also be macro cracks formed by a variety of processes involving gas entrapment. Other possible disparate defects can include regions of binder deficiency, where cohesion between filler particles is poor, inclusions usually refractory metal carbides, spongy regions of excess binder, voids left by vaporization of inclusions and ñreorganizedò graphite, where an impurity produced a region of ordered graphite unlike that of the filler and binder residue. It is possible to manufacture graphite with different average grain sizes. Fine grained material has grains smaller than 100 µm, and superfine, ultrafine, and micro fine has sizes smaller than 50 µm, 10 µm and 2 µm respectfully, medium-grained smaller than 4 mm and coarse-grained material has grains larger than 4 mm. Nuclear graphiteôs has typical grain sizes ranging from medium to ultrafine grains. Manufactured graphite is either molded or extruded which gives the resulting grain structure a biased orientation. Material properties are often measured with the grain (parallel to the extrusion direction and perpendicular to the molding axis) or against the grain

(perpendicular to the extrusion direction and parallel to the molding axis). Thus, graphite strength is anisotropic (transversely isotropic), where newer grades tend to be more isotropic (within 10% or even less), which is a desirable property. Graphite strength increases with increase in temperature (in a non-oxidizing environment) up to 2500 ęC and there exists a high resistance to thermal shock. Graphite is similar to other brittle materials and it does not exhibit plastic deformation and thus shows a wide scatter in strength. Where it does differ from other brittle materials is that it can have nonlinear stress-strain response and large amounts of acoustic emission (damage accumulation from micro cracking) prior to rupture. This behavior is referred to as quasi-brittle behavior. Strain in graphite is a few tenths of 1% in tension and 1-2% in compression, making it considerably stronger in compression than in tension. In nuclear graphite the compression strength is usually 3 to 4 times the tensile strength.

General Atomics (1988 for H-451) reported that bulk graphite tends to be weak in tension, with strength in the order of 11-15 MPa, depending on whether it is measured against the grain or with the grain and poses a low fracture toughness. To explain the fracture of graphite, can be a complex process, for different grades of graphite potentially have different failure behaviors. Fracture is influenced by pre-existing flaws or inherently weak regions in the material, which makes graphite brittle or quasi-brittle, with little or no plasticity prior to failure. Porosity is another factor, which can be important in the fracture process. Cracking can be initiated or the crack path can be influenced by stress concentrations at or very near pores, and so the crack path can be arrested at a pore until a higher stress is applied. Tensile fractures are caused by local concentrations of micro cracks that develop and join together to form a macro crack of critical size.

Tucker et al (1993) reported that crack growth tends to be transgranular (through the grain) and that the crack path within the individual grain corresponds to the crystallite cleavage plane according to Jenkins (1962) and Knibbs (1967). Thus the ultimate fracture path tends to extend from one large defect to another. Micro cracks that form early usually do not propagate directly to fracture, and fractography of fracture surfaces has usually not located the earliest initiating flaws. However in other brittle materials like ceramics and glasses it has been reported by Quinn (2007) that the science and art of fractography can often trace the source of fracture in a specimen or

component to a single originating flaw. Moreover these originating flaws can be caused by individual pores, porous regions, and agglomerates, compositional in homogeneities, inclusions, and large gains, cracks, machining damage, handling damage, surface pits, surface pores, or damage or chipping along sharp corners. These flaw populations or flaw types are very broadly classified either as, volume-distributed, surface-distributed, or edge-distributed and are considered to be separate and competing failure modes.

Nemeth (2003) suggests that when the probability of a component surviving loading is evaluated, it is performed as a function of either the component volume or the component surface, or even the component edges and that this is referred to as volume-flaw reliability analysis or surface-flaw reliability analysis. In graphite, the failure process of the material is usually considered to be a function of the material volume, and therefore the reliability analysis is performed over the volume of the component, assuming that the identity and location of the earliest originating flaws usually cannot be established and because the subsequent growth and accumulation of damage through micro cracking can be diffusely distributed within the material volume (at least for uniaxial tension) prior to a final assessment of damage and formation of macro crack. It is expected that under flexural loading surface flaws would play some role in the fracture of the material, however the role that surface flaws may play in the fracture if graphite is not clearly established. Nemeth (2009) states that literature can be found of any studies that examine the strength of nuclear-grade graphite flexural specimens as a function of the grit size of the abrasive that was used to grind the specimen surface. This may be due to that the size of exposed pores on the specimen surface is often larger than the grit size of the abrasive, making characterization of surface roughness from the grinding process pointless and indicating that the size of surface pores, rather than the damage which is caused during the grinding process, will control the strength response in flexure.

2.6 Conclusions and Research Aim

Acoustic emission (AE), ultrasonic testing and impulse excitation techniques were evaluated and their advantages and disadvantages and applicability to graphite were considered.

AE was found to be a passive method for in situ monitoring of the response of a material to an applied load, ensuring a 100% volumetric control. AE technique is not depended on direction, as the emitting source radiate the energy in every direction. AE is sensitive to defect growth and changes in the material rather than to static presence of defects. AE technique can be applied only if the material is adequately stressed i.e. if plastic deformation, gliding processes (dislocation movement), crack formation and growth or fracture phenomena etc. occur.

Ultrasonic testing was found to be a valuable method to evaluate the inner porous conditions of graphite, such as the porosity and pore size, which are changed by oxidation. Interrogation of a test specimen by ultrasonic pulses yields information relating to material properties and specimen dimension.

It was decided to use the Hammer Impulse Excitation technique, which falls under the category of RI techniques to determine the natural frequency of NBG-18 graphite. This decision was based upon reason that AE requires a localized source within the material to generate a stress situation in order to emit ñacoustic emissionsò. This is not in-line with the test objectives which requires the determination of the natural frequency of graphite, without subjecting the material to any stress situation.

The aim of the study evolved to apply the HIE technique to determine fatigue life of NBG-18 graphite from natural modal frequencies.

In order to be able to determine if modal frequency parameters can be correlated with fatigue life, a suitable uniaxial fatigue test specimen geometry needed to be obtained.

CHAPTER 3

3. SPECIMEN SAMPLING

3.1 Introduction

NBG-18 graphite blocks are manufactured by SGL Carbon, and are vibrationally molded, which results in an almost homogeneous material containing an isotropic, pitch coke and low ash content. (See detail of process presented in **Appendix F**). The material has the following properties:

- Mass Density 1873.24 kg/m^3
- Modulus of Elasticity 11.9 GPa
- Poisson's Ratio 0.21
- Shear Modulus of Elasticity 4917.4 N/mm^2
- Thermal Coefficient of Expansion 4.54e-6 1/°C

3.2 NBG-18 Specimen Cutting Plan

The SGL graphite blocks used for this research had nominal dimensions of 2000 mm x 500 mm x 540 mm in the X, Y and Z directions as shown in Figure 10 and Figure 11 respectively. The direction of vibration during manufacturing is in the Z-direction, causing any preferred grain orientation to be in the XY-plain. Only two axis orientations were used for the alignment of the uniaxial specimens, namely the Z-axis and X-axis orientations. Alignment with the Z-axis is expected to yield worst results strength wise, since the coke particles tend to align perpendicular to the direction of compaction of the block during manufacturing. If the graphite is anisotropic, alignment of the uniaxial specimens with the X-axis is expected to yield better results strength wise, since the X-orientation is parallel to the grain direction of the material.

Due to the reasons presented, a specimen cutting plan was generated from which two-hundred and sixty-five uniaxial specimens were manufactured out of the two separate blocks of unirradiated NBG-18 graphite. The orientation of the specimens taken from the blocks were chosen in such a manner that an even amount of specimens were orientated in the preferred orientation of the coke particles (grain orientation) referred to as parallel-to-grain, and an even amount in the perpendicular-to-grain direction. The cutting plan ensured that a similar ratio of centre and edge, and near-centre and near-edge specimens were taken from the two separate blocks of graphite. The cutting plan further presents the maximum variation in test results, expected in the blocks of SGL graphite used for the purpose of this research.

The specimens were cut from two NBG-18 blocks and represented by the small red cylinders shown in Figure 10 and Figure 11. The blocks were numbered as block Q20 5087260 and block Q20 5087261. Detail of the cutting plan is presented in **Appendix A**.

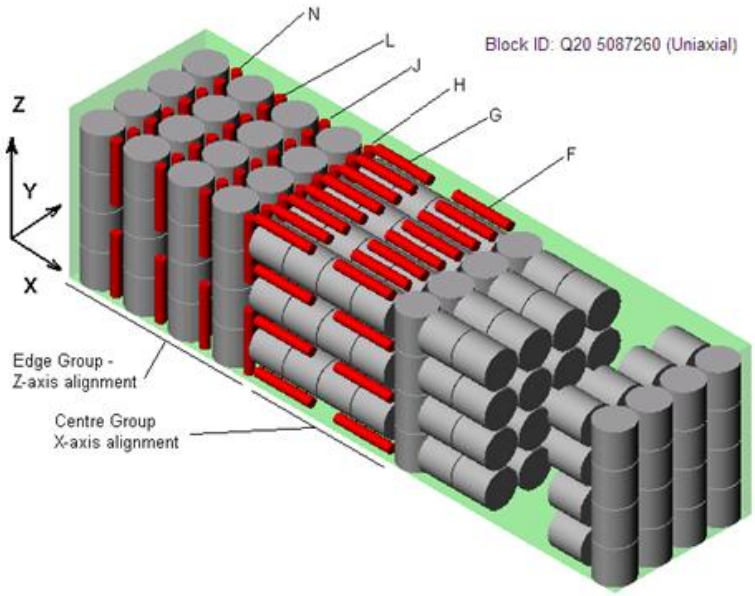

Figure 10: NBG-18 graphite block Q 20 5087260

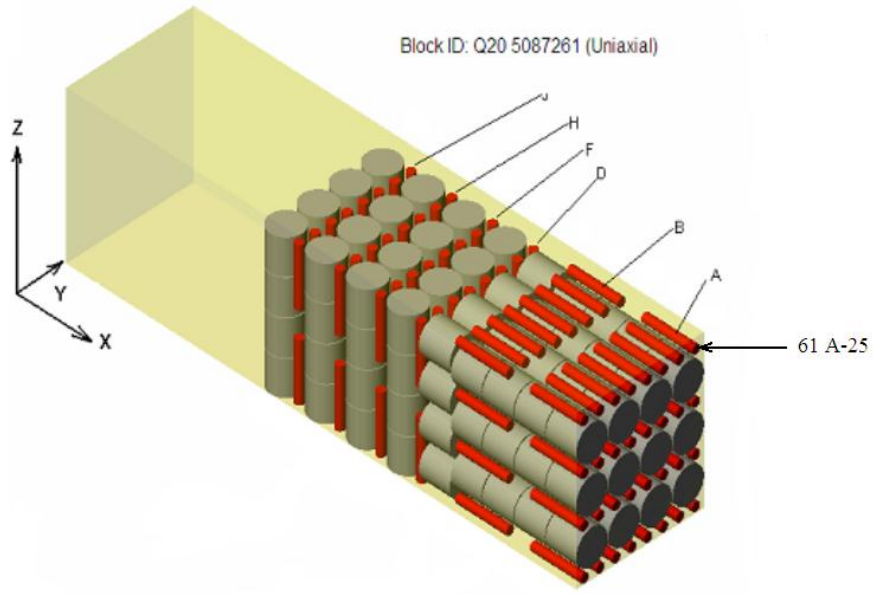

Figure 11: NBG-18 graphite block Q 20 5087261

Specimens were assigned serial numbers with the following numbering structure:

XX Y-Z

Where:

XX	ſ	Last two numbers of the Block Identity Number (60 or 61)
Y	ſ	Section plane in Cut Layout Drawings (A, B, D, F, G, H, J, L or N)
Z	ſ	Serial Number within section plane as shown on drawings (1, 2, 3 ext.)

Specimen 61 A-25 is an example of an assigned specimen shown in Figure 11. Where serial numbers XX, represent block 61, serial number Y represents the section plane A and serial number Z represents the specimen number 25.

3.3 Specimen Geometry Design

Uniaxial specimens for use in the planned frequency response and fatigue test experiments were manufactured to a design of Roberts (2007: 2-10). Roberts (2007:4-8) evaluated the design and geometry of several published uniaxial fatigue test specimens, and chose the geometry shown in Figure 12 because of its applicability to the KTA-3232 failure criterion[1]. The criterion states that the probability of failure of

graphite is dependent on the volume weighted stress in the material. With this rule serving as background the design of the specimens were based on the geometry of a metallic axial fatigue specimen which features a circular cross section and tangentially blended fillets according to ASTM E 466-96 (2002), which specifies the standard practice methodology for conducting force controlled constant amplitude axial fatigue tests of metallic materials.

A generic requirement for the design of the specimen geometry, according to ASTM C749-92 (2005) was that the minimum thickness of the gauge section should be approximately 5 x the maximum grain size of the material. ASTM C749-92 which specifies the standard geometry of static tensile strength testing of graphite required that the minimum thickness of the gauge section had to fall between 3 and 5 times the maximum grain size. The average and maximum grain size of the vibrationally molded graphite was 0.7 and 1.6 mm respectively according to SGL Carbon. The specimens had the following geometry specifications:

- Diameter of the gauge section: 13 mm
- Diameter of the area of grip 26 mm
- Length of the area of grip 26.6 mm
- Tangent fillet radius 105 mm
- Length of whole specimen 150 mm

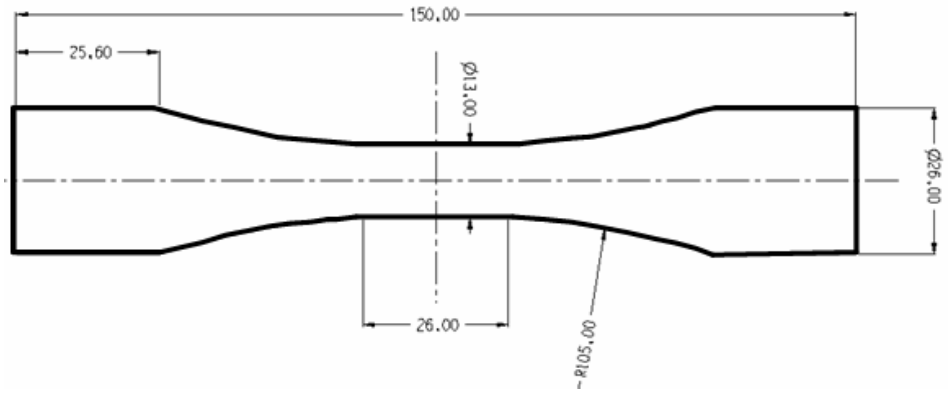

Figure 12: Uniaxial Graphite Test Specimen

[1]The design of the HTR of the PBMR is done according to the KTA 3232 design rule (Schmidt, 2003). Detail on this rule is presented in **Appendix G**.

CHAPTER 4

4. EXPERIMENTAL MODAL TESTING

4.1 Introduction

This chapter deals with considerations related to the practical implementation of the modal frequency analysis procedure in testing graphite. Strategies are discussed, then the experiences obtained from performing the experimental procedures are outlined which eventually leads to the formulation of the recommended practice.

4.2 Test Procedure

The specimen was placed on a sponge, in order to simulate a no-constraints, free-free test situation to generate the natural resonant frequencies of the specimen. The specimen was excited by hitting it once at the position indicated on Figure 13 with an impulse hammer. Induced vibrations caused by the hammer blow were captured by one uniaxial accelerometer, mounted on the opposite end of the hammer impact zone. The accelerometer detected the frequency response, from which the necessary Frequency Response Functions (FRFôs) were acquired, and on which a Fast Fourier Transform (FFT) was applied by using a FFT analyzer. Two-hundred and fifty-six specimens were subjected to this procedure. The data of the experimentally obtained natural frequencies, Mode 1 and Mode 2 are presented in Table 1 in **Appendix B**.

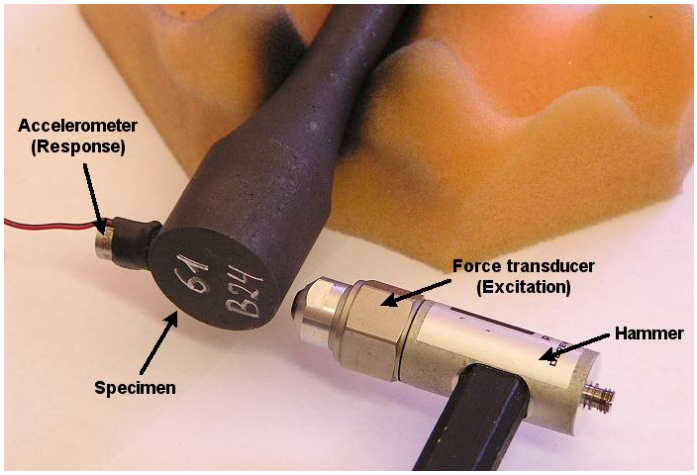

Figure 13: Test setup - accelerometer mounting and impact blow position

4.3 Particulars of the Test Set-up

4.3.1 Transducer Selection

A piezoelectric acceleration-based PCB Piezotronics 309A transducer (accelerometer) was used. The transducer has a 10 mV/g sensitivity and is capable of yielding a frequency range of 5-10000 Hz. Avitabile (1998) states that there are two principle features which are important when selecting the amplitude and frequency range of the measurable vibration. These are the amplitude range which is determined by the sensitivity of the transducers and the frequency range which is dictated by their resonant frequency. The vibration response of the specimen to the impulse excitation was limited to a frequency range between 0 to 4 kHz.

4.3.2 Accelerometer Mounting

One accelerometer was mounted on the opposite end of the hammer impact zone, as shown in Figure 13 to acquire the Frequency Response Functions (FRFôs). The FRF model used in determining the natural frequencies of a uniaxial fatigue test specimen can be represented by the following linear model shown in Figure 14.

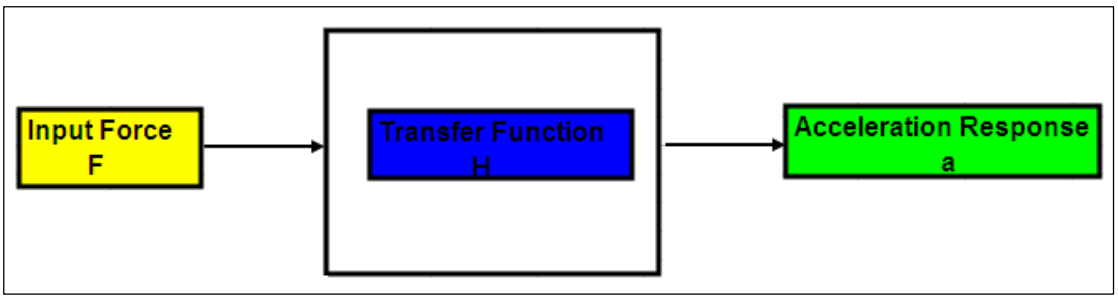

Figure 14: Frequency Response Function Model

In this model, (*F*) is the input force, (*H*) is the transfer function and (*a*) is the acceleration response function. The relationship in Figure 14is presented by the following equation:

$$H(\omega) = \frac{a(\omega)}{F(\omega)} \qquad (4.1)$$

Where:
ω = Angular velocity [rad/s]

Furthermore, a good accelerometer bond was essential for it is assumed that the transducer motion is identical to that of the system. Taking the curvature of the test specimen in consideration, the accelerometer was mounted with beeswax directly onto the graphite.

4.3.3 Excitation Source Selection

A PCB Piezotronics modally tuned hammer with model number 086C01 was used as a source of excitation to excite the specimens because of its applicability on a curved surface due to the particulars of the test cases. The impact hammer measured the exciting force signal by means of a force transducer. In order to achieve a satisfactory signal to noise ratio, the impact-hammer had to be capable of exciting the specimen above the ambient vibration level.

The quality of the measurements depends strongly on the proficiency and the consistency of the impact-hammer operator. Deviations in the excitation location or angle of the higher order modes of the graphite test specimens may stimulate different modes and degrade the consistency of the acquired natural frequencies as well as the quality of the mode shape definitions. Therefore, special care had to be taken to hit the predefined points on all of the different specimens with optimum driving force.

To achieve an optimum excitation level, according to Sezer Atamturktur *et al.* (2006)the following criteria had to be met: the graphite test specimen must be excited evenly and uniformly, while the system behaviour must be kept in the linear range and the response amplitude must be kept in the detectable measurement range of the equipment.

The specimen was recorded to undergo a magnitude of frequency response function (accelerance) of between 40 $(m/s^{2)}/N$ up to 450 $(m/s^{2)}/N$ which yielded a signal to noise ratio of approximately 80 dB. Based on these observations a hard tip impulse hammer with a hammer mass of 0.1 kg, a head diameter of 1.57 cm and a tip diameter of 0.63 cm was decided to be suitable for the purpose of these experiments. A steel tip hammer with a sensitivity of 11.2 mV/N and no additional mass was chosen as the preferred tool, since it offers a frequency range of up to 9.5 kHz and a measurement

range of ± 445 N pk for a ± 5V output. When applied in the case of NBG-18 graphite samples, the steel tip excited amplitudes of frequencies of up to 4 kHz.

4.3.4 Data Analyzer

A Spectral Dynamics SD 390Z-4 four channel Fast Fourier Transform (FFT) analyzer was used for data acquisitioning. The FFT analyzer calculates six linear averages in a frequency range of 0-1 kHz with 800 lines.

The interpretation of the extracted modal characteristics from the measured quantities is discussed in the subsequent chapter.

CHAPTER 5

5. Results and Modelling of Natural Frequency Data

5.1 Frequency Response Function and Extracted Modal Parameters

The velocity magnitude response to the frequency range was recorded by the vibrometer. Figure 15 displays as example typical measurement signals of the velocity magnitude response in $(m/s^2)/N$ to frequency range below 4 kHz for specimen 60 J-15 obtained. Two distinct resonance peaks occurring at frequencies 925 Hz and 3155 Hz are noticed in the magnitude of the frequency response function, with associated residue values at 320 $(m/s^2)/N$ and 133 $(m/s^2)/N$. Coherence values at each mode frequency are indicated from the coherence function curve to indicate the linearity and accuracy of the obtained results. Higher values in average coherence for the accelerometer generally represent better data quality, and the overall data quality is very good. The average coherence quality of all acquired data was used as a post-test guide to overall data quality. However this function does not indicate whether an individual FRF has good quality, but the average coherence does give an overall confidence in a complete data set.

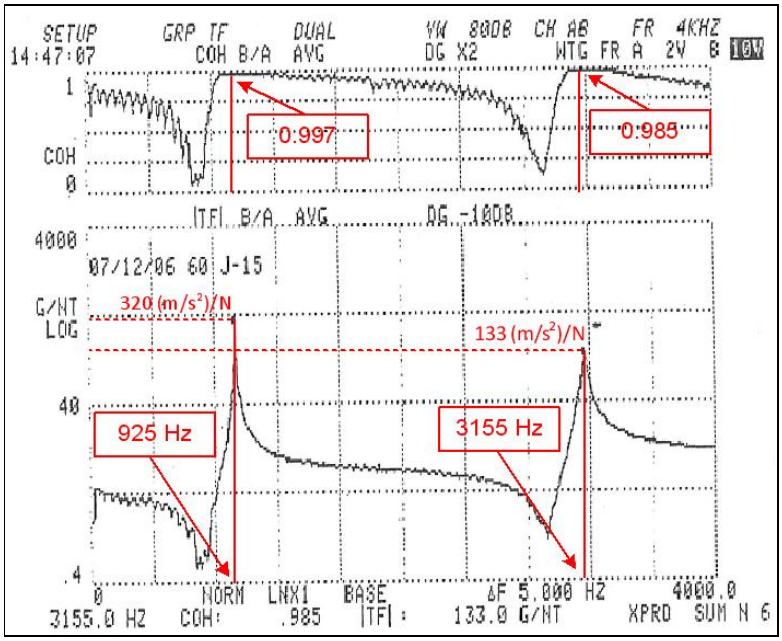

Figure 15: Frequency response plot from vibrometer for specimen 60 J-13, range of 0-4 kHz

5.2 Natural Frequencies

The results of the experimentally obtained frequencies are discussed in this section. Figure 16 and Figure 17 shows graphical presentations of the experimentally obtained magnitudes of natural frequencies Mode 1 and Mode 2. The natural frequencies are plotted against the number of samples tested, indicated by the green blocks. In order to gain perspective on the distribution of the frequencies, a black line representing the density distribution function was plotted on each graph.

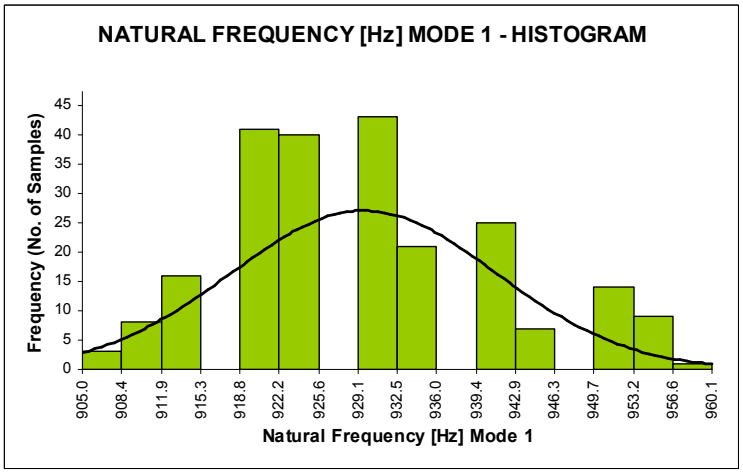

Figure 16: Histogram for natural frequency Mode 1

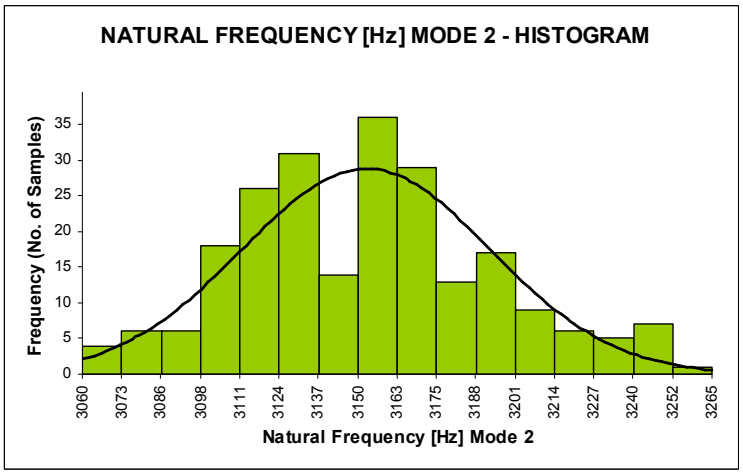

Figure 17: Histogram for natural frequency Mode 2

Statistical parameters of the experimentally obtained data were determined by making use of an Excel add-in histogram-plot function. The results are presented in Table 1.

Table 1: Statistical Distribution Results of Natural Frequency Data

Parameters	Mode 1 [Hz]	Mode 2 [Hz]
Population Mean	929.6	3152.5
Standard Deviation	11.585	40.423
Minimum Frequency	905	3060
Maximum Frequency	960	3265
95 % CI Mean	928.09 → 931.12	3147.2 → 3157.75
95 % CI Sigma	10.61 → 12.76	37.02 → 44.52

5.3 Modelling

5.3.1 Introduction

In order to evaluate the validity and accuracy of the experimentally obtained natural frequency data, it was decided to simulate the natural frequencies of uniaxial specimens, by importing a CAD (computer-aided design) model created in SolidWorks[1] of the sample geometry into Algor[2] and applying the appropriate simulation parameters.

5.3.2 Parameter Selection

The design scenario simulated was a single analysis type with static stress and linear elastic material properties and natural frequency (modal) parameters. Analysis parameter settings included the number of frequencies or modes to be calculated in some cases as 5 modes and in other cases as 10 modes. The lower cut-off frequency was set at 10 cycles/s and the upper cut-off frequency was set at 4000 cycles/s. The constraints set were chosen as free-free and no load set was applied to the specimens under consideration. These parameters were chosen in order to simulate the test setup explained in Section 4.2.

[1]SolidWorks is a 3D mechanical CAD program that runs on Microsoft Windows developed by SolidWorks Corporation.
[2]Algor is a general-purpose multiphysics finite element analysis software package developed by ALGOR Incorporated for use on the Microsoft Windows and Linux computer operating systems.

5.3.3 Experimental FEA Results

By applying the nominal material and geometry parameters shown in Section 3.1 and Figure 12, the following output windows presented in Figure 18 and Figure 19 were generated.

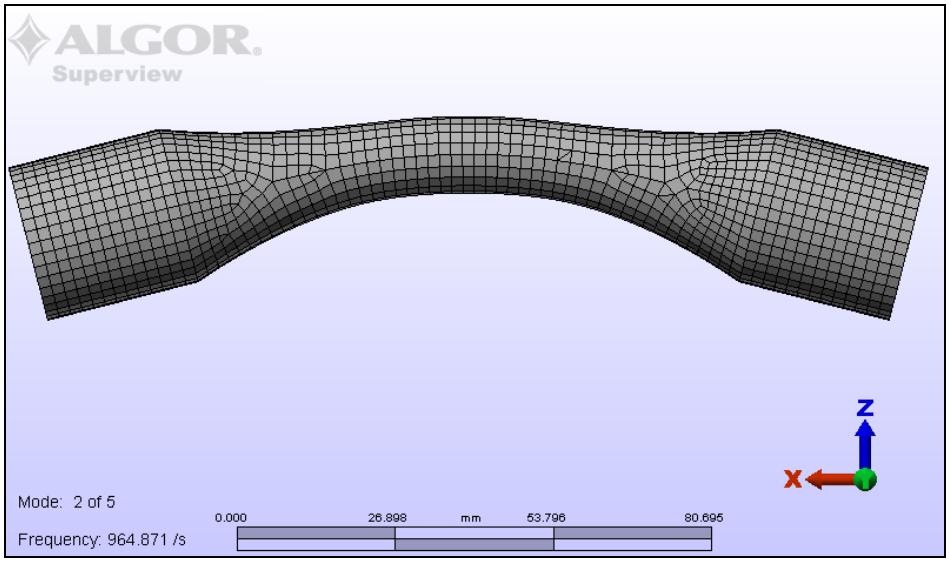

Figure 18: Window showing the deformation association with natural frequency mode 2 of the specimen with average parameters

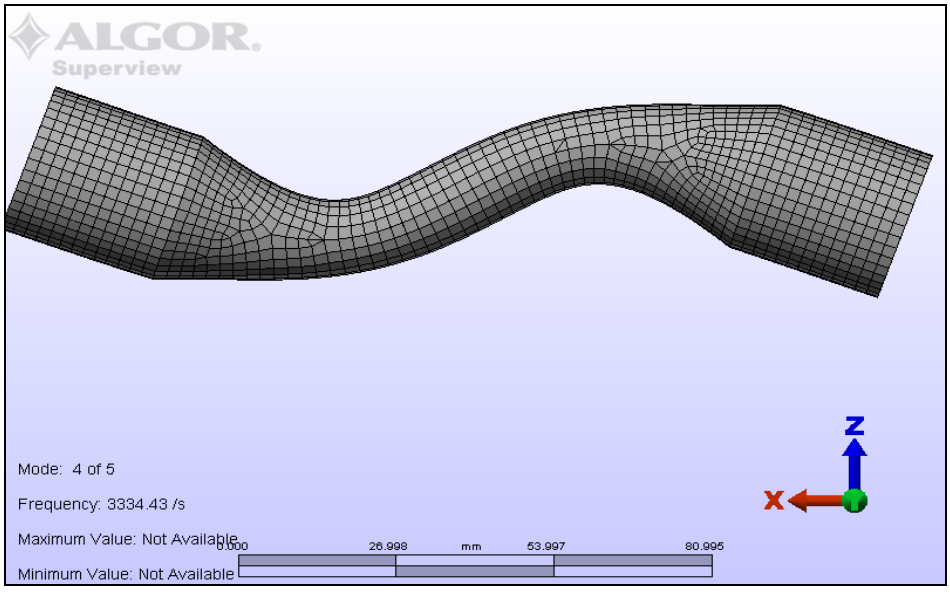

Figure 19: Window showing the deformation association with natural frequency mode 4 of the specimen with average parameters

Figure 18 shows the first amplitude of natural frequency referred to as Mode 1 with an obtained value of 964.871 Hz. Figure 19 shows the second amplitude of natural frequency referred to as Mode 2 with a value obtained of 3334.43 Hz.

A comparison between the experimentally obtained natural frequencies Mode 1 and Mode 2 and the FEA results for maximum and minimum obtained values, are presented in Table 3.

Table 2: Comparison between the Experimental and FEA Data.

Set-up	Mode 1 (max.) [Hz]	Mode 2 (max.) [Hz]	Mode 1 (min.) [Hz]	Mode 2 (min) [Hz]
Experimental	950	3245	908	3080
FEA	967	3403	944	3263

Because a variation in the geometry tolerances occur during machining, it can give rise to a variation in parameters like the density, the mass and the bulk modulus of elasticity in each specimen. In order to simulate the variations that occurred in the total population of uniaxial specimens, three different FEA models were created. To establish the amount by which the parameters should vary in the three FEA models, the mass and test section diameter were calculated for each specimen (See Section 6.2 for details on procedure).

From these results it was found that the parameters vary by an amount of 2ů (two standard deviations) from each other, and thus a deviation of 2% was introduced in the three FEA models. The first model were given nominal values of nominal density and modulus of elasticity as explained in Section 3.1 and nominal geometry tolerances as explained in Section 3.3. In the second and third simulation models one of these parameters were changed by an amount of 2ů, and the other two were kept at the nominal values. The results of the obtained natural frequencies mode 1 and mode 2 for the three FEA models are presented in Table 3.

Table 3: Results of Natural Frequency Mode 1 and Mode 2 for a change in nominal parameters presented.

Parameters	Mode 1 [Hz]	Mode 2 [Hz]
Volume (Nominal)	**964.871**	**3334.43**
Volume (High)	**967.084**	**3333.42**
Volume (Low)	**967.082**	**3333.44**
ΔE (High)	**984.932**	**3403.76**
ΔE (Low)	**944.382**	**3263.62**
Δρ (High)	**964.809**	**3334.22**
Δρ (Low)	**964.932**	**3334.64**

5.4 Discussion and Conclusions

The validation of the experimentally obtained Natural Frequencies Mode 1 and Mode 2 with the FEA results proved to be satisfactory as shown by the comparison in Table 2. These results indicate that the parameters chosen for the experimental setup of the modal frequency testing were sufficient in producing valid results.

CHAPTER 6

6.EXPERIMENTAL UNIAXIAL FATIGUE TESTS

6.1 Introduction

The load ratio concept used in fatigue loading is given by equation (6.1) according to Shigley *et al.* (2004). The load ratio is defined by the minimum to maximum stress in the time domain stress waveform, and is produced by cyclic loading. The load ratio is given by:

$$R = \frac{\sigma_{min}}{\sigma_{max}} \tag{6.1}$$

where: $R = Load\ Ratio$

$\sigma_{min} = Minimum\ stress\ [MPa]$

$\sigma_{max} = Maximum\ stress\ [MPa]$

Figure 20 is a presentation of the stress amplitude as a function of midrange stress and presents the load ratios used for the NBG-18 graphite uniaxial fatigue tests. Shown in the figure are the two horizontal lines of constant load ratio loci for ñstatic tensileò and ñstatic compressionò stress waveforms respectively, and the seven radial lines of constant load ratio loci for cyclic stress waveforms. The small inset drawings added to each load ratio, represent the relative stress waveforms containing a single cycle for each load ratio in order to relate the physical stress cycle to each load ratio.

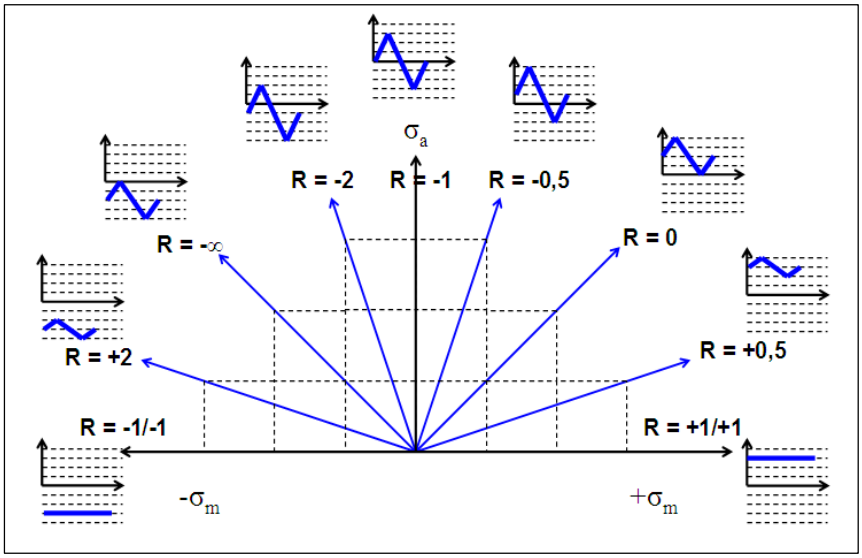

Figure 20: Graphical presentation of load ratios used for graphite tests, illustrating the cyclic waveform stress patterns

6.2 Experimental Work

6.2.1 Machining Requirements and Specimen Condition

Machining requirements based on research done by Roberts (2007, 4-16) stipulated that the specimens had to be machined in a single run from a pre-machined bar. This was implemented to ensure that the specimens had no radial run-out, or no other run-out apart from that induced by the running accuracy of the machine spindle. Another requirement was that the cutting methods, to obtain the shape of the raw material as well as the final specimens, had no clamping loads producing stresses larger than 5 MPa applied to the test section of the material.

The specimens were supplied in the as-machined condition by the PBMR. The test section diameter was calculated for each specimen, by averaging four measurements for each specimen, using a Tesa micrometer with an accuracy of ± 2 εm shown in Figure 21. The mass of the specimens were measured on a Sartorius model L420P mass balance, with an accuracy of ± 1 mg shown in Figure 22. The calibration certificate for the Sartorius mass balance is presented in **Appendix E**.

Figure 21: Tesa micrometer for geometric measurement of S70 specimen

Figure 22: Sartorius mass balance for weighing of S70 specimen

Furthermore, a surface treatment was applied to the gripping areas using Quality Stone Chip Sealer (Luxor Paints) to improve the coefficient of friction between the graphite rod and the collet.

6.2.2 Fatigue Testing Machine

The type of machine used to conduct the uniaxial fatigue tests was an Instron 8801 100 kN Servo hydraulic testing machine, shown in Figure 23 with a 25 kN calibrated load cell (see **Appendix E** for calibration certificates). A sinusoidal shaped forcing function, with a frequency that varies between 1 and 30 Hz was used.

Continuous measurement throughout testing was established by means of computer-based data acquisition. The data acquisition system for these tests was designed to conform to the ASTM E 1942-98 (2002) standard, which specifies the requirements for data acquisition systems used in cyclic fatigue and fracture mechanics. A simultaneous sample-hold Digital Signal Processing (DSP) card was used for data capture. To preserve a common count base for all load ratios, failure during the first excursion cycle, irrespective of the direction of the load path was counted as one.

The noise level of the data acquisition system was not measured, but all necessary precautions were taken to avoid EMI (electromagnetic interference) induced noise in the data signals. The instrument cables were shielded and grounded according to best practice.

Figure 23: Instron 8801 servo-hydraulic fatigue test machine

6.2.3 Modification of Test Equipment

To be able to interact with the Instron 8801, aluminium end stops held in place by waved washers and adapter pieces had to be designed and manufactured. Collet grips and an anti-rotation bar (Fig. 24) had to be applied to the hydraulic ram of the Instron to prevent any unwanted torsional loads on the specimens.

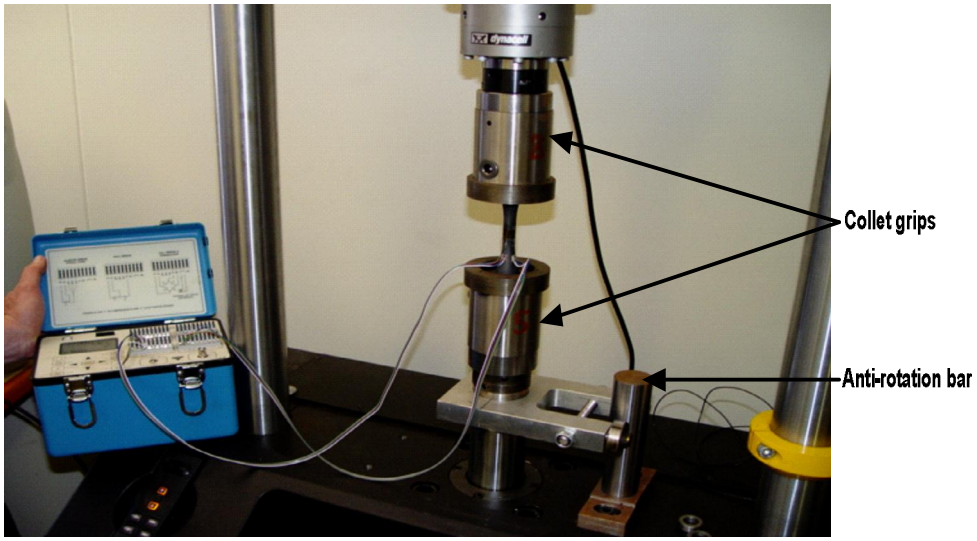

Figure 24: Instron 8801 with anti-rotation bar, collet grips and strain gauged uniaxial specimen

It was decided to use collet chucks for gripping the specimens, in order to remove axial play in the load train and to establish precision alignment. Because of the availability of standard collet chucks, the gripping diameter was constrained to a maximum of 26 mm. Furthermore the diameter of the gauge section was maximized within the prescribed geometry in order to maximize the fracture load.

Insufficient collet pressure can result in slipping of the test specimen according to Roberts (2007, 4-12). This was investigated by machining cylindrical graphite bars to the dimensions of the grip diameter used in the relevant test, and clamping the bars in a collet at different clamping pressures, by loading the specimens in compression with a hydraulic jack. The force at which the bar started to slip was then measured by making use of a 1000 kg load cell. From this investigation it became clear that a high contact pressure was required to prevent slippage and that at the moment the bar starts to slip a significantly higher gripping force would be required. The higher gripping force can be attributed to the local wear of the graphite, which forms a thin layer of graphite powder acting as a dry lubricant that makes it difficult to grip the component.

In order to solve the grip problem V-grooves were impinged in the dead length collet chuck, manufactured by Kalamazoo Industries Inc., Kalamazoo Michigan, USA at 5 mm axial intervals.

6.2.4 Alignment and Strain Gauge Calibration

The alignment of the specimen to load grips in the testing machine was of utmost importance to obtain high quality test results. ASTM E 1012-99 (2002), which is the standard practice for verification of specimen alignment under tensile loading, was used to verify the alignment of the grips during the uniaxial static and fatigue testing. The alignment verification for a single test (Type T) or for the test apparatus (Type A), using Method 2, which utilizes four strain gauges centered at the mid-length of the reduced section of the specimen, was used for this research. AlignPRO alignment fixtures and software was purchased from Instron in order to facilitate these test conditions. The alignment results are presented in **Appendix D**.

To enable the measuring of the stress-strain characteristics at each load setting it was decided to strain gauge one specimen per load ratio. HBM LY11-6/120 type gauges were connected to the graphite specimens using HBM X280 epoxy glue. The type of connection used was a full Wheatstone bridge, as shown in Figure 25 and explained in Section 6.3.3.

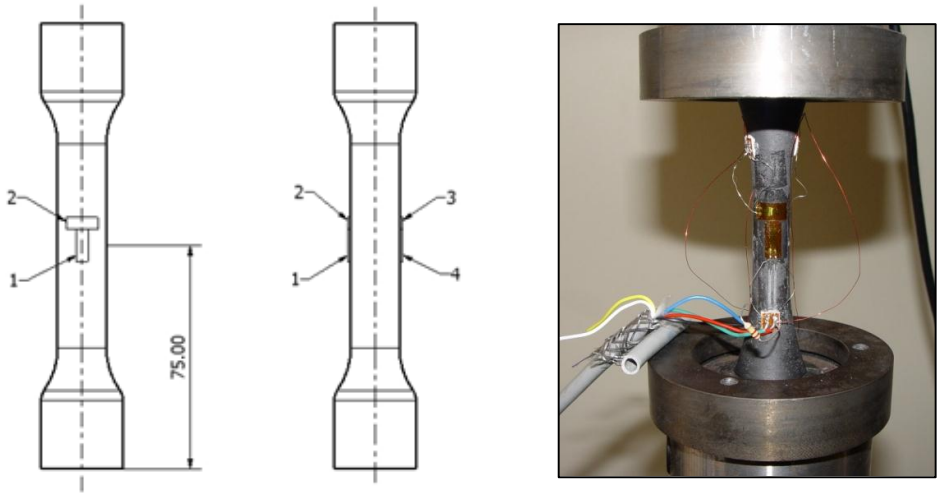

Figure 25: Gauge sample setup

6.2.5 Allocation of Specimens to Load Ratios and Test Procedures

The whole range of load ratios shown in Figure 20, ranging from static compression tests with a load ratio of R = -1/-1, to static tensile tests with a load ratio of R = +1/+1 were used to conduct uniaxial fatigue tests. The fatigue test load ratios used include ratios R = -∞, -2, -1, -0.5, 0, 0.5, and +2.Tests were conducted under the test conditions shown in Table 4.

Table 4: Test conditions for all load ratios

Load Ratio [-]	Temperature [°C]	Humidity [%]
R = -∞	22.3 - 27	39.2 - 72
R = -2	16 - 21.6	41.6 - 54
R = -1	20 - 28.6	51 - 75.1
R = -0.5	21.4 - 24	55 - 60
R = 0	25.2 - 28	46.7 - 73.5
R = 0.5	21 - 27	58 - 75.2
R = 2	18 - 25	50 - 80

As a starting point the first load for all tests were approximated at ±85% of the average maximum force (tensile or compression). The subsequent loads were then determined based on the results obtained from the first load. Failure was defined as complete separation and run-out was defined as $2x10^5$ cycles. There were eight specimens tested for each load ratio, taken from locations shown in Table 5.

Particulars of the test setup required that the tests conducted were to be load controlled. A frequency of 8 Hz and an ultimate tensile strength of 19.9 MPa were used for all load ratios. The test results and detail on the test conditions are presented in **Appendix C.**

Table 5: Specimen allocation for Load Ratios with reference to Figure 20

Load Combination	Load Amplitudes	Alignment	Location	Block	Qty.	No. R-values	Total Qty.
R = -1	4	X	Edge	A	4	1	4
R = -1	4	X	Centre	A	4	1	4
R = -1	4	Z	Edge	A	4	1	4
R = -1	4	Z	Centre	A	4	1	4
R = -1	4	X	Edge	A	4	1	4
R = -1	4	X	Centre	A	4	1	4
R = -1	4	Z	Edge	A	4	1	4
R = -1	4	Z	Centre	A	4	1	4
					Total Fatigue Samples		32
R = +1/+1 and -1/-1	1	X	Edge	A	1	2	2
R = +1/+1 and -1/-1	1	X	Centre	A	1	2	2
R = +1/+1 and -1/-1	1	Z	Edge	A	1	2	2
R = +1/+1 and -1/-1	1	Z	Centre	A	1	2	2
R = +1/+1 and -1/-1	1	X	Edge	B	1	2	2
R = +1/+1 and -1/-1	1	X	Centre	B	1	2	2
R = +1/+1 and -1/-1	1	Z	Edge	B	1	2	2
R = +1/+1 and -1/-1	1	Z	Centre	B	1	2	2
					Total Static Samples		16
R = -∞/–2/–1/–0.5/0/+0.5/+2	4	X	Edge	A	4	7	28
R = -∞/–2/–1/–0.5/0/+0.5/+2	4	X	Centre	A	4	7	28
R = -∞/–2/–1/–0.5/0/+0.5/+2	4	Z	Edge	A	4	7	28
R = -∞/–2/–1/–0.5/0/+0.5/+2	4	Z	Centre	A	4	7	28
R = -∞/–2/–1/–0.5/0/+0.5/+2	4	X	Edge	B	4	7	28
R = -∞/–2/–1/–0.5/0/+0.5/+2	4	X	Centre	B	4	7	28
R = -∞/–2/–1/–0.5/0/+0.5/+2	4	Z	Edge	B	4	7	28
R = -∞/–2/–1/–0.5/0/+0.5/+2	4	Z	Centre	B	4	7	28
					Total Fatigue Samples		224

6.3 Important Test Considerations

6.3.1 Alignment

The alignment of the machine was established by means of the ASTM E 1012-99 (2002) standard, explained in section 6.2.4. By assuming that the bending stress may not exceed 5% of the mean tensile stress according to ASTM C 749-92 (2005), it was possible to estimate the maximum allowable misalignment of a uniform diameter rod. This standard is applicable to graphite with grain size from 0.0254 mm to ± 6.4 mm, and is used to generate quality engineering data at room temperature or elevated temperature, with an emphasis on mean values and variances. The loading diagram, shear force diagram and bending moment diagram of a uniform diameter rod subjected to parallel and angular misalignment is shown in Figure 26.

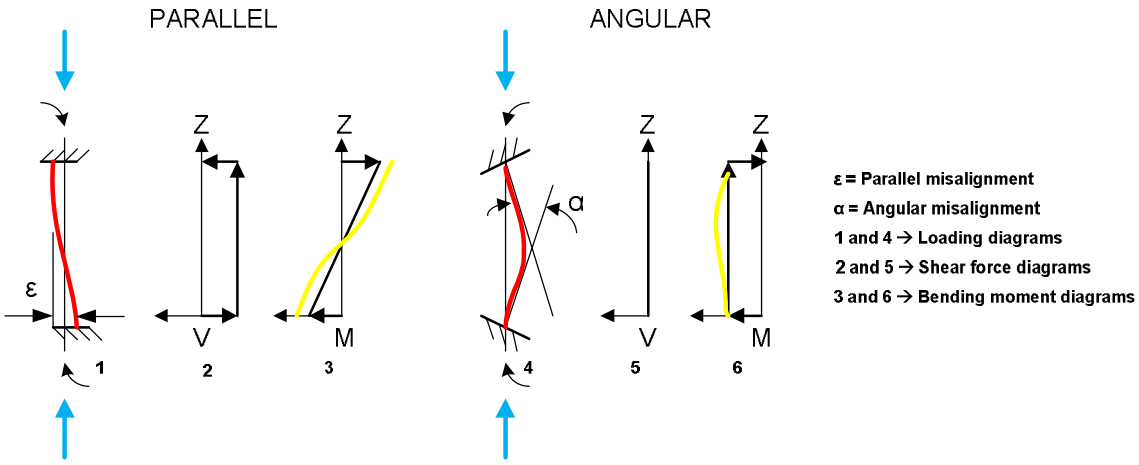

Figure 26: Uniform rod subjected to shear forces and bending moments induced by misalignment

An additional bending moment shown by the yellow lines in Figure 26 is caused by an axial force that increases the bending moment in the gauge section when it is compressed, and vice versa. For the purpose of this study the additional moment is neglected in the simplistic calculations of the two separate cases of misalignment, because in reverse loading, it adds in one case and subtracts in the other case. Thus for fully reversed loading the mean value will be zero.

The bending moment in angular misalignment remains constant along the gauge section and varies linearly from a positive to a negative value along the length of the gauge section in angular misalignment. Angular and parallel misalignment derived for the 5% allowable bending stress is given by equation (6.2) and equation (6.3) respectively.

Angular misalignment:

$$\alpha \leq F.\frac{0{,}4.l}{E.d^3} \tag{6.2}$$

Parallel misalignment:

$$\varepsilon \leq F.\frac{0{,}25.l^2}{3.\pi.E.d^3} \tag{6.3}$$

where:

$\alpha \equiv$ Angular misalignment angle relative to force line [rad]

$F \equiv$ Axial force [N]

$l \equiv$ Length of rod [mm]

$E \equiv$ Modulus of elasticity [MPa]

$\varepsilon \equiv$ Parallel misalignment [mm]

$d \equiv$ Uniform section diameter of the sample [mm]

By making use of a 1000 N axial force, the maximum allowable angular misalignment was calculated with Equation (6.2) to be $15{,}2 \times 10^{-3}$ rad, and the maximum allowable parallel misalignment was calculated with Equation (6.3) to be 3εm. Therefore, the maximum number of cycles where the axial load is the smallest determines the maximum allowable misalignment.

6.3.2 Clamping of Specimens

Sufficient gripping of the uniaxial tests specimens had to be established, which depended on the friction between the collet and the graphite according to Roberts (2007, 4-11). Roberts (2007, 4-11) determined the static coefficient of friction experimentally by placing a graphite part on a steel rail, and measuring the slope at

which the graphite part would start to slide down. The coefficient of friction was calculated to be approximately 0.7 for graphite on steel. An end stop in the gripping tool had to be designed to counteract the compression load, because the compressive strength of graphite is calculated to be four times higher, than that of its tensile strength.

The required clamping pressure to prevent slip in tension was calculated by deriving equation (6.4).

$$p = \frac{n.S_{ut}.d^2}{4.\mu.D.h} \tag{6.4}$$

where:

$p \equiv$ Clamping pressure between collet and graphite [MPa]

$S_{ut} \equiv$ Ultimate tensile strength of graphite [MPa]

$n \equiv$ Factor of safety

$d \equiv$ Diameter of the gauge section [mm]

$\mu \equiv$ Coefficient of friction between graphite and collet material

$D \equiv$ Grip diameter of specimen [mm]

$h \equiv$ Grip height in collet [mm]

A clamping pressure of 12 MPa on the full grip height for the uniaxial specimen was calculated with Equation (6.4).

6.3.3 Strain Calibration

The Wheatstone bridge connection resulted in a bridge factor of V.G.(1+ν)/2, and the gauge factor (G) for the gauges was taken as 2.06. The Wheatstone bridge connection is shown in Figure 27.

Calibration was done by means of a shunt resistor, and two resistors were used depending on the strain difference to be measured. The two measured resistance values were 119.7kΩ and 11.88 kΩ respectively. The 119.7 kΩ resistor was then used

for samples subjected to lower strain values (± 4000 μm/m), and an 11.88 kΩ resistor was used for samples subjected to large strain values (±12000 μm/m). In order to simulate an output voltage, the shunt resistor was connected across gauge one during the calibration process. The simulated strain was calculated using Equation (6.5) and a poisonôs ratio of v = 0.21.

$$\varepsilon_c = \frac{R_1}{G.2.(1+\nu).(R_1.R_c)} \tag{6.5}$$

where:

R_c = shunt resistor value

R_1 = 120 Ω (gauge one resistance)

G = strain gauge factor

ε_c = simulated strain

ν = Poissonôs ratio

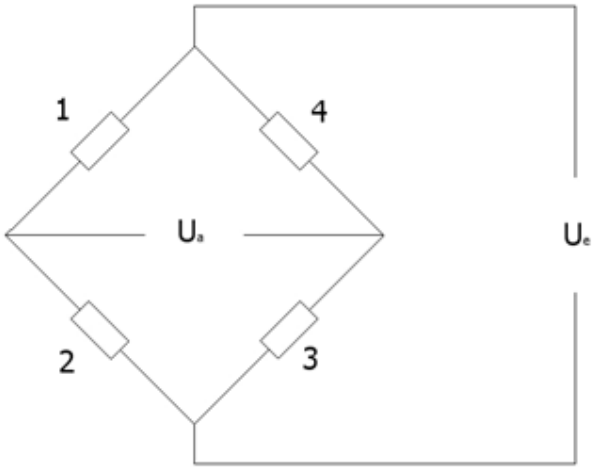

Figure 27: Wheatstone bridge Configuration

The simulated strain calculated for the 119.7 shunt resistor was -200.9 μm/m, and the simulated strain calculated for the 11.88 kΩ resistor was -2005.9μm/m.

CHAPTER 7

7. Results of the Uniaxial Fatigue Tests

7.1 Experimental Uniaxial Fatigue Data

The tests focussed on the nominal stress required to cause a fatigue failure in the uniaxial test specimens after a certain number of cycles, using the load ratios explained in Section 6.2.5.

R = -1 is an important load ratio, because the minimum and maximum (valley and peak) value in the stress-time waveform had the same magnitude, but opposite sign that represented the fully reversed stress cycle. The stress amplitude was equal to the maximum tensile and compressive stress, and had a midrange stress of zero.

The test results for each load ratio are shown in Figure 28 to Figure 34, as scatter plots of either the maximum or minimum applied load versus the number of cycles to failure (N). A logarithmic regression was performed to get a best-fit straight line through the data points, by making use of a logarithmic N scale. The regression equation and R^2-value (correlation coefficient) is presented on each graph. Run-out (non-failure) was defined to be approximately 200 000 cycles, and failure was defined as complete separation.

7.1.1 Tension Dominant Load Ratios

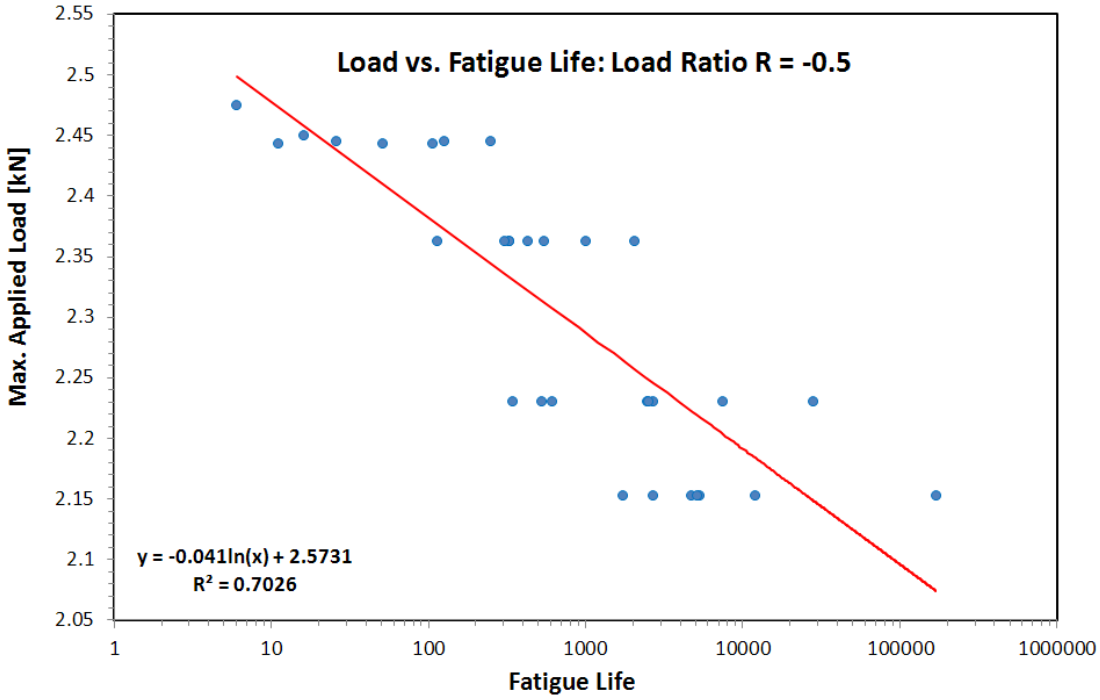

Figure 28: Maximum applied load versus no. of cycles to failure for load ratio R = -0.5

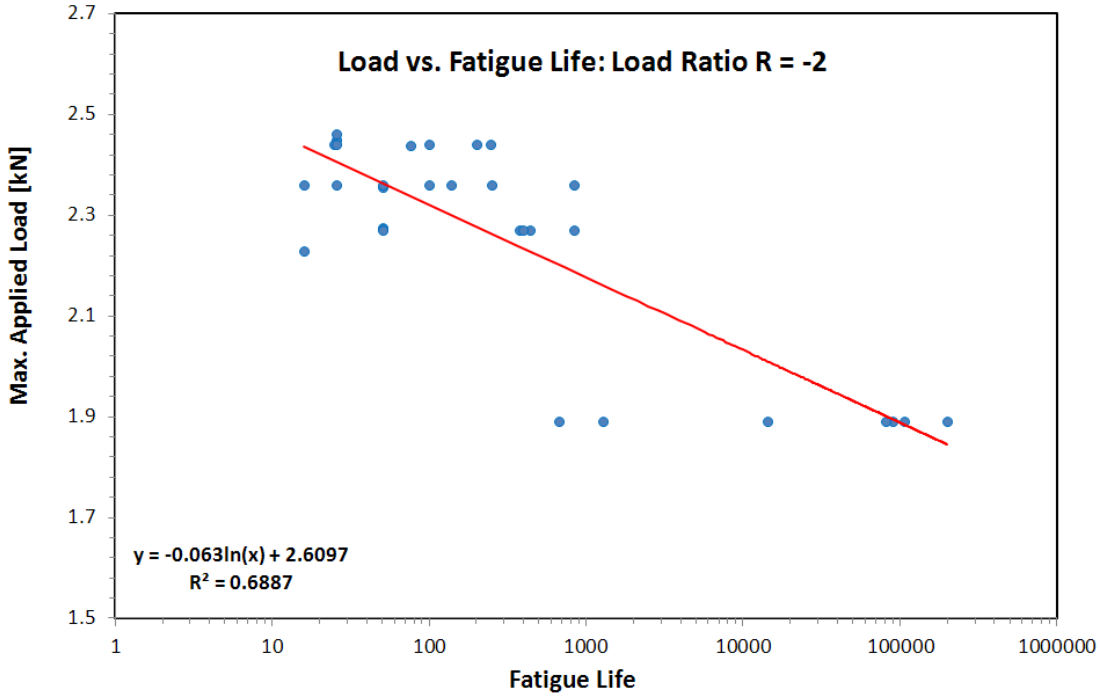

Figure 29: Maximum applied load versus no. of cycles to failure for load ratio R = -2

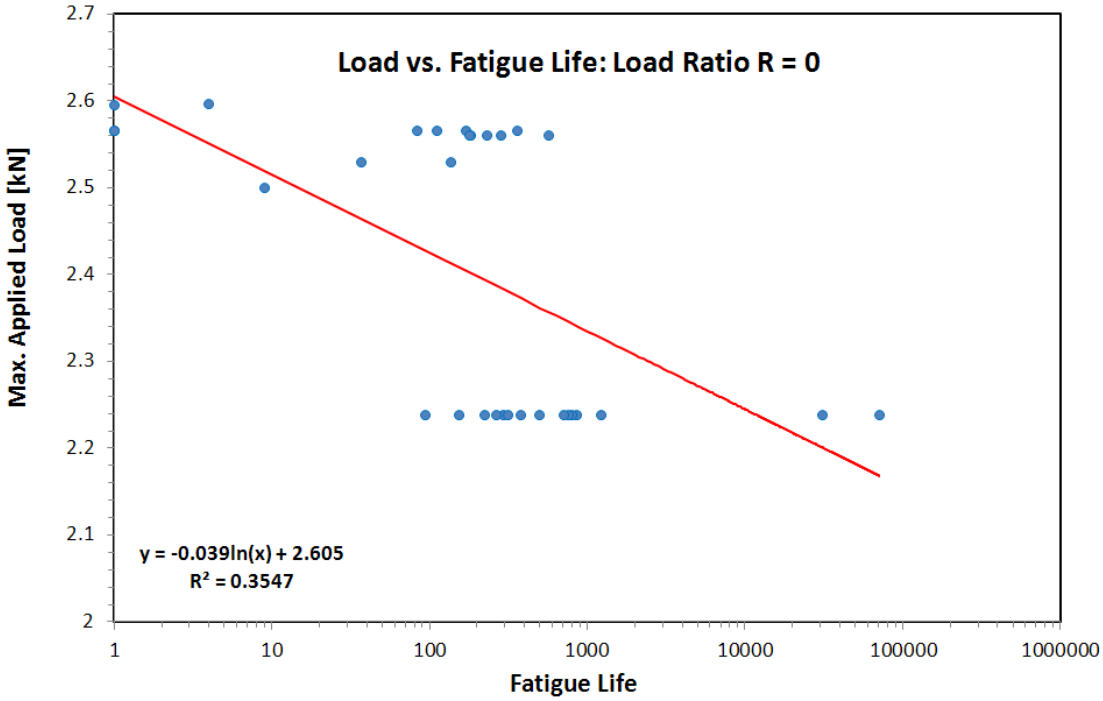

Figure 30: Maximum applied load versus no. of cycles to failure for load ratio R =0

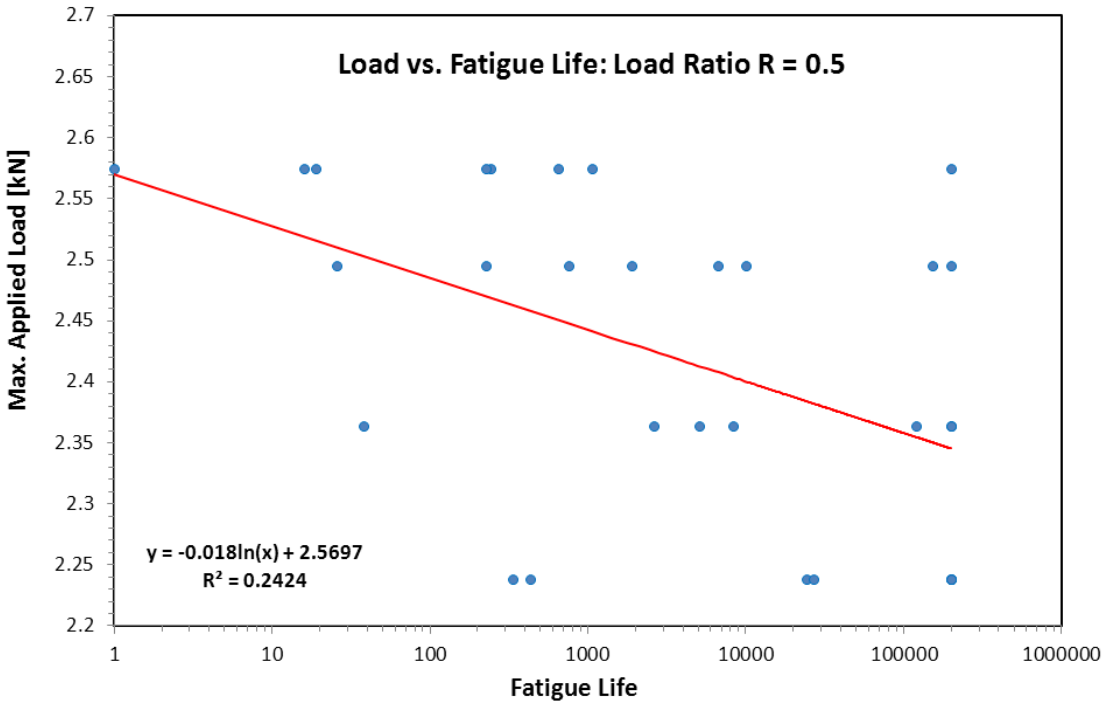

Figure 31: Maximum applied load versus no. of cycles to failure for load ratio R = 0.5

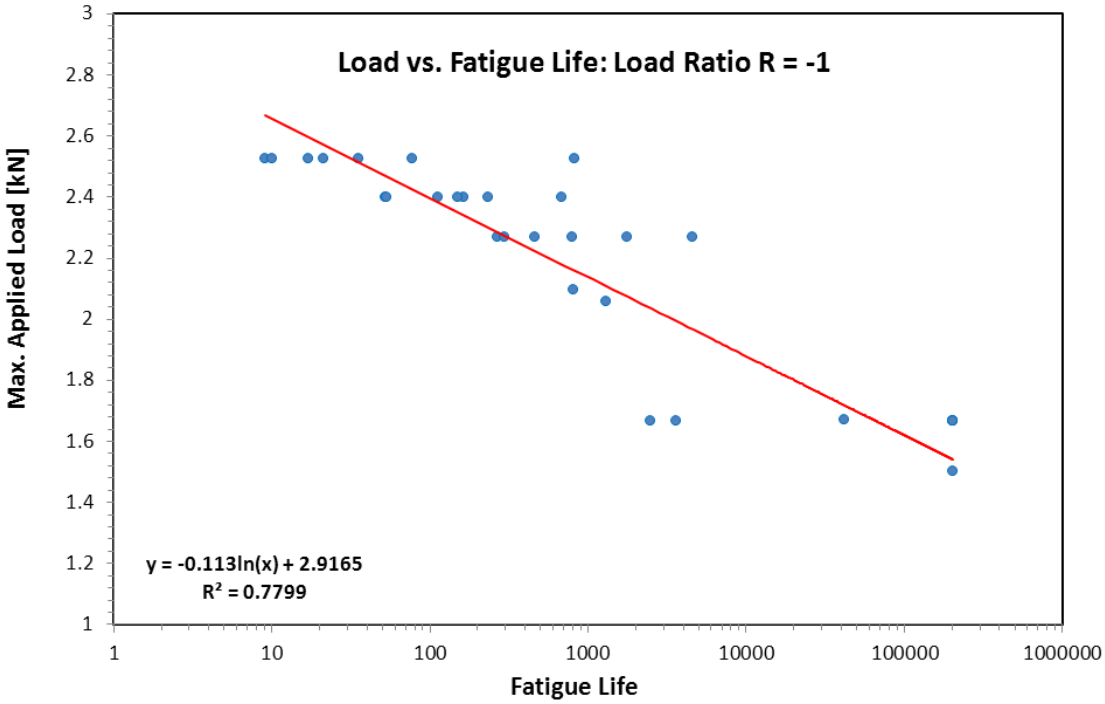

Figure 32: Maximum applied load versus no. of cycles to failure for load ratio R = -1

7.1.2 Compression dominant Load Ratios

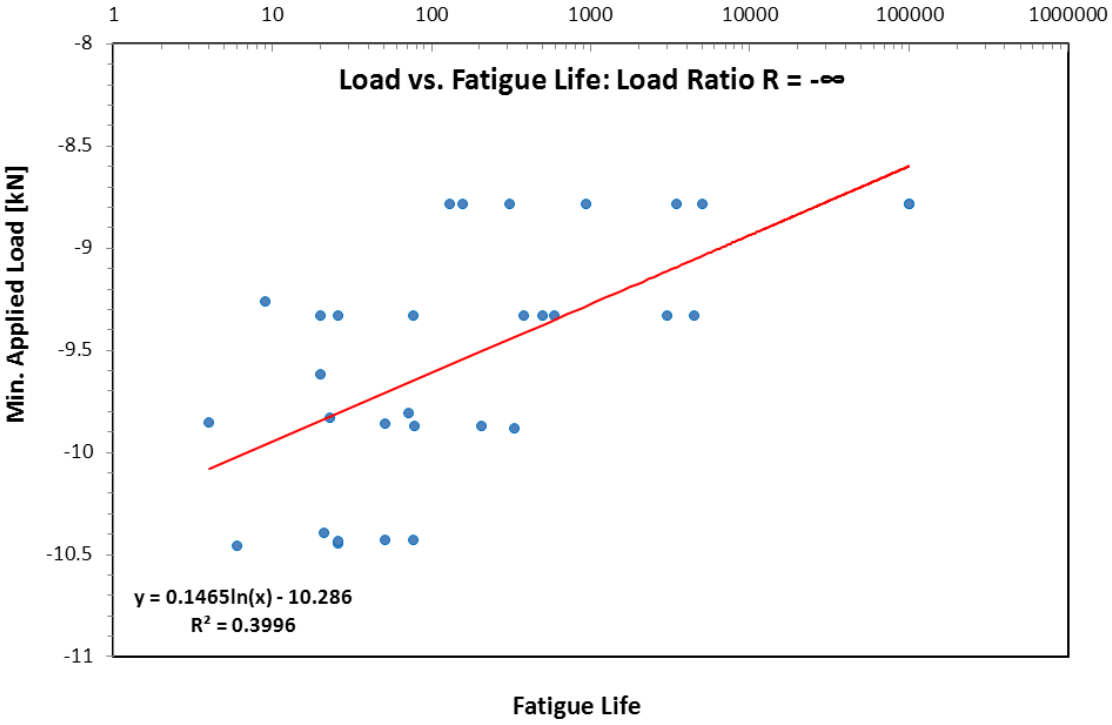

Figure 33: Minimum applied load versus no. cycles to failure for load ratio R = -∞

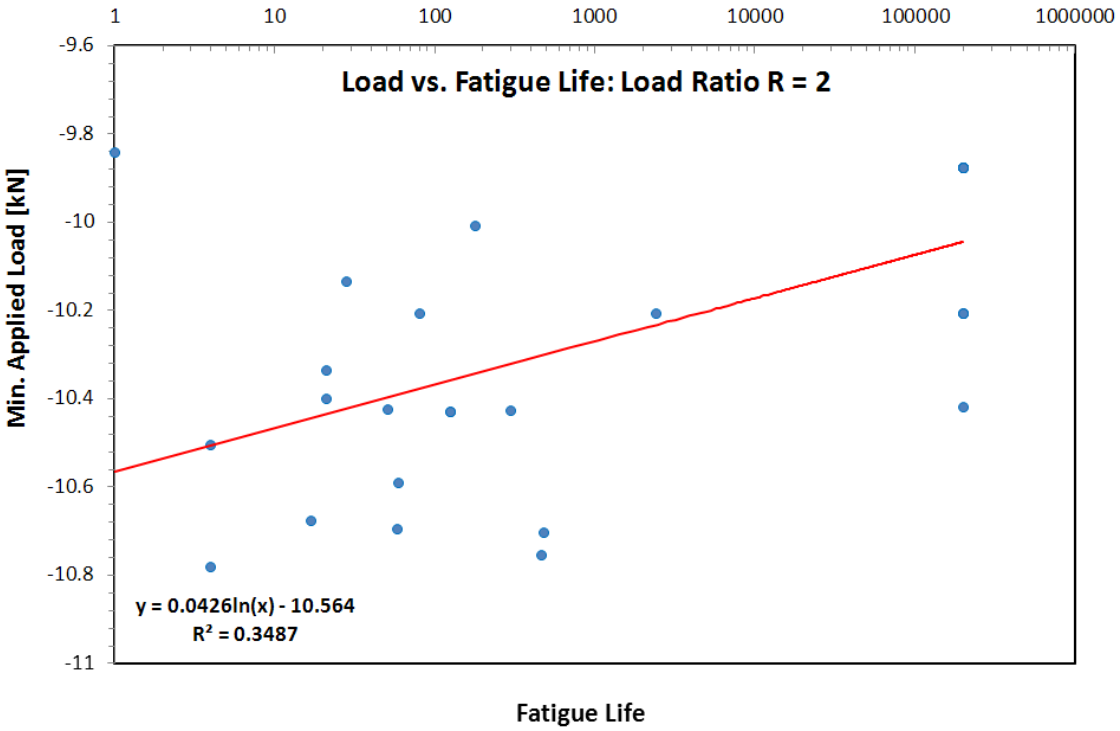

Figure 34: Minimum applied load versus no. of cycles to failure for load ratio R = +2

7.2Discussion and Conclusions

The six load ranges which includes R = +1/+1, R = 0.5, R = 0, R = -0.5, R = -1 and R = -2 are all governed by the tensile strength of the graphite and the other three load ranges which include R = -∞, R = 2 and R = -1/-1 are governed by the compressive strength of the graphite. According to Roberts (2007: 4-30) this is due to the fact that the Ultimate Tensile Strength/ Ultimate Compressive Strength ($S_{ut}/S_{uc)}$ ratio for this specific grade of graphite is close to being a ¼ of the magnitude of tensile and compressive strength, in comparison to the ratio for R = -2 which is close to being a ½ of the magnitude of tensile and the compressive strength. Data captured at load ratios R = 0 and R = 0.5 is not acceptable, because of the large scatter of data points on the diagram, which is aggravated by the small slopes on the load versus number of cycles to failure curves. The other curvesô data points has a better grouping about the slope of the line on the diagram, and can be accepted as satisfactory although more tests at the load ratio R = -1 can improve the level of confidence. This is due to the fact that load ratios with high midrange stress and low stress amplitudes caused least damage to the graphite and vice versa, where R = -1 caused the most damage.

CHAPTER 8

8. RELATIONSHIP BETWEEN THE NATURAL FREQUENCY AND THE FATIGUE LIFE OF NBG-18 GRAPHITE

8.1 Introduction

This section investigates the relationship between the natural frequency and the fatigue life of uniaxial test specimens, with regards to orientation in the sample block from which it was manufactured, for the different fluctuating principle stress ratios used to which the samples were subjected.

Section 3.2 explains the particulars of grain orientation in sample block Q20 5087260 (block 60) and sample block Q20 5087261 (block 61), as well as the centre and edge positions of the specimens in each sample block. An X-axis orientation in sample block 60 implies that the specimens are located in the centre of the block and for the same orientation in sample block 61; the specimens are located at the edge of the block and vice versa for Z-axis orientation.

8.2 Relationship between Natural Frequency and Fatigue Life

8.2.1 Introduction

The strength of relationship between the experimentally obtained natural frequencies and fatigue life of the uniaxial specimens can be derived in terms of the correlation coefficient. The correlation coefficient makes it possible to determine whether there is a possible linear relationship between natural frequency and fatigue life, and if so the strength of relationship between natural frequency and fatigue. Thus, if natural frequency increase does the fatigue life tend to increase or decrease? This relation is expressed as a number that ranges from -1 to +1. The population correlation is

expressed by the Greek letter *rho* (ρ) and the correlation coefficient is given by the letter (r). The Pearson correlation coefficient (r) measures how well a straight line fits through a scatter of points when plotted on a xy-axis. The correlation coefficient can be calculated by the following formulas, where fatigue life is represented by the letter X and natural frequency is represented by the letter Y:

$$S_{xx} = \sum_{i=1}^{n}\left(X_i - \bar{X}\right)^2 \tag{8.1}$$

$$S_{yy} = \sum_{i=1}^{n}\left(Y_i - \bar{Y}\right)^2 \tag{8.2}$$

$$S_{xy} = \sum_{i=1}^{n}\left(X_i - \bar{X}\right)\left(Y_i - \bar{Y}\right) \tag{8.3}$$

where $S_{xy} = S_{yx}$. Using this notation the sample variance of the X and Y variables can be defined as:

$$S_x^2 = \frac{S_{xx}}{n-1} \tag{8.4}$$

and

$$S_y^2 = \frac{S_{yy}}{n-1} \tag{8.5}$$

respectively, and the covariance is calculated by:

$$S_{xy} = \frac{S_{xy}}{n-1} \tag{8.6}$$

From these equations the Pearson correlation coefficient can be calculated, which is a measure of the linear relationship between the fatigue life and natural frequency and is given by the following formula:

$$r = \frac{S_{xy}}{\sqrt{S_{xx}S_{yy}}} = \frac{S_{xy}}{S_x S_y} \tag{8.7}$$

The correlation coefficient is not depended on units of measurement, and when the coefficient is close to +1 or -1 there is a strong correlation and the points are scattered along a straight line. The closer a correlation is to 0, the weaker the relationship will be and the cloud of data points will not be close to a straight line. The strength of a correlation can generally be defined as follows:

Strong: $|r| \geq 0.8$

Moderate: $0.5 < |r| < 0.8$

Weak: $|r| \leq 0.5$

A linear regression was performed, to get the best-fit line through the relevant data points, namely the experimentally obtained natural frequencies versus fatigue life. The fatigue life was plotted against a log scale axis. From the best-fit line the R^2-value was obtained to give an indication of the overall goodness of fit. The Pearson correlation coefficient (*r*-value) was calculated by making use of an embedded GraphPad Prism Correlation Function to quantify the association between the natural frequency and fatigue life and to verify the *r*-value, obtained from the R^2-value from the best-fit line. The results were verified with equation (8.1) through to equation (8.7).

The linear regression plots of natural frequency versus fatigue life for specimens taken from sample block 60 and block 61 with different fluctuating load ratios are shown in Figure 35 to Figure 48in the subsequent sections. For each fluctuating load ratio a plot is shown for the uniaxial specimenôs alignment in both the Z-axis and X-axis. Each graph in addition also presents the Pearson correlation coefficients *r*-value obtained.

8.2.2 Relationship between Natural Frequency Mode 1 and Fatigue Life for Load Ratio R = -1, for sample block 60 and 61

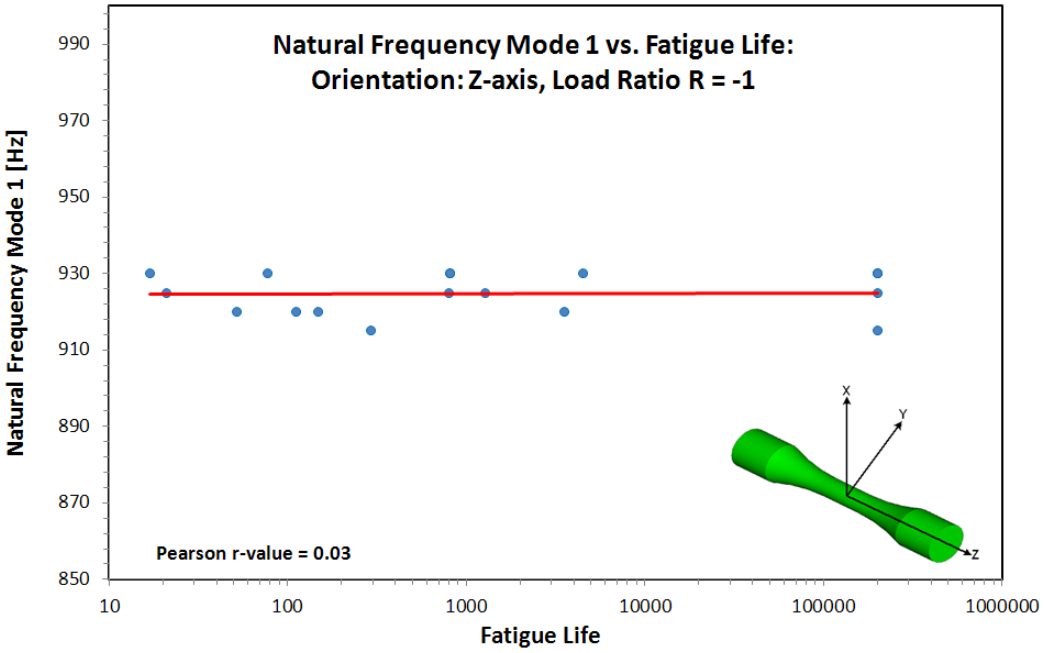

Figure 35: Natural frequency mode 1 vs. fatigue life for grain orientation in the Z-axis and load ratio of R = -1

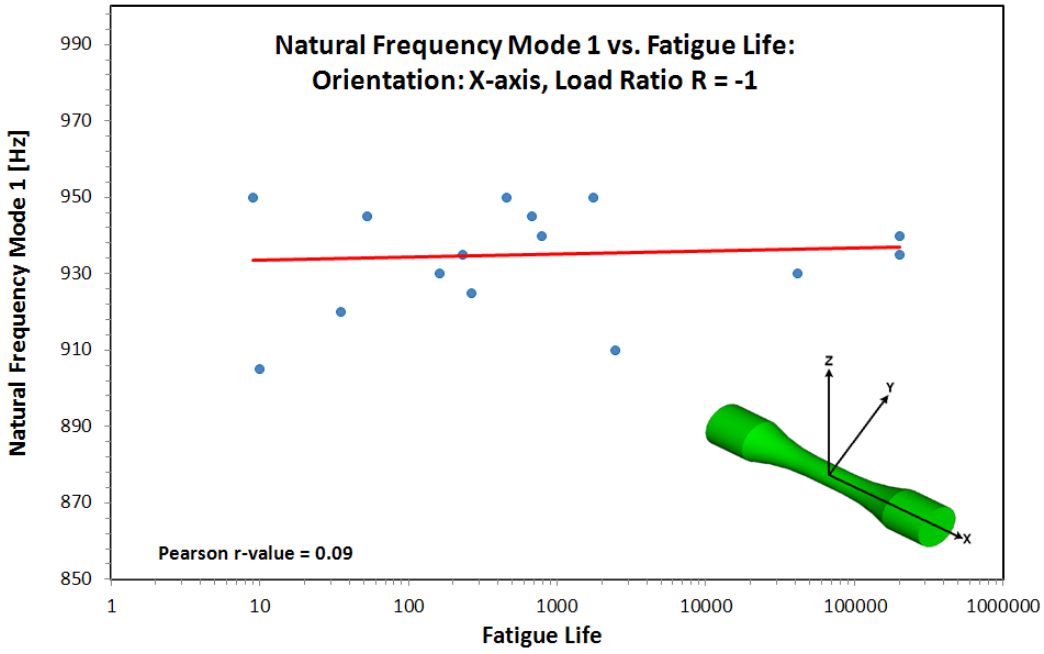

Figure 36: Natural frequency mode 1 vs. fatigue life for grain orientation in the X-axis and load ratio of R = -1

8.2.3 Relationship between Natural Frequency Mode 1 and Fatigue Life for Load Ratio R = - 2, for sample block 60 and 61

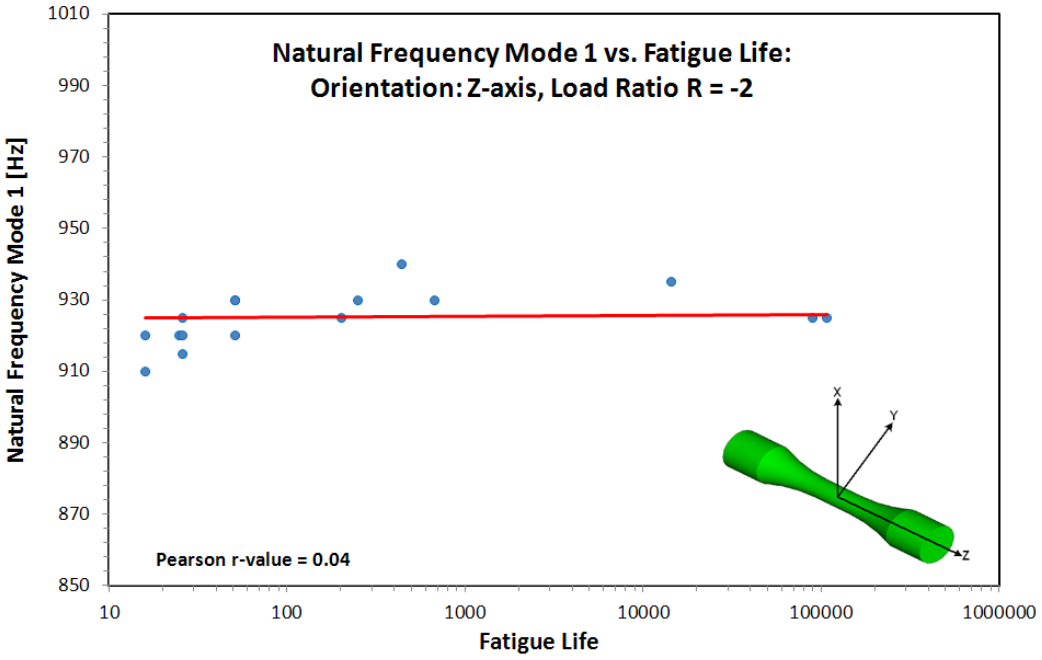

Figure 37: Natural frequency mode 1 vs. fatigue life for grain orientation in the Z-axis and load ratio of R = -2

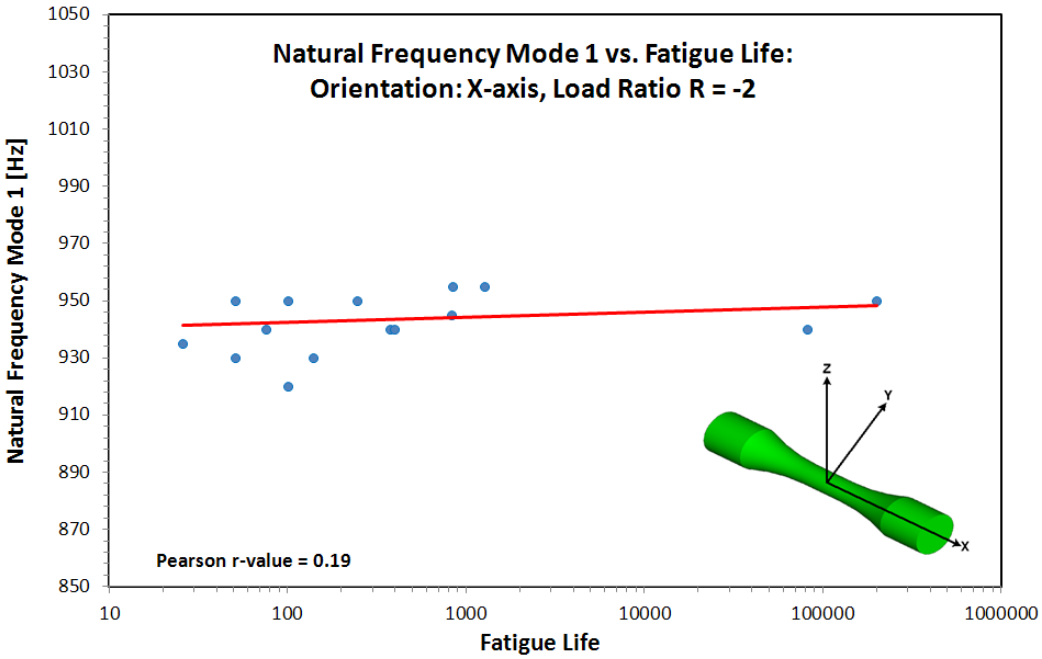

Figure 38: Natural frequency mode 1 vs. fatigue life for grain orientation in the X-axis and load ratio of R = -2

8.2.4 Relationship between Natural Frequency Mode 1 and Fatigue Life for Load Ratio R = - ∞, for sample block 60 and 61

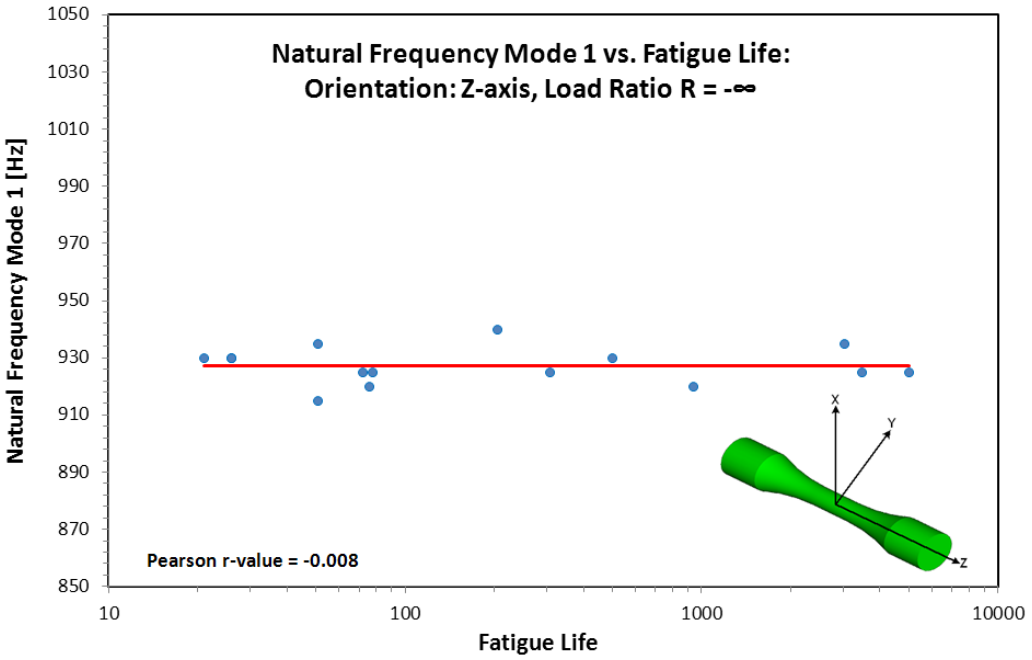

Figure 39: Natural frequency mode 1 vs. fatigue life for grain orientation in the Z-axis and load ratio of R = -∞

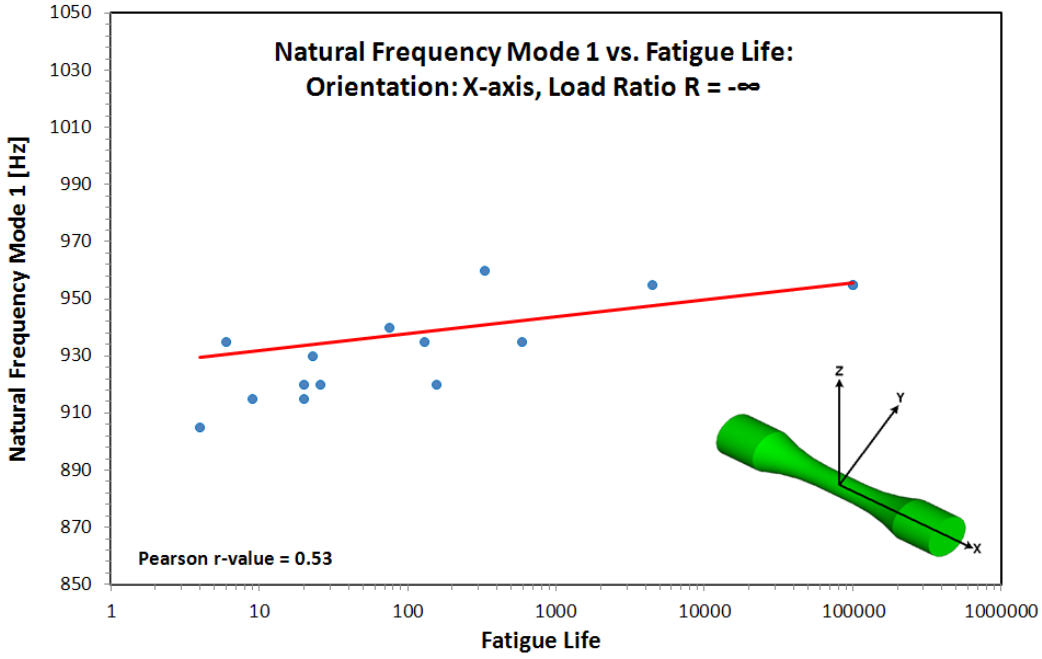

Figure 40: Natural frequency mode 1 vs. fatigue life for grain orientation in the X-axis and load ratio of R = -∞

8.2.5 Relationship between Natural Frequency Mode 1 and Fatigue Life for Load Ratio R = +2, for sample block 60 and 61

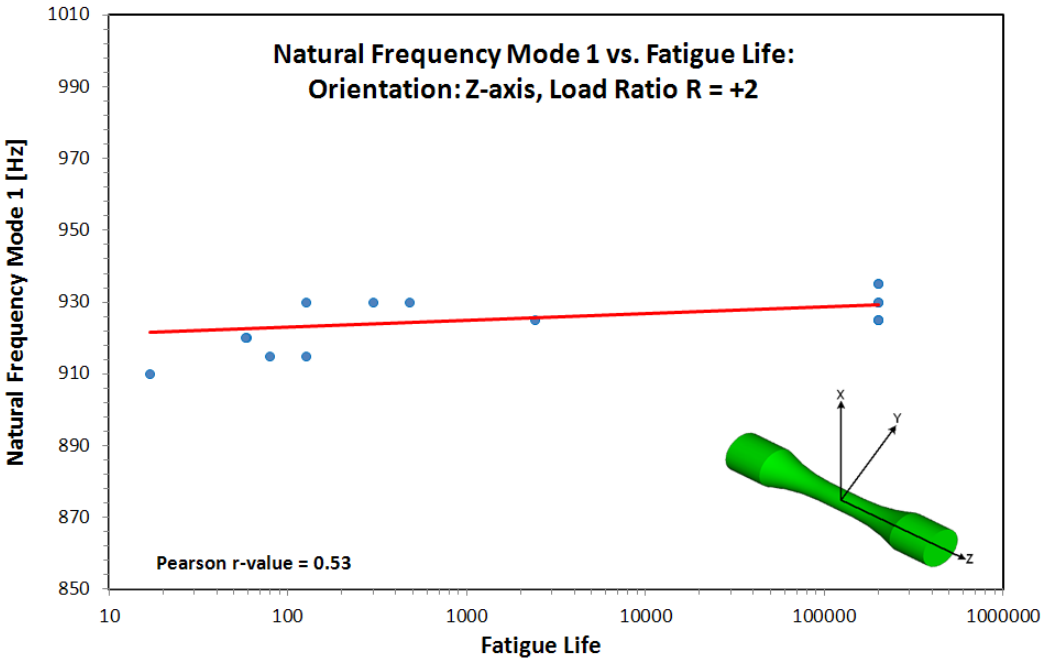

Figure 41: Natural frequency mode 1 vs. fatigue life for grain orientation in the Z-axis and load ratio of R = +2

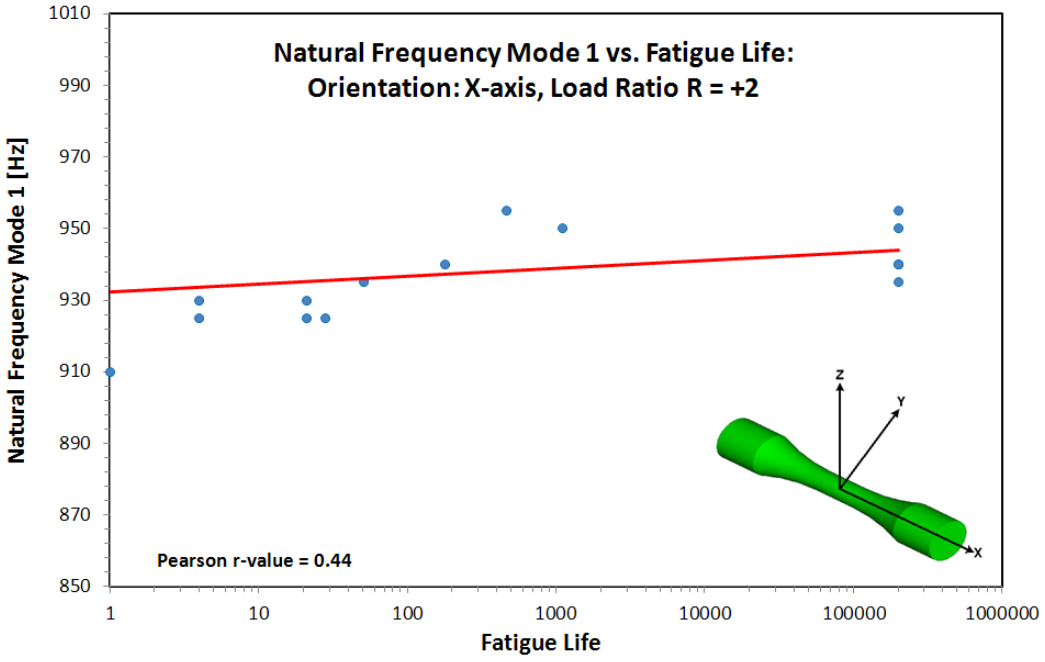

Figure 42: Natural frequency mode 1 vs. fatigue life for grain orientation in the X-axis and load ratio of R = +2

8.2.6 Relationship between Natural Frequency Mode 1 and Fatigue Life for Load Ratio R = -0.5, for sample block 60 and 61

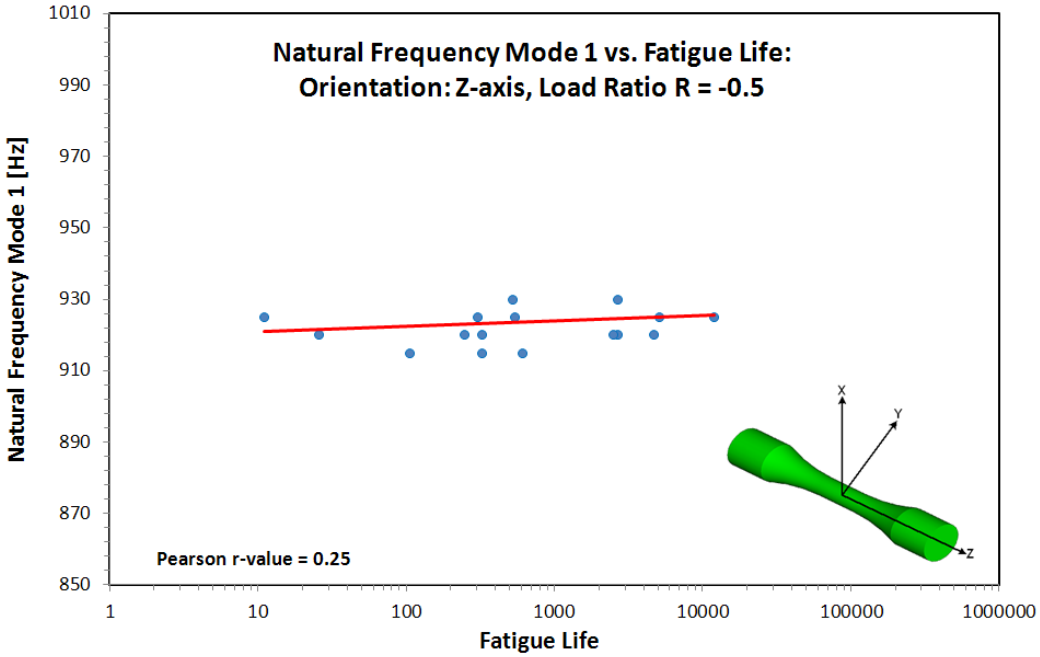

Figure 43: Natural frequency mode 1 vs. fatigue life for grain orientation in the Z-axis and load ratio of R = -0.5

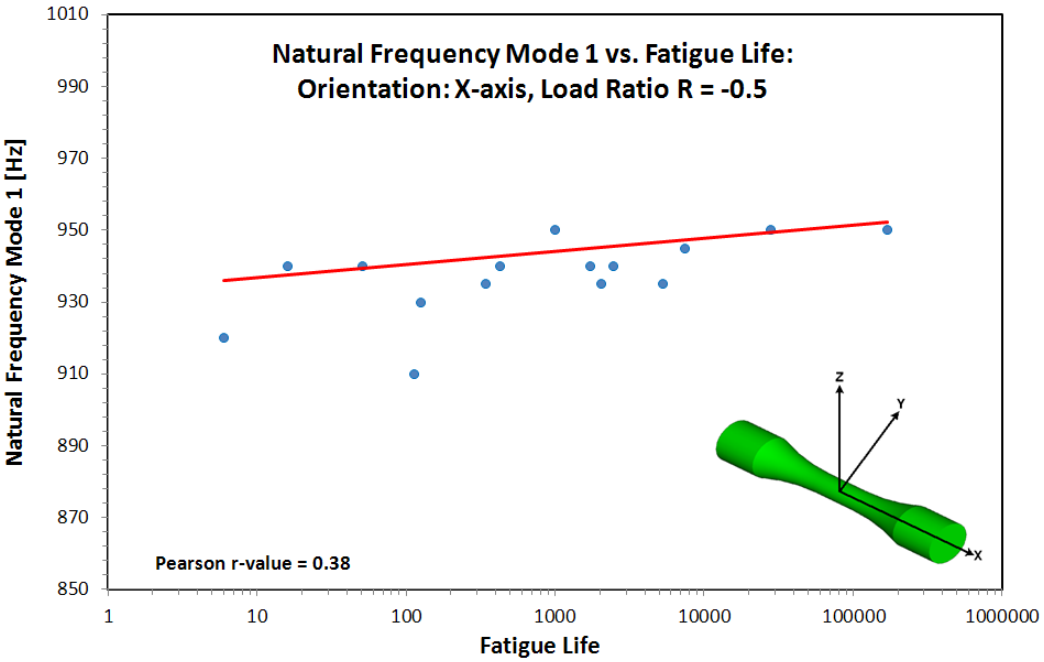

Figure 44: Natural frequency mode 1 vs. fatigue life for grain orientation in the X-axis and load ratio of R = -0.5

8.2.7 Relationship between Natural Frequency Mode 1 and Fatigue Life for Load Ratio R = 0, for sample block 60 and 61

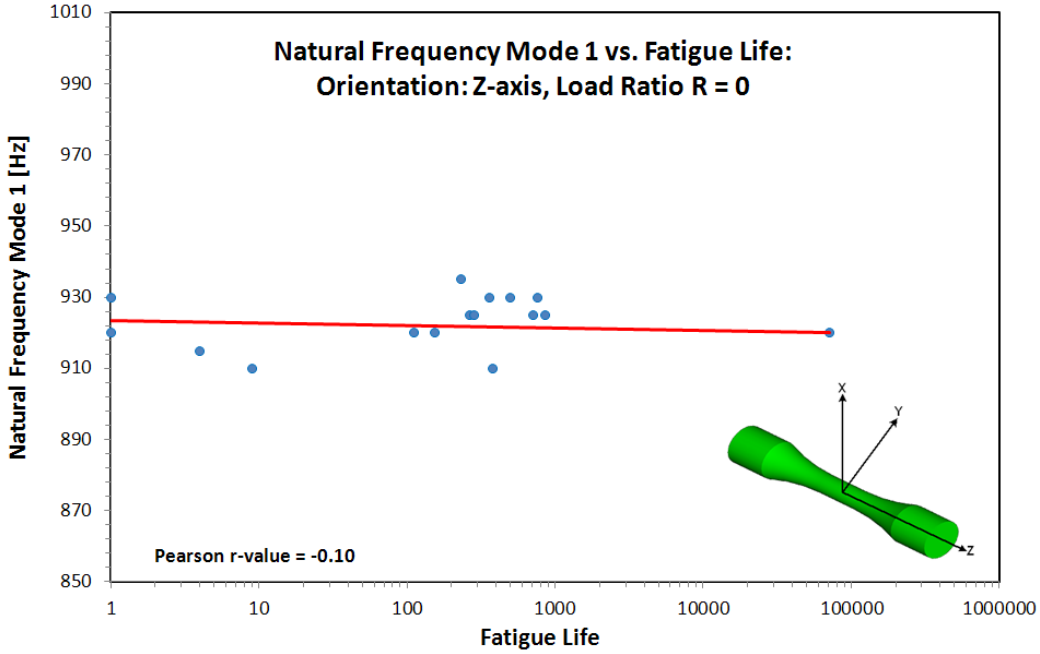

Figure 45: Natural frequency mode 1 vs. fatigue life for grain orientation in the Z-axis and load ratio of R = 0

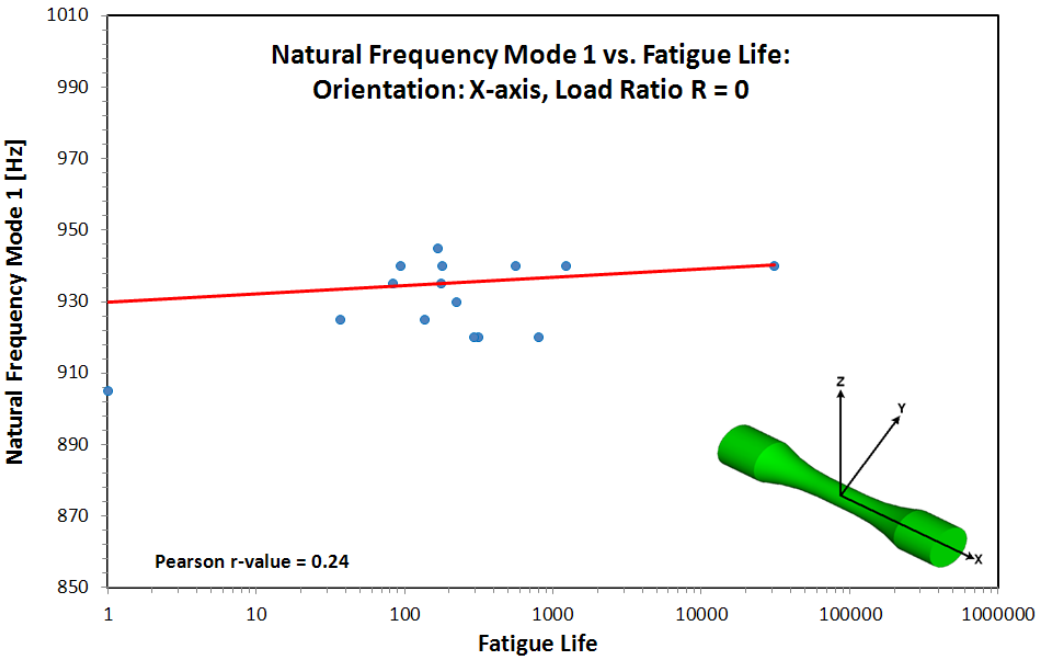

Figure 46: Natural frequency mode 1 vs. fatigue life for grain orientation in the X-axis and load ratio of R = 0

8.2.8 Relationship between Natural Frequency Mode 1 and Fatigue Life for Load Ratio R = +0.5, for sample block 60 and 61

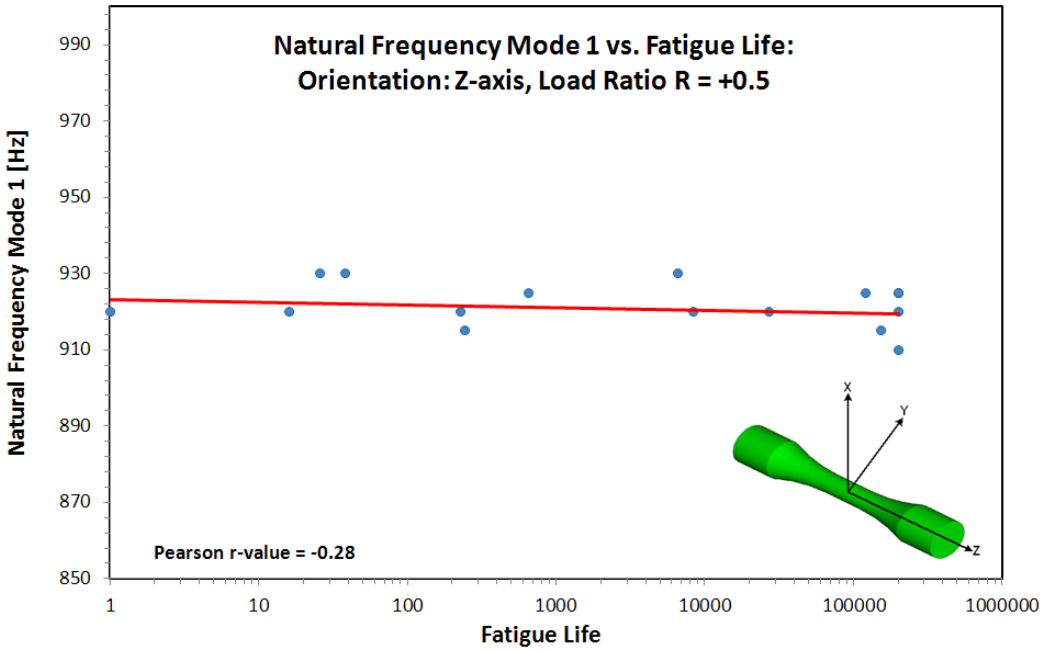

Figure 47: Natural frequency mode 1 vs. fatigue life for grain orientation in the Z-axis and load ratio of R = +0.5

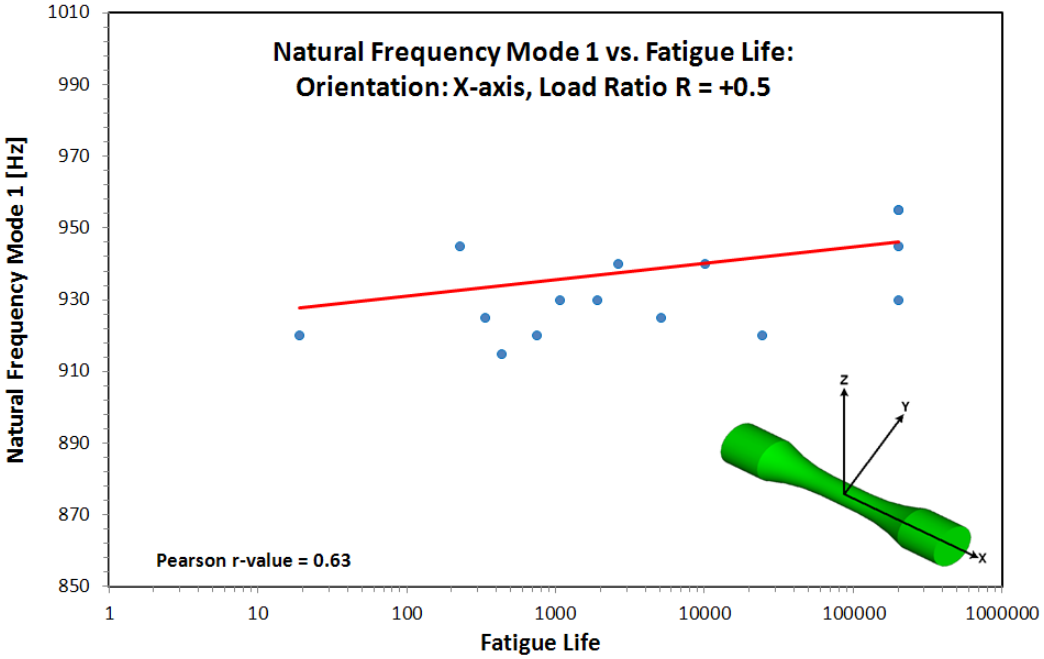

Figure 48: Natural frequency mode 1 vs. fatigue life for grain orientation in the X-axis and load ratio R = +0.5

Table 6 presents the results of the Pearson correlation coefficients calculated by means of equation 8.1 through to 8.7 for all load ratiosô grain orientations in the X and ï Z-axis in both sample block 60 and sample block 61.

Table 6: Pearson correlation coefficient (*r*-value) of natural frequency (mode 1 & mode 2) versus fatigue life, for all load ratios and block 60 and 61

Load Ratio	Block 60 (x-axis) Mode 1	Block 60 (x-axis) Mode 2	Block 61 (x-axis) Mode 1	Block 61 (x-axis) Mode 2	Block 60 (z-axis) Mode 1	Block 60 (z-axis) Mode 2	Block 61 (z-axis) Mode 1	Block 61 (z-axis) Mode 2
R = -1	0.49	0.33	-0.14	-0.24	-0.09	-0.05	0.27	-0.03
R = -2	0.38	0.19	0.05	-0.28	0.57	0.5	0.36	0.6
R = -∞	0.78	0.75	0.6	0.61	0.05	-0.55	-0.38	-0.5
R = +2	0.29	0.35	0.52	0.38	0.54	0.31	0.67	0.78
R = -0.5	0.55	0.39	0.55	0.52	0.14	0.01	0.38	0.25
R = 0	0.52	0.3	0.21	0.04	0.53	0.58	-0.26	-0.14
R = +0.5	0.02	0.23	0.56	0.62	-0.46	-0.57	-0.45	-0.35

8.3 Conclusions

Concerning the strength of correlations obtained between the natural frequency mode 1 and mode 2 versus the fatigue life of the specimens and considering Section 8.2.1, which explains the strength of Pearson correlations, it is clear from the results obtained (moderate to weak) that there is no noticeable trend between natural frequency mode 1 or natural frequency mode 2 with the fatigue life.

CHAPTER 9

9. CONCLUSION AND RECOMMENDATIONS

9.1 Modal Analysis Tests

The hammer impulse excitation technique proved to be an easy and reliable technique in determining natural frequencies of the NBG-18 graphite specimens. Two distinct resonance peaks in the magnitude of the frequency response function was successfully measured.

The consistency of the experimentally obtained data indicates that the parameters chosen for the experimental setup were sufficient in producing valid results. The experimental results were compared to FEA results, to further validate that the experiments were sufficient.

9.2 Uniaxial Fatigue Tests

The results obtained represent the average low end characteristics, since the specimens were taken from different orientations and locations from two graphite sample blocks of lower end acceptable strength.

The specimen design and the gripping alignment procedures proved to be satisfactory for the uniaxial fatigue tests. The fatigue tests conducted was exploratory, but statistically less accurate, because more load ratios were covered, with fewer specimens per load ratio. Although additional tests can improve the reliability of the data, the critical load ratios were identified. These were the fluctuating load ratios that produced the most damage in the material and include load ratios R = -0.5, R = -2 and R = -1.

9.3 The Feasibility of Application of the HIE Technique to predict the Fatigue Life of NBG-18 graphite.

The ability of modal testing by making use of the hammer impulse excitation technique to predict the fatigue life of NBG-18 graphite specimens has been investigated in this study.

Linear regression analysis was applied to correlate the modal parameter obtained namely the natural frequency to fatigue life as an output of fatigue tests performed at different fluctuating load ratios. Load ratios R = -∞ and R = +2 tested proved to show the highest *r*-values for the Pearson correlation coefficients obtained, however per definition the strength of these correlation still classifies as weak to moderate as explained in section 8.2.1. No significant trend (relationship)could be found between the natural frequency and the fatigue life. In the context of this research, the hammer impulse excitation technique failed to predict the fatigue life of NBG-18 graphite.

9.4 Recommendations for further research

Taking into consideration the results and limitations of this research, the following proposals are made for further investigation:

Modal parameters are by definition functions of the physical properties of materials i.e. mass, stiffness or modulus of elasticity and hence of mechanical properties. The uniaxial fatigue test specimens were machined into cylindrical shapes with defined dimensions before being dynamically tested to minimize the effect of other parameters, namely shape variations that could affect the modal results. Thus, the result of the dynamic properties was mainly due to microstructure variations that occur in the graphite.

Literature shows that natural frequency is sensitive to modulus of elasticity dimensions and shape, and that metallurgical characteristics explained by the type and phases play a crucial role in determining the mechanical properties such as the fatigue behaviour of a material. Moreover, natural frequency is dependent on material

stiffness that is affected by the microstructure of the material as shown by Damir *et.al* (2005), in a study performed to investigate the feasibility of using modal analysis for grey and ductile cast iron to predict the fatigue life of components.

Whether damping ratio could be a parameter used to predict the fatigue life of NBG-18 graphite remains unclear, but could be an interesting topic for future study.

REFERENCES

ANON. 2006, *Acoustic Emission,* http://www.twi.co.uk

ASTM E 466-96, 2002, *Standard Practice for Conducting Force Controlled Constant Amplitude Axial Fatigue Tests of Metallic Materials,* ASTM standards, Vol. 03.01, West Conshohocken, PA: ASTM

ASTM E 610-82, 2005, *Standard Definitions of Terms Relating to Acoustic Emission,* ASTM International.

ASTM C 651, *Test Method for Flexural Strength of Manufactured Carbon and Graphite Articles using Four-Point Loading at Room Temperature,* ASTM International

ASTM C 695, *Test Method for Compressive Strength of Carbon and Graphite,* ASTM International

ASTM C 747, *Test Method for Moduli of Elasticity and Fundamental Frequencies of Carbon and Graphite Materials by Sonic Resonance*, ASTM International

ASTM C749ï 92, 2005, *Standard test method for tensile stress-strain of carbon and graphite,* ASTM Standards, Vol. 05.05 West Conshohocken, PA: ASTM

ASTM E 1012-99, 2002,*Standard Practice for Verification of Specimen Alignment under Tensile Loading,* ASTM standards, Vol. 03.01, West Conshohocken, PA: ASTM

ASTM E 1876-01, *Standard Test Method for Dynamic Young's Modulus, Shear Modulus, and Poisson's Ratio by Impulse Excitation of Vibration,* ASTM International

ASTM E 1942-98, 2002, *Standard Guide for evaluating Data Acquisition Systems used in Cyclic Fatigue and Fracture Mechanics Testing,* ASTM International

Avitabile P. *Experimental Modal Analysis (A simple non-mathematical presentation),* Modal Analysis and Controls Laboratory, Mechanical Engineering Department, University of Massachusetts Lowell, Massachusetts USA.

Bedewi N.E., Kung D.N., *Effect of fatigue loading on the modal properties of composite structures and its utilization for prediction of residual life*, Compos. Struct1997;37(3/4):357ï 71.

Bishop R.E.D., Gladwell GML., *An investigation into the theory of resonance testing*, Proc Roy Soc Phil Trans 1963, 255:241.

Borum K.K., McGugan M, Brøndsted, *Condition Monitoring of Wind Turbine Blades,* Risø National Laboratory, DK-4000 Roskilde, Denmark.

Bosomworth P., *An exciting technique for quality analysis: the impulse excitation technique is finding widespread use in the high-tech ceramic industry as an easy-to-use research and quality control tool*, Access My Library, February 1, 2005.

BreyH. L.*Historical Background and Future Development of the High Temperature Gas Cooled Reactor,* presented at Seminar on HTGR Application and Development, Institute of Nuclear Engineering Technology, Tsinghua University, March 19 -21, 2001, Beijing China.

Burchell T.D., Cooke B., McEnaney B., Pickup I.M., Carbon 23, 739 (1985)

Damir A.N., *Characterization of progressive fatigue using modal analysis*, M.Sc. thesis, Production Engineering Department, Alexandria University; 2004.

Doebling S.W., Farrar C.R., Prime M.B., Shevitz D.W., *Damage identification and health monitoring of structural and mechanical systems from changes in their vibration characteristics: a literature review*, Los Alamos National Laboratory Report LA-13070-MS;1996.

El Tobgy M.S., *The use of modal analysis as a non-destructive testing tool for predicting fatigue life of components and structures*, M.Sc.Thesis, Production Engineering Department, Alexandria University;April 2002.

Eto M., Kurosawa T. Imai H., Nomura S., Oku T., *Estimation of Graphite Materials Corrosion with Water-vapour in Coolant of the VHTR and Oxidation Effect on the Materials Properties,* Japan Atomics Energy Research Institute, Tokai Mura, Ibaraki-ken 319-11, Japan (1983).

Friedrich C, et al., *The World's First 800 mm Diameter Graphite Electrode for a DC Electric Furnace*, MTP International 2002; 23 (2): 42-49.

General Atomics. *Graphite Design Handbook*, U.S. Department of Energy, DOE-HTGR-88111, 1988.

Hands G. *Resonant Inspection a "new" NDT technique,* NDTnet - July 1997, Vol.2 No.07

[a]Ioka I., [b]Yoda S., [c]Konishi T., *"Acoustic Emission for Polycrystalline Graphite under Compressive Loading"*, [a]Japan Atomic Energy Research Institute, Tokai-mura, Ibaraki-ken, 319-11, Japan, [b]National Space Development Agency of Japan, 2-4-1 Hamamatsu-cho, Minato-ku, Tokyo, 105 Japan., [c]Toyo Tanso Co. Ltd., Ohnohara-cho, Kagawa-ken, 769-16, Japan.

Irvine T, *An introduction to Frequency Response Functions,* Aug 2000.

Internet Web Site of the company SGL Carbon, www.sglcarbon.com, 2008

Ishihara, M., Iyoku,T., Shiozawa, S., and Kambe, M., *"Application of ultrasonic testing as acceptance test for the graphite component of HTTR,"* Trans. of 13th Int. Conf. on Structural Mechanics in Reactor Technology(SMiRT13) Vol.I, pp.575-580, Porto Alegre, Brazil, 1995.

Jenkins, G.M., *Fracture in reactor graphite*. J. Nucl. Mater. 5, 280-286, 1962.

Kessler SS et al. *Damage detection in composite materials using frequency response methods.* Composites: B 2002; 33: 87-95.

Macnaughtan M.P., *The cast iron brake disc developments for the 21st century*, MIRA new technology 2002, Available from: http://www.atalink.co.uk/mira.htm.

McClung R.W. *Non-destructive testing methods,* Metals and Ceramics Division, Oak Ridge National Laboratory, Post Office Box X, Oak Ridge, Tennessee37830.

McMaster R.C., 1959, *Non-destructive Testing Handbook*, Columbus, Ohio, The American Society for Non-destructive Testing, Inc., 43, p 36-37.

Migliori A., Visscher W.M., *Resonant Ultrasonic Inspection,* Industrial Applications Office, Los Alamos National Laboratory, November 1991.

Neighbour G.B., McEnaney B., Philips M., *"Acoustic Emissions Responses from Cyclic Loading of a Nuclear Graphite"*, School of Materials Science, University of Bath, Bath, BA2 7AY, U.K., Carbon Vol. 30. No. 3. Pp. 359-363, 1992.

Nemeth, N.N.Bratton, R, L., *Overview of statistical models of fracture for non-irradiated nuclear graphite components*. NASA Glenn Research Centre, Cleveland, OH, USA, Idaho National Laboratory, Idaho Falls, ID USA.

Nomura S., Kurosawa T., Imai H., Eto M., Oku T. 1986. *A graphite corrosion rate equation under high concentration water-vapour in helium and an estimation of the VHTR support post corrosion and strength.* (A Specialists graphite meeting on component structural design - JAERI Tokai (Japan), 8-11 September. International Atomic Energy Agency, Vienna (Austria). International working group on gas cooled reactors. IWGGCR ï 11, pp. 195 ï 200).

Ooka, N., Iyoku, T., et al., 1993. *"Ultrasonic examination of nuclear graphite for acceptance test in HTTR,"* JAERI-M93-003. [in Japanese]

[a]Pardini L.C., [b]Neto F.L., [c]De Almeida Fereira J.L., ñ*Damping Behaviour of Synthetic Graphite Beams"*, [a]CTA/AMR, 12225-904 São José Campos ï SP, Brazil., [b]UnB/FT/ENM, 70910-900 Brasilia ï DF, Brazil.

Pears C.D., Sanders H.G., *A Strength Analysis of a Polygraphite,* Air Force Materials Laboratory Report AFML-TR-69-204, Part 2, 1970.

Pebble Bed Modular Reactor Brochure, PBMR (Pty) Ltd, 2003

Quasar International Inc., *Using Quasar resonant inspection in a production environment*, 2000. Available from: http://www.quasarintl.com/.

Quinn, G.D., *Fractography of Ceramics and Classes*. National Institute of Standards and Technology, Special Publication 960-16, U.S. Government Printing Office.

Roberts, J.G. 2007. *Determination of Fatigue Characteristics of NBG-18 Graphite,* Potchefstroom: NWU, (Thesis ï PhD) 166 p.

Shigley, J.E., Mishke C.R., Budynas R.G., 2004, Mechanical Engineering Design, 7th edition, New York, McGraw-Hill.
Sezer Atamturktur H., Hanagan L.M., Boothy T.E. *Extensions of Large-Scale Modal Analysis Techniques to Historic Masonry Vaults,* Department of Architectural Engineering, The Pennsylvania State University, University Park, PA 16802, 2006.

Shibata, T. and Ishihara, M.,*"Ultrasonic signal characteristics by pulse-echo technique and mechanical strength of graphite materials with porous structure,"* Department of HTTR Project, Oarai Research Establishment, Japan Atomic Energy Research Institute, 3607 Oarai-machi,Higashiibaraki-gun, Ibaraki-ken 311 -1394, Japan.

Shibata, T., Ishihara, M., *"Ultrasonic Signal Characteristics by Pulse-echo Technique and Mechanical Strength of Graphite Materials with Porous Structure,"* Nucl. Eng. and Des, 203, pp133-141, 2001.

Shibata[a], T., Sumita[a], J., Tada[b], T., Hanawa[b], S., Sawa[a], K., Iyoku[a], T., *"Non-destructive evaluation methods for degradation of IG-110 and IG-430 graphite,"*[a]High Temperature Fuel and Material Group, Japan Atomic Energy Agency, 4002 Oarai-machi, Ibaraki-ken 311-1393, Japan, [b]Technology Development Division, Japan Atomic Energy Agency, 4002 Oarai-machi, Ibaraki-ken 311-1393, Japan.

Takatsubo, J.,Yamamoto, S., *"Study on the Propagation Mechanism of Ultrasonic Waves in Porous Ceramics (1st Report, Theory),"* Trans. Jpn. Soc. Mech. Eng., 60-577(A), pp.2126-2131, 1994. [in Japanese].

Schmidt A., 2003, Regulations for the design of the internals of the high temperature reactor. (Explanatory report no.GBRA 065942, Westinghouse Reactor GmbH, (May version) Mannheim, Germany, (Unpublished).

Stepinski T, *Resonance Ultrasound Spectroscopy – A Tool for Quality Control of Steel Products,*Signals and Systems Group, Department of Material Science, P. O.Box 528, 751 20 Uppsala University, Sweden, 2002.

Tucker, M.O., McLachian, N., *Fracture and microstructure if graphite's*, J.Phys.D: Appl. Phys. 26, 893-907.
TWI, *Acoustic Emission,* Copyright ©2006 TWI Ltd, http://www.twi.com.

Tuncel S, *Latest developments in the field of NDT Technologies: Acoustic Emission,*3rd International Non-Destructive Testing Symposium and Exhibition, Istanbul Turkey, April 2008, 12p.

Appendix A

Specimen Cutting Plan

Appendix B

Natural Frequency Tests Results Tables

Load Ratio: R = 2

Specimen ID	Natural Frequency [Hz] Mode 1	Natural Frequency [Hz] Mode 2	Block Orientation
60F31	935	3180	X
61J6	930	3155	Z
60N10	930	3140	Z
61B8	910	3060	X
61B29	930	3165	X
60N12	914.99	3150	Z
61J15	935	3170	Z
60F27	925	3120	X
60G32	950	3215	X
60N6	920	3135	Z
60N9	910	3120	Z
61B23	955	3245	X
61B28	930	3150	X
61J5	930	3125	Z
61J8	920	3110	Z
60G27	925	3130	X
60N7	925	3145	Z
60N13	914.99	3095	Z
61B16	950	3205	X
61B30	939.99	3185	X
61J13	930	3160	Z
61J16	925	3155	Z

Load Ratio: R = -2

Specimen ID	Natural Frequency [Hz] Mode 1	Natural Frequency [Hz] Mode 2	Block Orientation
61A24	950	3240	X
61F7	930	3140	Z
60G15	930	3150	X
60G5	920	3120	X
61B11	945	3210	X
60L4	925	3150	Z
60N8	920	3135	Z
61D14	930	3175	Z
60G12	939.99	3185	X
60G24	935	3175	X
60J7	914.99	3125	Z
60L5	920	3125	Z
61A31	950	3220	X
61B14	950	3210	X
61F5	925	3135	Z
61F8	920	3115	Z
60G10	930	3170	X
61F6	930	3150	Z
60G13	939.99	3180	X
60L3	920	3110	Z
60J8	910	3085	Z
61F15	939.99	3170	Z
61A23	955	3220	X
61B19	939.99	3190	X
60J15	925	3155	Z
60L6	925	3135	Z
61F16	930	3165	Z
61B22	950	3205	X
61F13	935	3175	Z
61A32	955	3245	X
60G20	939.99	3175	X

Load Ratio: R = -∞

Specimen ID	Natural Frequency [Hz] Mode 1	Natural Frequency [Hz] Mode 2	Block Orientation
60G21	935	3175	X
60G25	955	3230	X
60J16	925	3115	Z
60L12	920	3115	Z
61A6	920	3100	X
61A7	914.99	3115	X
61F14	935	3160	Z
61H7	930	3140	Z
60G26	935	3180	X
60G28	920	3115	X
60L7	925	3110	Z
60L13	925	3130	Z
61A14	955	3240	X
61H5	925	3145	Z
61A15	955	3245	X
61H8	920	3125	Z
60F7	920	3120	X
60G29	914.99	3105	X
60L8	914.99	3125	Z
60L11	925	3135	Z
61A28	930	3150	X
61B32	960	3265	X
61H6	925	3140	Z
61H15	939.99	3160	Z
60F19	939.99	3175	X
60L14	930	3120	Z
60L15	930	3140	Z
61A29	935	3180	X
61B7	905	3090	X
61H11	935	3165	Z
61H16	930	3155	Z

Load Ratio: R = -0.5

Specimen ID	Natural Frequency [Hz] Mode 1	Natural Frequency [Hz] Mode 2	Block Orientation
60H11	930	3150	Z
60F20	939.99	3190	X
60G1	935	3160	X
60J4	920	3130	Z
60L1	914.99	3105	Z
61B10	945	3190	X
61B12	950	3200	X
61H9	920	3100	Z
60G8	910	3070	X
60F21	935	3160	X
60L2	920	3115	Z
60J5	914.99	3115	Z
61B18	939.99	3175	X
61B13	950	3215	X
61H10	925	3165	Z
60H14	925	3135	Z
60G3	920	3135	X
60G17	930	3160	X
60J3	920	3110	Z
60L9	920	3130	Z
61A19	939.99	3195	X
61B25	939.99	3160	X
61J1	914.99	3105	Z
61J3	925	3165	Z
60G11	935	3155	X
60J6	920	3110	Z
60L10	930	3150	Z
61A22	950	3215	X
61A26	939.99	3190	X
61J2	925	3160	Z
61J4	925	3145	Z

Load Ratio: R = 0.5

Specimen ID	Natural Frequency [Hz] Mode 1	Natural Frequency [Hz] Mode 2	Block Orientation
60F17	920	3135	X
60F6	914.99	3110	X
60H1	910	3105	Z
60H4	920	3125	Z
61A2	930	3160	X
61A4	925	3140	X
61D9	920	3095	Z
61D11	925	3150	Z
60F24	930	3150	X
60F14	939.99	3200	X
60H2	920	3140	Z
60H5	914.99	3095	Z
61A10	945	3230	X
61A5	920	3085	X
61D10	930	3150	Z
61F3	930	3155	Z
60F24	930	3150	X
60F28	920	3120	X
60H9	920	3120	Z
60H12	914.99	3115	Z
61A17	945	3185	X
61A12	955	3230	X
61F1	920	3105	Z
61F4	925	3115	Z
60F29	925	3115	X
60H10	925	3120	Z
60H13	920	3105	Z
61B17	939.99	3190	X
61F2	925	3115	Z
61A13	955	3210	X
61F11	930	3165	Z

Load Ratio: R = 0

Specimen ID	Natural Frequency [Hz] Mode 1	Natural Frequency [Hz] Mode 2	Block Orientation
60F13	939.99	3180	X
60J10	925	3120	Z
61B2	920	3110	X
61B5	920	3100	X
61H13	930	3165	Z
61H2	925	3145	Z
61H4	920	3130	Z
60F10	930	3160	X
61F9	920	3130	Z
60J1	910	3085	Z
60H3	925	3135	Z
61A20	939.99	3235	X
61D12	930	3155	Z
60F4	920	3095	X
61A25	939.99	3190	X
60F5	925	3130	X
60F16	925	3120	X
60H6	920	3100	Z
60J2	920	3125	Z
61A21	945	3200	X
61B9	935	3170	X
61F10	930	3150	Z
61F12	930	3135	Z
60F12	939.99	3215	X
60F18	935	3165	X
60J9	914.99	3065	Z
61H12	935	3175	Z
61B17	939.99	3190	X
61B4	905	3080	X
61H1	910	3070	Z
61H3	925	3165	Z

Load Ratio: R = -1

Specimen ID	Natural Frequency [Hz] Mode 1	Natural Frequency [Hz] Mode 2	Block Orientation
60J14	925	3130	Z
60J11	920	3125	Z
60J12	914.99	3085	Z
60J13	920	3085	Z
61D5	930	3150	Z
61J11	930	3180	Z
61J12	925	3145	Z
61A8	930	3160	X
61B3	910	3190	X
61D15	930	3175	Z
60G18	935	3190	X
60G22	939.99	3160	X
60H15	925	3145	Z
60G2	930	3150	X
60G14	935	3200	X
60H7	920	3115	Z
61A18	945	3240	X
61B20	945	3210	X
61J9	920	3120	Z
60G9	925	3140	X
60G19	939.99	3170	X
61B21	950	3190	X
61B26	950	3210	X
60H8	914.99	3120	Z
61J10	930	3170	Z
60G4	920	3125	X
60H16	925	3130	Z
61A16	950	3205	X
61D13	930	3170	Z
61B6	905	3095	X
61J11	930	3180	Z
61D16	930	3185	Z

Appendix C

Uniaxial Fatigue Tests Results Tables

C-1 Compression Dominant Load Ratios

Load Ratio: R = 2

Specimen ID	Max Load (Theoretical)	Min Load (Theoretical)	Max Load (Actual)	Min Load (Actual)	No. of Cycles	Mass [g]	Gauge Section diameter [mm]	Block Orientation
60F22	-4.939	-9.878	-4.939	-9.878	200000	91.09	12.995	X
60G31	-4.939	-9.878	-4.939	-9.878	200000	91.08	12.999	X
60L16	-4.939	-9.878	-4.939	-9.878	200000	91.05	13.003	Z
61J7	-4.939	-9.878	-4.939	-9.878	200000	90.46	13.002	Z
61H14	-4.939	-9.878	-4.939	-9.878	200000	91.01	12.998	Z
61B27	-4.939	-9.878	-4.939	-9.878	200000	90.36	12.995	X
61B15	-4.939	-9.878	-4.939	-9.878	200000	90.8	12.994	X
60N4	-4.939	-9.878	-4.939	-9.878	200000	90.72	12.999	Z
60F30	-5.213	-10.426	-5.256	-10.336	21	90.21	12.996	X
60F31	-5.213	-10.426	-5.213	-10.424	51	90.83	12.996	X
61J6	-5.213	-10.426	-5.215	-10.43	126	90.39	13.001	Z
60N10	-5.213	-10.426	-5.228	-10.428	301	90.53	13	Z
61B8	-5.213	-10.426	-5.165	-9.841	1	88.67	12.995	X
61B29	-5.213	-10.426	-5.217	-10.4	21	89.9	12.996	X
60N12	-5.213	-10.426	-5.213	-10.429	126	90.24	12.998	Z
61J15	-5.213	-10.426	-5.213	-10.42	200000	90.99	13.004	Z
60F27	-5.378	-10.756	-5.301	-10.782	4	90.36	12.993	X
60G32	-5.378	-10.756			1100	91.59	12.999	X
60N6	-5.378	-10.751	-5.395	-10.592	59	90.69	12.999	Z
60N9	-5.378	-10.751	-5.429	-10.676	17	90.31	13.002	Z
61B23	-5.378	-10.751	-5.38	-10.754	465	90.65	12.995	X
61B28	-5.378	-10.751	-5.549	-10.504	4	90.07	12.996	X
61J5	-5.378	-10.751	-5.396	-10.703	477	90.59	12.998	Z
61J8	-5.378	-10.751	-5.391	-10.696	58	90.02	13.002	Z
60G27	-5.103	-10.207	-5.127	-10.134	28	90.45	12.999	X
60N7	-5.103	-10.207	-5.103	-10.207	200000	90.58	12.998	Z
60N13	-5.103	-10.207	-5.103	-10.207	80	90.41	13	Z
61B16	-5.103	-10.207	-5.103	-10.207	200000	90.48	12.995	X
61B30	-5.103	-10.207	-5.163	-10.007	180	90.07	12.999	X
61J13	-5.103	-10.207	-5.103	-10.207	200000	91.01	13.005	Z
61J16	-5.103	-10.207	-5.103	-10.207	2420	90.45	13.003	Z

Load Ratio: R = -∞

Specimen ID	Max Load (Theoretical)	Min Load (Theoretical)	Max Load (Actual)	Min Load (Actual)	No. of Cycles	Mass [g]	Gauge Section diameter [mm]	Block Orientation
60G21	0	-9.329	0	-9.329	588	91.34	13.001	X
60G25	0	-9.329	0	-9.329	4453	91.56	12.996	X
60J16	0	-9.329	0	-9.329	376	91.21	13.002	Z
60L12	0	-9.329	0	-9.329	76	90.44	13.006	Z
61A6	0	-9.329	0	-9.329	26	88.91	12.998	X
61A7	0	-9.329	0	-9.329	20	88.52	12.996	X
61F14	0	-9.329	0	-9.329	3039	91.02	13.003	Z
61H7	0	-9.329	0	-9.329	501	90.65	12.998	Z
60G26	0	-8.78	0	-8.78	130	90.77	12.996	X
60G28	0	-8.78	0	-8.78	157	90.15	12.998	X
60L7	0	-8.78	0	-8.78	3466	90.75	13.007	Z
60L13	0	-8.78	0	-8.78	307	90.55	13.003	Z
61A14	0	-8.78	0	-8.78	100000	90.57	12.995	X
61H5	0	-8.78	0	-8.78	5016	90.54	13.002	Z
61A15	0	-8.78	0	-8.78	100000	90.55	12.992	X
61H8	0	-8.78	0	-8.78	940	90.08	12.998	Z
60F7	0	-9.878	0	-9.619	20	90.16	13	X
60G29	0	-9.878	0	-9.26	9	90.08	13.001	X
60L8	0	-9.878	0	-9.859	51	90.38	13.004	Z
60L11	0	-9.878	0	-9.869	78	90.52	13.007	Z
61A28	0	-9.878	0	-9.828	23	89.74	12.991	X
61B32	0	-9.878	0	-9.88	329	90.83	12.996	X
61H6	0	-9.878	0	-9.808	72	90.55	13.001	Z
61H15	0	-9.878	0	-9.868	205	91.01	12.998	Z
60F19	0	-10.426	0	-10.427	76	90.93	12.983	X
60L14	0	-10.426	0	-10.444	26	90.71	13.003	Z
60L15	0	-10.426	0	-10.435	26	90.97	13.003	Z
61A29	0	-10.426	0	-10.457	6	89.69	12.993	X
61B7	0	-10.426	0	-9.851	4	88.77	12.996	X
61H11	0	-10.426	0	-10.428	51	91.1	12.996	Z
61H16	0	-10.426	0	-10.394	21	90.69	12.998	Z

C-2 Tension Dominant Load Ratios

Load Ratio: R = 0

Specimen ID	Max Load (Theoretical)	Min Load (Theoretical)	Max Load (Actual)	Min Load (Actual)	No. of Cycles	Mass [g]	Gauge Section diameter [mm]	Block Orientation
60F13	2.238	0	2.238	0	31042	91.02	12.998	X
60J10	2.238	0	2.238	0	860	90.68	13	Z
61B2	2.238	0	2.238	0	296	89.91	12.998	X
61B5	2.238	0	2.238	0	804	89.76	13	X
61H13	2.238	0	2.238	0	761	90.95	12.995	Z
61H2	2.238	0	2.238	0	265	90.78	12.994	Z
61H4	2.238	0	2.238	0	71237	90.52	12.993	Z
60F10	2.37	0	2.238	0	225	90.63	12.997	X
61F9	2.37	0	2.238	0	155	90.92	12.994	Z
60J1	2.37	0	2.238	0	377	90.25	13.001	Z
60H3	2.37	0	2.238	0	710	90.78	13.002	Z
61A20	2.37	0	2.238	0	94	90.33	12.99	X
61D12	2.37	0	2.238	0	496	90.74	12.996	Z
60F4	2.37	0	2.238	0	316	90.04	12.989	X
61A25	2.37	0	2.238	0	1233	90.32	12.992	X
60F5	2.53	0	2.53	0	137	89.99	12.99	X
60F16	2.53	0	2.53	0	37	90.57	13	X
60H6	2.53	0	2.566	-0.559	1	90.73	13.004	Z
60J2	2.53	0	2.566	-0.559	112	90.72	13.002	Z
61A21	2.53	0	2.566	-0.559	169	90.29	12.992	X
61B9	2.53	0	2.566	-0.559	83	90.63	12.997	X
61F10	2.53	0	2.566	-0.556	1	91.15	12.998	Z
61F12	2.53	0	2.566	-0.556	359	90.86	12.996	Z
60F12	2.651	0	2.56	0	181	90.9	12.998	X
60F18	2.651	0	2.56	0	178	90.72	12,987	X
60J9	2.651	0	2.596	0	4	90.58	13.001	Z
61H12	2.651	0	2.56	0	231	90.94	12.995	Z
61B17	2.651	0	2.56	0	565	90.57	12.994	X
61B4	2.651	0	2.595	-0.764	1	89.29	12.995	X
61H1	2.651	0	2.5	0	9	90.37	12.995	Z
61H3	2.651	0	2.56	0	283	90.68	12.993	Z

Load Ratio: R = -2

Specimen ID	Max Load (Theoretical)	Min Load (Theoretical)	Max Load (Actual)	Min Load (Actual)	No. of Cycles	Mass [g]	Gauge Section diameter [mm]	Block Orientation
61A24	2.363	-4.725	2.355	-4.724	51	90.02	13	X
61F7	2.363	-4.725	2.36	-4.72	251	90.44	12.994	Z
60G15	2.363	-4.725	2.36	-4.72	140	91.04	12.999	X
60G5	2.363	-4.725	2.36	-4.72	101	90.3	12.998	X
61B11	2.363	-4.725	2.36	-4.72	838	91.02	12.997	X
60L4	2.363	-4.725	2.36	-4.72	26	90.66	13.002	Z
60N8	2.363	-4.725	2.36	-4.72	16	90.32	13.001	Z
61D14	2.363	-4.725	2.36	-4.72	51	90.79	12.994	Z
60G12	2.44	-4.88	2.437	-4.88	76	91.31	13.002	X
60G24	2.44	-4.88	2.448	-4.88	26	91.1	13.004	X
60J7	2.44	-4.88	2.461	-4.906	26	90.78	13.002	Z
60L5	2.44	-4.88	2.441	-4.96	25	90.81	13.003	Z
61A31	2.44	-4.88	2.44	-4.876	101	90	12.992	X
61B14	2.44	-4.88	2.44	-4.876	247	90.77	12.994	X
61F5	2.44	-4.88	2.44	-4.88	203	90.44	12.992	Z
61F8	2.44	-4.88	2.439	-4.88	26	89.93	12.993	Z
60G10	2.27	-4.54	2.274	-4.538	51	90.84	13.002	X
61F6	2.27	-4.54	2.271	-4.541	51	90.42	12.992	Z
60G13	2.27	-4.54	2.27	-4.54	379	91.27	13.002	X
60L3	2.27	-4.54	2.27	-4.542	51	90.57	12.997	Z
60J8	2.27	-4.54	2.229	-4.621	16	90.45	13.002	Z
61F15	2.27	-4.54	2.27	-4.54	444	90.96	12.991	Z
61A23	2.27	-4.54	2.27	-4.54	842	90.27	12.989	X
61B19	2.27	-4.54	2.27	-4.54	399	90.75	12.994	X
60J15	1.89	-3.78	1.89	-3.78	106985	91.12	13	Z
60L6	1.89	-3.78	1.89	-3.78	89695	90.84	13.002	Z
61F16	1.89	-3.78	1.89	-3.78	678	90.64	12.992	Z
61B22	1.89	-3.78	1.89	-3.78	200000	90.68	12.998	X
61F13	1.89	-3.78	1.89	-3.78	14424	90.88	12.991	Z
61A32	1.89	-3.78	1.89	-3.78	1284	90.33	12.999	X
60G20	1.89	-3.78	1.89	-3.78	82018	91.22	13	X

Load Ratio: R = 0.5

Specimen ID	Max Load (Theoretical)	Min Load (Theoretical)	Max Load (Actual)	Min Load (Actual)	No. of Cycles	Mass [g]	Gauge Section diameter [mm]	Block Orientation
60F17	2.238	1.119	2.238	1.119	24583	90.02	12.991	X
60F6	2.238	1.119	2.238	1.119	432	89.94	12.986	X
60H1	2.238	1.119	2.238	1.119	200000	90.13	12.999	Z
60H4	2.238	1.119	2.238	1.119	27114	90.79	13.002	Z
61A2	2.238	1.119	2.238	1.119	200000	89.69	12.995	X
61A4	2.238	1.119	2.238	1.119	336	89.36	13.001	X
61D9	2.238	1.119	2.238	1.119	200000	90.82	12.99	Z
61D11	2.238	1.119	2.238	1.119	200000	90.88	12.997	Z
60F24	2.494	1.247	2.495	1.25	1916	90.75	12.99	X
60F14	2.494	1.247	2.495	1.25	10118	90.94	13.005	X
60H2	2.494	1.247	2.495	1.25	227	90.64	12.998	Z
60H5	2.494	1.247	2.495	1.25	152151	90.68	13	Z
61A10	2.494	1.247	2.495	1.25	200000	90.66	12.994	X
61A5	2.494	1.247	2.495	1.25	755	89.15	12.998	X
61D10	2.494	1.247	2.495	1.25	26	91.09	12.999	Z
61F3	2.494	1.247	2.495	1.25	66 49	90.55	12.993	Z
60F24	2.574	1.287	2.574	1.287	1066	90.75	12.99	X
60F28	2.574	1.287	2.574	1.287	19	90.05	12.993	X
60H9	2.574	1.287	2.574	1.287	1	90.99	13.004	Z
60H12	2.574	1.287	2.574	1.287	242	90.58	13.003	Z
61A17	2.574	1.287	2.574	1.287	227	90.37	12.992	X
61A12	2.574	1.287	2.574	1.287	200000	90.71	12.999	X
61F1	2.574	1.287	2.574	1.287	16	90.47	12.997	Z
61F4	2.574	1.287	2.574	1.287	649	90.46	12.994	Z
60F29	2.363	1.182	2.363	1.182	5113	90.05	12.992	X
60H10	2.363	1.182	2.363	1.182	120948	90.91	13.003	Z
60H13	2.363	1.182	2.363	1.182	8435	90.79	13.002	Z
61B17	2.363	1.182	2.363	1.182	2615	90.57	12.994	X
61F2	2.363	1.182	2.363	1.182	200000	90.67	12.996	Z
61A13	2.363	1.182	2.363	1.182	200000	90.7	12.996	X
61F11	2.363	1.182	2.363	1.182	38	90.92	12.996	Z

Load Ratio: R = -1

Specimen ID	Max Load (Theoretical)	Min Load (Theoretical)	Max Load (Actual)	Min Load (Actual)	No. of Cycles	Mass [g]	Gauge Section diameter [mm]	Block Orientation
60J14	2.047	-2.047	2.06	-2.08	1279	90.62	13	Z
60J11	1.67	-1.67	1.67	-1.69	3546	90.61	13.003	Z
60J12	0.88	-0.88	0.9	-0.9	201423	90.45	13.002	Z
60J13	2.4	-2.4	2.4	-2.41	52	90.61	13.001	Z
61D5	1.5	-2.1	1.504	-1.503	200000	90.37	12.992	Z
61J11	2.27	-2.27			815	91.12	13.004	Z
61J12	2.1	-1.67	2.1	-2.1	802	90.91	13.004	Z
61A8	1.67	-1.67	1.672	-1.67	41331	89.58	12.996	X
61B3	1.67	-1.67	1.67	-1.67	2476	89.39	12.997	X
61D15	1.67	-1.67	1.67	-1.67	200000	90.81	12.997	Z
60G18	1.67	-1.67	1.67	-1.67	200000	91.06	13	X
60G22	1.67	-1.67	1.67	-1.67	200000	91.43	13.005	X
60H15	1.67	-1.67	1.67	-1.67	200000	91.18	13.006	Z
60G2	2.4	-2.4	2.4	-2.4	161	90.61	12.998	X
60G14	2.4	-2.4	2.4	-2.4	231	91.19	13.003	X
60H7	2.4	-2.4	2.4	-2.4	112	90.78	13.003	Z
61A18	2.4	-2.4	2.4	-2.4	677	90.44	12.992	X
61B20	2.4	-2.4	2.4	-2.4	53	90.75	12.993	X
61J9	2.4	-2.4	2.4	-2.4	149	90.93	13.004	Z
60G9	2.27	-2.27	2.27	-2.27	266	90.39	13.003	X
60G19	2.27	-2.27	2.27	-2.27	790	91.22	13.004	X
61B21	2.27	-2.27	2.27	-2.27	458	90.78	12.995	X
61B26	2.27	-2.27	2.27	-2.27	1747	90.79	12.995	X
60H8	2.27	-2.27	2.27	-2.27	292	90.42	13.004	Z
61J10	2.27	-2.27	2.27	-2.27	4516	91.28	13.003	Z
60G4	2.53	-2.53	2.53	-2.53	35	90.29	12.999	X
60H16	2.53	-2.53	2.53	-2.53	21	91.28	13.007	Z
61A16	2.53	-2.53	2.53	-2.53	9	90.15	12.993	X
61D13	2.53	-2.53	2.53	-2.53	17	90.73	12.994	Z
61B6	2.53	-2.53	2.53	-2.53	10	89.03	12.998	X
61J11	2.53	-2.53	2.53	-2.53	815	91.12	13.004	Z
61D16	2.53	-2.53	2.53	-2.53	77	90.65	12.995	Z

Load Ratio: R = -0.5

Specimen ID	Max Load (Theoretical)	Min Load (Theoretical)	Max Load (Actual)	Min Load (Actual)	No. of Cycles	Mass [g]	Gauge Section diameter [mm]	Block Orientation
60H11	2.231	-1.115	2.231	-1.115	527	90.76	13.004	Z
60F20	2.231	-1.115	2.231	-1.115	2462	90.99	12.992	X
60G1	2.231	-1.115	2.231	-1.115	343	90.48	12.998	X
60J4	2.231	-1.115	2.231	-1.115	2664	90.85	13.001	Z
60L1	2.231	-1.115	2.231	-1.115	606	90.05	12.997	Z
61B10	2.231	-1.115	2.231	-1.115	7417	90.9	12.997	X
61B12	2.231	-1.115	2.231	-1.115	27996	90.81	12.995	X
61H9	2.231	-1.115	2.231	-1.115	2506	90.94	12.997	Z
60G8	2.363	-1.182	2.363	-1.182	113	90.1	13.002	X
60F21	2.363	-1.182	2.363	-1.182	2027	91.01	12.991	X
60L2	2.363	-1.182	2.363	-1.182	324	90.51	12.996	Z
60J5	2.363	-1.182	2.363	-1.182	326	90.83	13.001	Z
61B18	2.363	-1.182	2.363	-1.182	426	90.69	12.994	X
61B13	2.363	-1.182	2.363	-1.182	1000	90.81	12.996	X
61H10	2.363	-1.182	2.363	-1.182	540	91.24	12.995	Z
60H14	2.363	-1.182	2.363	-1.182	302	91.02	13.001	Z
60G3	2.441	-1.22	2.475	1.231	6	90.43	12.997	X
60G17	2.441	-1.22	2.445	1.221	126	90.52	12.999	X
60J3	2.441	-1.22	2.445	1.221	247	90.84	13.001	Z
60L9	2.441	-1.22	2.445	1.221	26	90.62	13.002	Z
61A19	2.441	-1.22	2.45	1.23	16	90.38	12.993	X
61B25	2.441	-1.22	2.444	1.22	51	90.72	12.994	X
61J1	2.441	-1.22	2.444	1.22	106	90.57	12.999	Z
61J3	2.441	-1.22	2.444	1.238	11	90.74	12.999	Z
60G11	2.153	-1.076	2.153	-1.076	5311	91.18	13.003	X
60J6	2.153	-1.076	2.153	-1.076	4719	90.88	13.003	Z
60L10	2.153	-1.076	2.153	-1.076	2669	90.76	13.004	Z
61A22	2.153	-1.076	2.153	-1.076	169104	90.35	12.991	X
61A26	2.153	-1.076	2.153	-1.076	1712	90.16	12.991	X
61J2	2.153	-1.076	2.153	-1.076	11885	90.87	12.999	Z
61J4	2.153	-1.076	2.153	-1.076	5118	90.6	13	Z

Appendix D

Alignment Reports for Uniaxial Fatigue Tests

Report 1: AlignPro device

Operator:	G Gouws and DG Hattingh
Reference Nº:	Initial Alignment Test Set-Up
Temperature:	21°C
Frame ID:	Instron Fatigue Machine 25kN Load Cell
Time & Date:	07:31AM& 2007/02/22
Project No:	NO001
Specification:	ASTM E1012 : 1999
Unit System:	S.I.
Hardware ID:	AP-USB-350-01 [A]
Description:=	16 ch - 16 bit device with USB interface
Alignment Cell Type:	Standard
Alignment Cell:	Instron 8000-171 Cylindrical 8 Gauges – ALIGN
Cell Description:	Cylindrical - 8 Gauges
Material:	Alloy Steel 817M40
Total Length (lt):	185 mm
Length (l):	50 mm
Diameter (Ø):	8 mm
No Gauges:	8
Type Gauges:	350 ohms
Gauge Factor:	2.05
Separation (lg):	37.5 mm
Alignment Load:	4.2 kN
Test Comments:	Customised load train.

Alignment Data Summary:

Field Designation	e1 (µE)	e2 (µE)	e3 (µE)	e4 (µE)	Ave.	b1 (µE)	b2 (µE)	b3 (µE)	b4 (µE)	Max bending (µE)	% Bending
Top Gauges (1 to 4)	377.930	372.903	377.650	374.704	**375.797**	2.133	-2.894	1.853	-1.092	0.912	**0.243**
Bottom Gauges (5 to 8)	374.303	370.855	373.045	372.672	**372.719**	1.585	-1.864	0.326	-0.047	1.105	**0.297**

Report 2: AlignPro device

Operator:	G Gouws
Reference Nº:	Alignment Test Set-Up before commencement of Fatigue tests.
Temperature:	26°C
Frame ID:	Instron Fatigue Machine 25kN Load Cell
Time & Date:	12:08:44 PM 2007/03/07
Project No:	NO001
Specification:	ASTM E1012 : 1999
Unit System:	S.I.
Hardware ID:	AP-USB-350-01 [A]
Description:=	16 ch - 16 bit device with USB interface
Alignment Cell Type:	Standard
Alignment Cell:	Instron 8000-171 Cylindrical 8 Gauges – ALIGN
Cell Description:	Cylindrical - 8 Gauges
Material:	Alloy Steel 817M40
Total Length (lt):	185 mm
Length (l):	50 mm
Diameter (Ø):	8 mm
No Gauges:	8
Type Gauges:	350 ohms
Gauge Factor:	2.05
Separation (lg):	37.5 mm
Alignment Load:	3 kN
Test Comments:	Customised load train. Test Loads are estimated to be around 2kN

Alignment Data Summary:

Field Designation	e1 (µE)	e2 (µE)	e3 (µE)	e4 (µE)	Ave.	b1 (µE)	b2 (µE)	b3 (µE)	b4 (µE)	Max Bending (µE)	% Bending
Top Gauges (1 to 4)	216.323	215.572	211.139	215.543	**214.644**	1.679	0.928	-3.505	0.899	2.592	**1.208**
Bottom Gauges (5 to 8)	214.819	209.682	211.065	217.439	**213.251**	1.567	-3.569	-2.186	4.188	4.309	**2.020**

Report 3: AlignPro device

Operator:	G Gouws
Reference Nº:	First Alignment Test during Fatigue tests.
Temperature:	23
Frame ID:	Instron Fatigue Machine 25kN Load Cell
Time & Date:	23 March 2007 at 12:00
Project No:	NO001
Specification:	ASTM E1012 : 1999
Unit System:	S.I.
Hardware ID:	AP-USB-350-01 [A]
Description:=	16 ch - 16 bit device with USB interface
Alignment Cell Type:	Standard
Alignment Cell:	Instron 8000-171 Cylindrical 8 Gauges – ALIGN
Cell Description:	Cylindrical - 8 Gauges
Material:	Alloy Steel 817M40
Total Length (lt):	185 mm
Length (l):	50 mm
Diameter (Ø):	8 mm
No Gauges:	8
Type Gauges:	350 ohms
Gauge Factor:	2.05
Separation (lg):	37.5 mm
Alignment Load:	2.4kN
Test Comments:	Test done after completion R = -1

Alignment Data Summary:

Field Designation	e1 (µE)	e2 (µE)	e3 (µE)	e4 (µE)	Ave.	b1 (µE)	b2 (µE)	b3 (µE)	b4 (µE)	Max Bending (µE)	% Bending
Top Gauges (1 to 4)	237	241	239	238	**239**	-1.93	2.49	0.26	-0.82	**1.99**	**0.83**
Bottom Gauges (5 to 8)	236	237	242	237	**238**	-1.45	-1.37	4.11	-1.29	**2.78**	**1.17**

Report 4: Align Pro device

Operator:	G Gouws
Reference Nº:	Second Alignment Test during Fatigue tests.
Temperature:	26
Frame ID:	Instron Fatigue Machine 25kN Load Cell
Time & Date:	24 April 2007 at 12:30
Project No:	NO001
Specification:	ASTM E1012 : 1999
Unit System:	S.I.
Hardware ID:	AP-USB-350-01 [A]
Description:=	16 ch - 16 bit device with USB interface
Alignment Cell Type:	Standard
Alignment Cell:	Instron 8000-171 Cylindrical 8 Gauges – ALIGN
Cell Description:	Cylindrical - 8 Gauges
Material:	Alloy Steel 817M40
Total Length (lt):	185 mm
Length (l):	50 mm
Diameter (Ø):	8 mm
No Gauges:	8
Type Gauges:	350 ohms
Gauge Factor:	2.05
Separation (lg):	37.5 mm
Alignment Load:	3kN
Test Comments:	Test done before R = Ð

Alignment Data Summary:

Field Designation	e1 (µE)	e2 (µE)	e3 (µE)	e4 (µE)	Ave.	b1 (µE)	b2 (µE)	b3 (µE)	b4 (µE)	Max Bending (µE)	% Bending
Top Gauges (1 to 4)	308.5	307.9	309.7	307.4	**308.4**	0.12	-0.46	1.33	-0.99	**0.66**	**0.21**
Bottom Gauges (5 to 8)	303.6	304.3	305.3	309.9	**305.8**	-2.16	-1.49	-0.45	4.11	**2.92**	**0.96**

Report 5: Align Pro device

Operator:	G Gouws
Reference Nº:	Third Alignment Test during Fatigue tests.
Temperature:	23
Frame ID:	Instron Fatigue Machine 25kN Load Cell
Time & Date:	06 May 2007 at 15:00
Project No:	NO001
Specification:	ASTM E1012 : 1999
Unit System:	S.I.
Hardware ID:	AP-USB-350-01 [A]
Description:=	16 ch - 16 bit device with USB interface
Alignment Cell Type:	Standard
Alignment Cell:	Instron 8000-171 Cylindrical 8 Gauges – ALIGN
Cell Description:	Cylindrical - 8 Gauges
Material:	Alloy Steel 817M40
Total Length (lt):	185 mm
Length (l):	50 mm
Diameter (Ø):	8 mm
No Gauges:	8
Type Gauges:	350 ohms
Gauge Factor:	2.05
Separation (lg):	37.5 mm
Alignment Load:	3kN
Test Comments:	Test done before R =+2;-2

Alignment Data Summary:

Field Designation	e1 (µE)	e2 (µE)	e3 (µE)	e4 (µE)	Ave.	b1 (µE)	b2 (µE)	b3 (µE)	b4 (µE)	Max Bending (µE)	% Bending
Top Gauges (1 to 4)	316.8	311.7	310.8	316.8	**314**	2.783	-2.337	-3.228	2.782	**3.947**	**1.257**
Bottom Gauges (5 to 8)	312.1	312.7	313.2	314.7	**313.2**	-1.052	-0.472	0.02	1.504	**1.124**	**0.359**

Report 6: Align Pro device

Operator:	G Gouws
Reference Nº:	Third Alignment Test during Fatigue tests.
Temperature:	20˚C
Frame ID:	Instron Fatigue Machine 25kN Load Cell
Time & Date:	28 May 2007 at 12:30
Project No:	NO001
Specification:	ASTM E1012 : 1999
Unit System:	S.I.
Hardware ID:	AP-USB-350-01 [A]
Description:=	16 ch - 16 bit device with USB interface
Alignment Cell Type:	Standard
Alignment Cell:	Instron 8000-171 Cylindrical 8 Gauges – ALIGN
Cell Description:	Cylindrical - 8 Gauges
Material:	Alloy Steel 817M40
Total Length (lt):	185 mm
Length (l):	50 mm
Diameter (Ø):	8 mm
No Gauges:	8
Type Gauges:	350 ohms
Gauge Factor:	2.05
Separation (lg):	37.5 mm
Alignment Load:	3kN
Test Comments:	Test done before testing strain gauged samples

Alignment Data Summary:

Field Designation	e1 (µE)	e2 (µE)	e3 (µE)	e4 (µE)	Ave.	b1 (µE)	b2 (µE)	b3 (µE)	b4 (µE)	Max Bending (µE)	% Bending
Top Gauges (1 to 4)	300.06	301.53	303.62	297.19	**300.60**	-0.54	0.93	3.02	-3.41	**2.81**	**0.93**
Bottom Gauges (5 to 8)	300.33	301.24	296.77	299.25	**299.40**	0.93	1.84	-2.62	-0.15	**2.04**	**0.68**

Report 1: Graphite sample

Operator:	W. Rall, G. Gouws and D. Hattingh
Reference Nº:	Initial Test tests.
Temperature:	25C
Frame ID:	Instron Fatigue Machine 25kN Load Cell
Time & Date:	13:00&22/02/2007
Project No:	NO001
Specification:	ASTM E1012 : 1999
Unit System:	S.I.
Hardware ID:	DM 20 Strain Amplifier
Description:	4 channel
Alignment Cell:	Strain Gauged Graphite Sample
Material:	Graphite
Total Length (lt):	Mm
// **Length :**	50 mm
Diameter (Ø):	Mm
No Gauges:	4
Type Gauges:	120 ohms
Gauge Factor:	2.06
Alignment Load:	See Results table.
Test Comments:	None

Results:

LOAD	**N**	**895**	**912**	**796**	**915**	**879**
Strain gauge position	**Degrees**	**0**	**90**	**180**	**270**	**0**
Strain Measurement	e_1	630	603	535	606	613
	e_2	630	583	543	580	612
	e_3	610	592	570	589	580
	e_4	616	606	564	612	585
Average Strain	e_{ave}	**621.5**	**596**	**553**	**596.75**	**597.5**
$e_1 - e_{ave}$	**b1**	8.5	7	-18	9.25	15.5
$e_2 - e_{ave}$	**b2**	8.5	-13	-10	-16.75	14.5
$e_3 - e_{ave}$	**b3**	-11.5	-4	17	-7.75	-17.5
$e_4 - e_{ave}$	**b4**	-5.5	10	11	15.25	-12.5
$0.5 (x + y)^{0.5}$	**B**	12.2066	12.748	20.40833	18.11767	21.31901
$(b1 - b3)^2$	**x**	400	121	1225	289	1089
$(b2 - b4)^2$	**y**	196	529	441	1024	729
$(B/e_{ave})x100$	**$\%B_{Max}$**	**2.0**	**2.1**	**3.7**	**3.0**	**3.6**

Report 2: Graphite sample

Operator:	W. Rall, G. Gouws
Reference Nº:	Initial Test tests.
Temperature:	24C
Frame ID:	Instron Fatigue Machine 25kN Load Cell
Time & Date:	16:00&07/03/2007
Project No:	NO001
Specification:	ASTM E1012 : 1999
Unit System:	S.I.
Hardware ID:	DM 20 Strain Amplifier
Description:	4 channel
Alignment Cell:	Strain Gauged Graphite Sample
Material:	Graphite
Total Length (lt):	Mm
// **Length :**	50 mm
Diameter (Ø):	--mm
No Gauges:	4
Type Gauges:	120 ohms
Gauge Factor:	2.06
Alignment Load:	875N
Test Comments:	None

Results:

LOAD	**N**	**875**	**875**	**875**	**875**	**875**
Strain gauge position	**Degrees**	90	180	270	0	90
Strain Measurement	**e_1**	583	563	599	592	574
	e_2	616	573	570	594	608
	e_3	608	601	578	562	602
	e_4	573	594	600	561	570
Average Strain	**e_{ave}**	**595**	**582.75**	**586.75**	**577.25**	**588.5**
$E_1 - e_{ave}$	**b1**	-12	-19.75	12.25	14.75	-14.5
$e_2 - e_{ave}$	**b2**	21	-9.75	-16.75	16.75	19.5
$e_3 - e_{ave}$	**b3**	13	18.25	-8.75	-15.25	13.5
$e_4 - e_{ave}$	**b4**	-22	11.25	13.25	-16.25	-18.5
$0.5\ (x + y)^{0.5}$	**B**	24.86966	21.70829	18.30983	22.2991	23.60085
$(b1 - b3)^2$	**x**	625	1444	441	900	784
$(b2 - b4)^2$	**y**	1849	441	900	1089	1444
$(B/e_{ave})x100$	**$\%B_{Max}$**	**4.2**	**3.7**	**3.1**	**3.9**	**4.0**

Report 3: Graphite sample

Operator:	G. Gouws
Reference Nº:	Initial Test tests.
Temperature:	23C
Frame ID:	Instron Fatigue Machine 25kN Load Cell
Time & Date:	23 March 2007 at 13:45
Project No:	NO001
Specification:	ASTM E1012 : 1999
Unit System:	S.I.
Hardware ID:	DM 20 Strain Amplifier
Description:	4 channel
Alignment Cell:	Strain Gauged Graphite Sample
Material:	Graphite
Total Length (lt):	Mm
// **Length :**	50 mm
Diameter (Ø):	--mm
No Gauges:	4
Type Gauges:	120 ohms
Gauge Factor:	2.06
Alignment Load:	875N
Test Comments:	None

Results:

LOAD	**N**	**875**	**875**	**875**	**875**	**875**
Strain gauge position	**Degrees**	90	180	270	0	90
Strain Measurement	**e_1**	566	565	590	586	573
	e_2	571	560	566	558	587
	e_3	581	595	563	562	569
	e_4	584	581	573	588	580
Average Strain	**e_{ave}**	**575.5**	**575.25**	**573**	**573.5**	**577.25**
$E_1 - e_{ave}$	**b1**	-9.5	-10.25	17	12.5	-4.25
$e_2 - e_{ave}$	**b2**	-4.5	-15.25	-7	-15.5	9.75
$e_3 - e_{ave}$	**b3**	5.5	19.75	-10	-11.5	-8.25
$e_4 - e_{ave}$	**b4**	8.5	5.75	0	14.5	2.75
$0.5\ (x + y)^{0.5}$	**B**	9.92	18.31	13.95	19.21	4.03
$(b1 - b3)^2$	**x**	225	900	729	576	16
$(b2 - b4)^2$	**y**	169	441	49	900	49
$(B/e_{ave})x100$	**$\%B_{Max}$**	**1.7**	**3.2**	**2.4**	**3.3**	**0.7**

Appendix E

Calibration Certificates for Uniaxial Fatigue Tests

Appendix F

Vibratory Molding Process

According to SGL Carbon (2008) it is possible to manufacture NBG-18 graphite blocks in large sizes, which also makes further impregnation possible.

The full production line of vibratory molded graphite is shown schematically in Figure 71 and can be explained as follows. High quality raw materials are gathered from a secure source. The processing that follows includes crushing, milling, screening, binding, mixing and homogenizing. After these processes are completed, the material is vibration moulded. Baking of the material follows where carbonizing and redensification takes place. Graphitizing of the baked material allows for the formation of an ordered graphite matrix. Mechanical processing of the materials can include processes like turning, milling, grinding, drilling, lapping and finally polishing. Refining is the last step in the manufacturing process and can include impregnating, coating and purifying of the material.

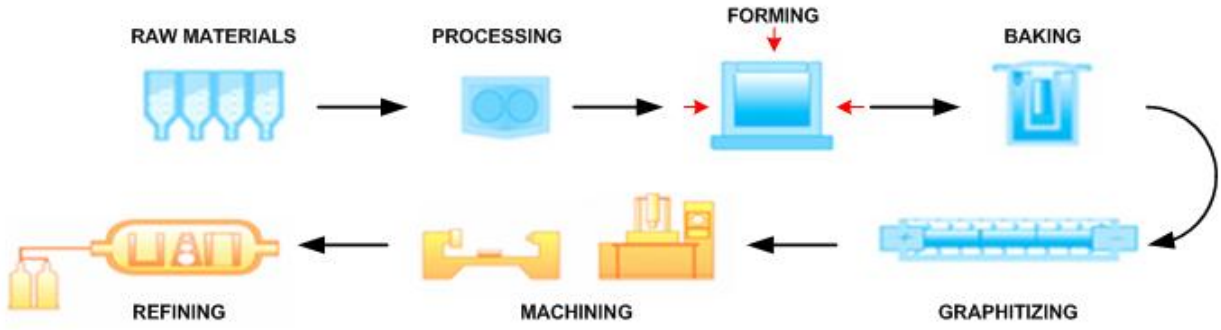

Figure 49: Vibration molding manufacturing process

Appendix G

KTA 3232 Design Rule and Developed MDE Stress

According to the KTA 3232 design rule, the governing stress equation to design for strength of graphite is the modified Maximum Deformation Strain Energy (MDE) criterion (Schmidt, 2001b).

The MDE stress criterion can be mathematically shown by Equation 1 and Equation 2:

$$\sigma_\nu = \left\{ \bar{\sigma}_1^{\,2} + \bar{\sigma}_2^{\,2} + \bar{\sigma}_3^{\,2} - 2.\nu.\left(\bar{\sigma}_1.\bar{\sigma}_2 + \bar{\sigma}_2.\bar{\sigma}_3 + \bar{\sigma}_3.\bar{\sigma}_1 \right) \right\} \le S_{ut}^{\,2} \qquad \text{... (1)}$$

Where:

$$\bar{\sigma}_i = \begin{Bmatrix} \sigma_i.1 & if\ \sigma_i \ge 0 \\ \sigma_i.f & if\ \sigma_i < 0 \end{Bmatrix} \qquad \text{é (2)}$$

And

$$f = \frac{S_{ut}}{S_{uc}}$$

σ = MDE Stress [MPa]

ν = Poissonôs ratio with loss of physical interpretation

S_{ut} = Ultimate Tensile Strength [MPa]

S_{uc} = Ultimate Compressive Strength [MPa]

σ_i = Principle Stress, i [MPa]

The probability of survival is calculated by using a two-parameter Weibull distribution, given by Equation (3):

$$L_c = e^{-\left\{ \sum_i \left(\frac{\sigma_i}{S_c} \right)^m . \frac{\nu_i}{\sum \nu_i} \right\}} \qquad \text{é (3)}$$

And the probability of failure (PF) of the component is determined by Equation (4):

$PF = 1 - L_c$

Where:

L_c = KTA 3232 Probability of survival

σ_i = Local MDE Stress [MPa]

S_c = Weibull characteristic strength (all tensile data) [MPa]

m = Weibull distribution shape parameter (all tensile data)

PF = Probability of failure